Atomistic Computer Simulations of Polymer Permeation:

Thermodynamics and Transport of Additives in Liquids and Polymeric Systems

Dissertation

Zur Erlangung des Grades

"Doktor der Naturwissenschaften"

am Fachbereich Chemie, Pharmazie und Geowissenschaften

der Johannes Gutenberg-Universität

in Mainz

Tuğba Arzu Özal

geboren in İstanbul, Türkei

Mainz 2007

Dedicated to my family

Zusammenfassung

Mit Molekulardynamik-Simulationen können Einblicke in molekulare Systeme und deren atomistische Struktur, sowie strukturelle, dynamische und thermodynamische Eigenschaften von weicher Materie (z. B. Flüssigkeiten oder Polymere) gewonnen werden. Diese Arbeit befasst sich mit atomistischen Simulationen von Additiven mit dem Ziel, die Permeation von Polymeren im Hinblick auf Löslichkeit und Diffusion zu untersuchen.

Die Thermodynamik des Lösungsprozesses einer unpolaren Substanz in niedermolekularen Flüssigkeiten, im Speziellen binären Mischungen von Dimethylsulfoxid (DMSO) in Wasser, wird untersucht. Dabei soll insbesondere der Einfluss der Wechselwirkungen zwischen Lösungsmittel und gelöster Substanz auf thermodynamischer Ebene betrachtet werden. Die Berechnung der Entropie zeigt, dass diese als treibende Kraft für den Lösungsprozess nicht in Frage kommt, da große kompensierende Terme auftreten. Die Beziehung zwischen diesen Größen und den Zustandgrößen des Lösungsmittel werden aus den Simulationsdaten zur DMSO-Wasser-Mischung berechnet. Durch Vergleich mit experimentellen Daten werden die zugrundeliegenden Simulationsmodelle und mögliche Verbesserungen (force-field-Parameter) diskutiert. Für die Untersuchung der Permeation von Polymeren ist der Lösungsprozess von besonderer Bedeutung. Die üblichen Methoden zur Bestimmung des chemischen Potentials in niedermolekularen Flüssigkeiten sind jedoch für dichte Polymersysteme nicht anwendbar. Aus diesem Grund wird ein neuerer Ansatz, "Störungstheoreticher Ansatz basierend auf einem einzelnen Referenzzustand mit weichen Potentialen", mit klassischen Ansätzen (thermodynamische Integration (TI) und durch Fast-Growth TI z.B. in Oktadekan und Bisphenol-A-Polykarbonat) verglichen. Abschliessend werden die Transportprozesse von Additiven in Polymersystemen untersucht und gezeigt, dass experimentelle Daten zur Diffusivität von Wassermolekülen in einem morphologisch mikrophaseseparierten Natriumsulfanat-Polyethylen-System (Na-PES) reproduziert werden können.

SUMMARY

Molecular dynamics (MD) simulations provide an atomic level description of molecular systems and driving forces behind structural, dynamic and thermodynamic properties of condensed matter systems (liquids and polymers). This thesis deals with atomistic simulation of additives in order to understand polymer permeation which has two aspects; solvation and diffusion.

Solvation thermodynamics of a nonpolar solute in low molecular liquids (binary mixtures of dimethyl sulfoxide (DMSO)/water) is investigated to observe how the preferential interactions between solute and solvent are reflected in thermodynamic terms; free energy, enthalpy, and entropy. The solute-solvent and solvent-solvent contributions of entropy are computed and total entropy is claimed not to be the driving force for solvation, since it involves a large compensating term. The relation between these terms and the solvent equation of state data in DMSO-water mixtures is examined quantitatively, and the optimization of computational models (force-field parameters) in relation with experimentally easily obtainable bulk properties of mixtures are discussed. Since permeation occurs through polymeric systems, solvation is particularly important in polymeric systems. The basic methodologies applied to obtain solvation chemical potentials in low molecular liquids are not applicable to dense polymer microstructures. Therefore, a new method, one-step perturbation (based on a soft-cavity reference state), is discussed via comparison of classical thermodynamic integration (TI) and Fast Growth TI in octadecane and bisphenol-A polycarbonate (BPA-PC). Finally, in a transport study of additives through polymeric systems, reproduction of experimental data on diffusivity of water molecules in a morphologically microphaseseparated sodium-Sulfonated Polyethylene (Na-PES) system was achieved.

Table of Contents

CHAPTER 1

Introduction

Computational chemistry, as the name implies, is a branch of chemistry which utilizes computers and numerical calculation methods to gain information on the chemical structures and properties of systems based on theoretical chemistry. Depending on the property of interest, the methods employed cover both static and dynamic situations. Static means that one can either perform quantum mechanical calculations or observe the microscopic orientation of the atoms as well as the effects related with their structure formation in complex systems via molecular dynamics (MD) simulations. Dynamics illustrates how particles behave under the impact of both internal and/or external forces. In this thesis, we will mainly focus on how to gain information from atomic scale MD simulations to explain systematically the properties of additive molecules within various systems, including aqueous solutions and polymers. In general, the system simulated can be a single molecule or a group of molecules. Accordingly, the computational effort increases rapidly with the size and complexity of the systems being studied. Also, variability of the interactions within a system counts in the complexity of the system. Furthermore, as the complication of the system varies, the methods applied or

the approaches used differ as well with respect to their accuracy or feasibility. In the next chapter, chapter 2, we will start with introducing the theory of basic methodologies used in this thesis, concentrating on molecular dynamics.

As the title of this thesis indicates, our interest focuses on atomistic scale computer simulations of polymer permeation. For a clear understanding of permeation, we drew attention to the thermodynamics and transport of additives in liquid and polymeric systems. Permeation involves both a dissolution and diffusion process: first a molecule dissolves in a medium and then diffuses across that medium. Both dissolution (solubility) and diffusion depend on the interactions that the molecule experiences with its surrounding. The medium can be a (synthetic) polymer membrane, or a lipid membrane, a thin film, etc. We tried to explain how these specific interactions are reflected in the quantities that are macroscopically observable, such as free energy, enthalpy and entropy changes.

In this thesis, we study the thermodynamics of dissolved molecules in fluid media with particular interest on how molecular rearrangements in the fluid medium affect the thermodynamic properties. This is achieved by studies starting from binary liquid solutions. The reason that we start up with binary solutions is that, in these kinds of low molecular weight systems any molecule can explore through the system freely within the time constraints of simulations making it possible to sample the configuration space easily. This enables us to use the basic thermodynamic approaches. In binary solutions, there is preferential interaction of one of the components of the cosolvent with the solute molecule. The question we want to answer is that whether these preferential interactions are reflected in the basic thermodynamic quantities like free energy, enthalpy and

entropy. Moreover, we would like to see whether we can relate the spatial rearrangements of the solvent molecules around certain species in the solution to some numerical thermodynamic results. To go beyond the phenomenological thermodynamics, we separated the basic quantities into solute-solvent and solvent-solvent contributions by the help of the statistical mechanics. Thus, splitting the entropy and enthalpy changes brings about exploring the solvation and reorganization of solvent molecules in a superior way.

In our initial study which we present in Chapter 3, we worked on solvation of methane in organic cosolvent/water mixtures to explore the preferential interactions. For that, a binary mixture of Dimethyl Sulfoxide (DMSO)/ water was taken as a solvent system at various proportions to relate the structural properties to thermodynamic quantities. While the solute is a simple non-polar molecule, the solvent system was chosen as a complex two component mixture in which two very polar compounds are mixed. Trends in the free energy change with respect to cosolvent amount in the aqueous mixture show whether the solvation is more preferential or not with the increasing cosolvent content. This may give a clue about the preferential interaction between the additive molecule and the cosolvent. However, when there is a term in enthalpy and entropy which totally cancels out in the free energy, then we come up with a pinpoint that basic thermodynamic quantities free energy, enthalpy and entropy does not necessarily give an exact explanation for the molecular driving forces of solvation. Actually, if the compensating term dominates, looking at the basic quantities can be even misleading. At that point, going beyond the basic thermodynamic quantities by splitting up enthalpy and entropy into its solute-solvent and solvent-solvent contributions is required. So in chapter 3 we have characterized the relevance of these either basic or statistically derived

thermodynamic quantities to the internal mechanisms with atomic scale simulations of these kind of low molecular systems. Researches done on this kind of model systems can be used to gain insight into the thermodynamics of similar processes. Performing the simulations at an atomistic scale can provide an insight into molecular scale behaviors which cannot be easily observed by means of conventional experimental studies.

In chapter 4, we go further in detailed descriptions of thermodynamics within the binary solvent systems mentioned above and try to obtain the solvent reorganization contribution to the free energy terms from pure solvent data using equations of state. In principle, solvation occurs when an additive molecule fits into a proper cavity in the solvent. The availability of the proper cavity is determined by both the solute and the solvent characteristics. Yet, there is no exact theory that relates the bulk properties of solvent to the numerical thermodynamic solvation contributions of solute-solvent and solvent-solvent. We proposed that in the cases where the cavity formation occurs without a bias of any other interactions, these contributions should have been possible to derive from the volume fluctuations within the solvent matrix. Since in our case these fluctuations are directly related to creation and annihilation of the free volumes, approaches that relates pure solvent properties to thermodynamic quantity of solvent reorganization work quite well. However, the correlations we use are only applicable when there is weak solute-solvent interaction not biasing the additive insertion probability. The applicability of the approaches and methods we used were discussed later on in detail by Peter et.al. [1] They have given the cases in which the solvation is just a matter of creation of a proper-sized free volume enabling to obtain reorganization contributions from pure solvent data, and the deviations in the correlations affecting the

formulations. By that means, in similar cases to ours it is possible to evaluate reorganization terms and then relate these solute-solvent interaction terms via comparison of easily available experimental data on the bulk properties of solvents such as isothermal compressibility and isobaric expansion coefficient.

The improvement of the theories corresponding to observables enables us to assess the quality of the force fields. Improvement in the force fields, which includes the set of determining parameters in computational methods, affects the accuracy of simulations directing us to better outcomes. The computational results can be used both as complementary tools for the information obtained by chemical experiments and even more in some cases where experimental methods are insufficient or unfeasible they can predict hitherto unobserved chemical phenomena. To be able to gain accurate outcomes from the computational methods, the parameters imbedded in the force fields should be consistent with the real life properties of the system of under study. This is why, in chapter 4, we discuss the "back-of-the-envelope" methods to obtain or check the interaction contributions from the bulk properties.

After the low molecular weight liquids we would like to perform a similar study on polymers to gain more insight on permeation mechanisms. However, the latter type of systems evolve more slowly in a computer simulation time which disables us from using the same methodologies applied to liquid systems. Therefore, we first need to come up with an optimized method to overcome the sampling problems in polymer systems. In chapter 3 and 4, we have discussed how to obtain basic thermodynamic quantities and what kind of information we gain from those in low molecular weight systems. Since, free energy is a key concept in modeling solubilities of additives and we would like to

compute this term also for high molecular weight systems. For this case polymers are of interest as a solvent matrix, since they are made of long chains with many repeating units. Wherever there are functional groups in the repeating units, polymers can also be considered as code in code solvents. When a solute is involved in a polymer matrix, the local interactions are the main driving forces for many processes within such systems. In many selective membrane or barrier materials understanding these forces extends the scopes for the design of new polymer permeation materials and for their applications. For instance the importance of the permeation through the barrier coatings on metal surfaces is crucial in many industrial purposes. In such coating polymer materials, the desired property would be that oxidizing agents like water and oxygen should not be dissolved and nor transported through the material. In all similar cases, the question especially for the synthetic chemists is that which interior functional groups within a polymer should be chosen to control the mechanism in a desired way. There is an experimental history of this question started in 50s that people started to observe permeation of polymers where they develop a new material and measure the permeation. From these kinds of observations there exist some empirical rules. However, the structure and property relations are not still well explained at an atomic scale perspective.

For low molecular weight liquids, for an atomic scale perspective we used readily available methods while explaining the local scale interactions via solubility of molecules. There we used Widom test particle insertion (TPI). Widom TPI method is one of the basic methods widely applied for the free energy calculations [2,3] With this method one can calculate the solubility by probing the cavities in which insertion of solute is possible with a probability determined by the local atomic scale interactions.

Even though with this method it is possible to sample the entire solvent matrix for the available free volumes and to come up with the locations where the solute prefers to be in, this method is only applicable for weakly interacting small gas molecules in liquid and amorphous polymers. For small gas molecules it is enough to probe a proper sized-cavity without any bias of specific interactions by means of volume fluctuations within liquid or amorphous polymer solvents. On the hand for bigger and very polar molecules sampling just through the natural volume fluctuations within the solvent will not be sufficient. When the free volume sizes are not comparable for the insertion of the solute and in cases where stronger specific interactions between solute and solvent occur, an advanced method is required. Therefore, we come up with a combinatory method named as "single step perturbation". Given the basic theory of the methodologies in chapter 2, in chapter 5 we will discuss the feasibility of the free energy calculations on a variety of systems by applying this combinatory method, which is the free energy perturbation (FEP) based on a soft-core reference state. In that chapter, we will discuss the feasibility of performing the single step perturbation based on a soft-core reference state by comparison with the fast-growth thermodynamic integration data. Single step perturbation method based on a reference state is a combinatory method of Widom test particle insertion and thermodynamic integration. According to the FEP method we introduce a reference state and perturb this reference particle to a real solute. The idea here is to embed a soft core cavity which is actually a soft Lennard Jones (LJ) potential particle, in a polymer matrix. This virtual particle can travel through the system pretty fast since it can cut through polymer chains. Although it is soft enough to penetrate through the chains like a ghost, the reference particle is not infinitely soft, it has some hardness. In figure 1.1, the ghost

like soft-core particle is depicted for a better visualization of the reference state. By this means, it is possible to create some space within the solvent matrix, so that you can insert any other particle inside this cavity. In other words one can perturb the system by replacing this soft core reference particle with a real solute particle which is harder.

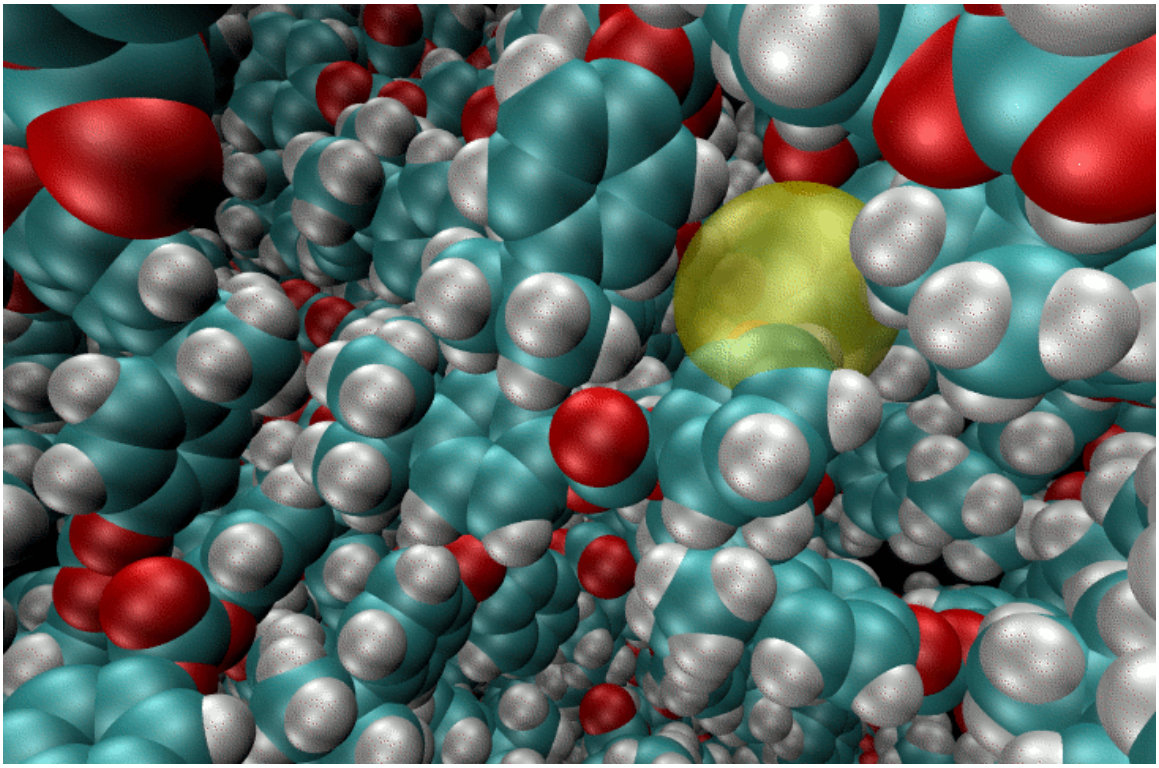

Figure 1.1: Snap-shot presenting a Soft-core Reference state (yellow transparent) in BPA_PC polymer matrix at 480 K used for the free energy calculation based on a combinatory method of Thermodynamic Integration (TI) and Free Energy Perturbation (FEP).

This method is used recently in free energy estimations for drug solubility in pharmaceutical industry [4] and to understand binding mechanisms of proteins to certain

structures such as RNAs in biochemistry where the accuracy is discussed. [5] Computational benefits to obtain converged free energy values, and choice of introducing a middle reference step in the thermodynamic cycle of solvation are explained systematically in chapter 5. This is accomplished by studying the method for the solvation process initially on a simple polymer melt of octadecane, and then on an artificially created viscous octadecane matrix close to its glass transition temperature (Tg) and thirdly on a real polymer matrix of Bisphenol-A-Polycarbonate (BPA-PC).

We close up with an application study on transport of additives in polymer systems again by molecular dynamic simulation means. There we introduce the convergence problems that one needs to overcome for meaningful dynamics in complex polymer systems. After discussing the solubility in the thesis we would like to focus on the other component of penetration through polymeric materials, which is the diffusion of additives. Molecular simulation using realistic models is not only a powerful tool for the elucidation of microscopic structure of polymers but also for the subsequent estimation of macroscopic physical properties. Interest on the diffusivity of polymers by computational means is the basic issue related to transport of additives. The studies on transport of additives within the solvents are not older than 10 years starting at the early 90s with the studies mainly on gas diffusion. [6,7] Currently, diffusion in complex polymeric microstructures (used in e.g. in polymer electrolyte fuel cells) is of interest. Transport of molecules through the polymeric materials that are especially used in membrane applications is a hot topic for researchers performing molecular dynamic simulations. [8,9] We have investigated a similar system of an ionomer, which is sulphonated polyethylene (SPE) swollen by water including sodium ions. Molecular interactions in

between hydrophilic and hydrophobic parts of the polymer matrix and ionic interactions play an important role in this kind of systems. How these interactions affect the structure and thermodynamics of these mixtures, is a central question. We will emphasize in chapter 6 how the simulation details have an impact on the convergence properties of a real polymer system via comparison with the diffusivity properties of water through an ionomer system. The important factors affecting the structural and dynamic equilibrium of the system considering the important constraint of finite time scales available to molecular dynamic simulations will be given. Throughout these studies after reaching an equilibration we have observed a microphase separation of the material. Accuracy of the transport behavior of water through the microphase separated channels will be discussed by comparison with the experimental data.

Molecular transport permeation, sorption and diffusion through membranes are still ongoing important properties studied also by experimental means, such as radiotracer experiments [10, 11] Design of new materials with similar properties is exciting for experimental chemists, for example in our institute recently poly(vinylphosphonic acid) is synthesized by free radical polymerization, where high-resolution NMR spectroscopy techniques are required to gain microstructure information [12] In this thesis we demonstrate that MD simulations of polymer models can reproduce both qualitatively and quantitatively important experimental results from related membrane processes. These models are therefore suited in principle to obtain a better insight in the atomistic dynamics. In addition, the knowledge about the underlying diffusion mechanism could be improved. In particular, molecular dynamics (MD) can simulate the time dependent behavior of molecular systems and provide the structure, dynamics and thermodynamics

of molecules in solution or polymeric systems. It is demonstrated that computer simulation has enough to offer to make it a useful tool when studying or designing new polymers. In the ionomer part we will also make use of a few quantum mechanical calculations to parameterize some of the non-bonded interaction parameters in the force fields. The sensitivity of the transport coefficients to the atomistic models (force fields) is another issue discussed here.

Finally, in chapter 7 we will give a general outlook depending on the studies we have performed. This part will include the summary of conclusions which will bring about beneficial knowledge on atomistic simulation of permeation process in both simple systems and in polymers. This will be achieved by systematic studies done in this thesis.

CHAPTER 2

Methods

2.1. Introduction

Looking at the modern molecular modeling methods today we see that roots of the developments in the methods lie at 50s. These methods, started with the investigations on an interior structure of atom and with the improvements both in processors and also in computational approaches today polymers containing thousands of atoms can be simulated. Many properties of materials are measurable with experimental methods such as X-Ray, NMR etc. However, besides the analytical knowledge, a systematic thought is required. For this reason, analogies of molecular systems are developed and studied by means of computational chemistry. By computational methods predictions of physical states and many related properties are available.

In general, the computational methods can be grouped into two main classes; quantum chemistry and statistical mechanics methods. Ab initio quantum mechanical (QM) method is the most detailed class including even the internal electronic properties in an atom. By means of QM, structural information can be acquired like molecular geometry, relative stabilities, vibrational spectra, dipole moments, reactivity, and atomic charges. In contrast to the vast of knowledge gained, this class of basic QM methods is applicable only to systems of a few numbers of atoms because of computational

expenses. For systems consisting of many atoms classical statistical mechanics methods of either Monte Carlo (MC) or molecular dynamics (MD) simulations are carried out. The latter methods are introduced to gain insight into properties and processes at the molecular scale. There exist also advanced multi-scale methodologies which combine quantum chemistry and dynamics with some approximation techniques permitting high level calculations with low cost on big systems like polymeric materials, proteins, etc.[13,14] Yet, in this thesis we will stay at the level of molecular dynamics simulations with atomistic details.

When starting any molecular modeling study, configurations of molecules with reasonable and reliable starting geometry are introduced in a simulation box. Configurations of atoms can be obtained from several sources; either from experimental sources such as X-ray methods where the X-rays are scattered by the electron cloud around an atom or from computational means like quantum optimizations. By quantum mechanical means, knowledge of the most stable conformation is gained from the global energy minimum structure. After having a reasonable starting configuration file representative of the system in a simulation box containing the x, y, z coordinates of the atoms or molecules, to perform the computer simulations another complementary input file including the parameters for structural information of each atom or particle type is required for simulations. Parameters so called force fields are constructed to describe bonded/nonbonded atomic interactions. In principle, QM can be employed to determine the interactions in small model species. In our case we have obtained parameters from both initially studied empirical force fields or in a few cases also by the help of QM calculations.

To start a simulation, according to the technique or optimization method to be applied a run-file should be fed stating the theory, approximations and variables. Variables are used in the MD for setting the simulation conditions like temperature and pressure as in the case of an experiment. Finally, in the dynamic simulations the atomic coordinates are varied under the effect of internal or/and external forces during the simulation time. Then, these Cartesian coordinates, subsequently the structure, can be analyzed by means of statistical mechanics and thermodynamics tools and can be easily displayed by molecular graphics for visualization.

Both MD and MC simulations generate information at the microscopic level, including atom positions but MD gives velocities as well. For the analysis, the conversion of this microscopic information to macroscopic observables such as pressure, energy, heat capacities, etc., requires statistical mechanics. Statistical mechanics methods are used to calculate average properties and then provide the link between these quantities and the atomistic description on a microscopic level. By that means, thermodynamic and structural bulk properties are related to the distribution and motion of the atoms and molecules of an *N*-body system.

In this thesis we are interested in the atomic-scale description of thermodynamics and transport of additives in simple liquid cosolvent systems, simple polymers and a complex system of a polymer membrane material, which is an ionomer. In all cases, the degree of resolution is such that an atom is the smallest elementary entity. The computational chemistry method needed in such a description relies on concepts of classical and statistical mechanics. Complex integrals are used in statistical mechanics to

study processes at an all-atom scale in condensed phases. They are computed to define relations between the fundamental molecular interactions and experimental observables.

Accordingly, this chapter is outlined as follows: First, an introductory knowledge on three computation methods; Quantum Mechanics, Monte Carlo, and Molecular Dynamics is given. The next section is focused on theoretical basis of molecular dynamics in detail, since molecular dynamics simulations were used for all my computational studies. Starting with a definition of MD, in that section the functional forms of force fields and typical force field parameterizations are also addressed. Algorithms used for integrations of equation of motions and how to control the external parameters (like pressure and temperature) and some computational methods for accuracy and ease are given there. After these, various basic principles of free energy calculations, such as Widom Test particle insertion, Thermodynamics integration, Fast-Growth Thermodynamic integration, which I used all through my doctorate study to analyze solvation effects, and energetic contributions and to discuss the feasibility of a new combinatory free energy calculation method will be presented.

2.1.1. Quantum Mechanical Methods

Quantum mechanical methods must be discussed, at least briefly, because they are very valuable additional tools in computational chemistry. In principle, by quantum mechanical means, knowledge of the most stable conformation is gained from the global energy minimum structure. Besides the geometry optimizations QM can also be used to gain complementary data for MD simulations. In MD, properties like molecular geometry and relative conformational energies can be calculated with high accuracy for a broad

variety of structures by a well-parameterized general force-field. However, if the force field parameters for a certain structure are not available in such cases quantum chemical methods can be used to obtain the parameters required for MD. From quantum means we got some assistance at some points of our force field parameterization for a set of our dynamic simulations in our last study on ionomer systems in chapter 6. We used quantum methods to obtain some of the force field parameters for the structural information of the functional sulphonate group, which is connected to a polyethylene backbone in the ionomer system. The dihedral potentials of the sulphonate group obtained by quantum means are used for the dihedral constant parameterization in the force field of dynamic studies. In addition, the results obtained from quantum calculations are considered together with comparison to the charge distributions in similar polymer structures for initial setting of the charge parameters.

In our case to obtain the dihedral constant we scan the relative potential energies through different conformations by shifting the dihedral angle, and then fitting the corresponding potential energies to the ones obtained by single step MD for that configuration of atoms. By the term single step MD it is meant that only the initial energy minimization step is performed as in the quantum case. We performed QM calculations at Moller Pleset Perturbation level with 6-31G* basis set. I will give a brief explanation of this method by introducing the basic information on QM as in the following paragraphs. Calculations of transition states or reaction paths as well as the determination of geometries influenced by polarization or irregular electron distribution in a molecule are the fields of quantum mechanical calculations. Their disadvantages relative to other methods are the computational costs and the limitation to rather small molecules. This is

why, the use of quantum mechanical methods are generally reserved for the treatment of special problems, such as in our case mentioned above. The objective in this section is to discuss the quantum mechanical methods very simply from a theoretical perspective and also to explain some practical hints for the application of semiempirical or ab initio programs. For more theoretical knowledge, the reader may refer to many books or reviews on this subject to gain more insight into the theoretical aspects of these methods [15-19]

In QM, microscopic systems are described by wave functions that completely characterize all physical properties of the system and there are quantum mechanical operators corresponding to each physical observable that, when applied to the wave function, allow one to predict the probability of finding the system to exhibit a particular value or range of values for that observable. There are several methods to obtain these values among those, for molecules Hartree-Fock (HF) is the central method for all ab initio quantum chemistry methods, which is an approximate method for the determination of the ground-state wavefunction and ground-state energy of a quantum many-body system in computational physics and chemistry. Solution of the equations yields the Hartree-Fock wavefunction and energy of the system, which are approximations of the exact ones. The Hartree-Fock method finds its typical application in the solution of the electronic Schrödinger equation of atoms, molecules and solids. The solutions to the resulting non-linear equations behave as if each particle is subjected to the mean field created by all other. The equations are almost universally solved by means of an iterative type algorithm.

What we used in our calculations on the sulphonate functional group was the second order Møller-Plesset perturbation theory (MP). MP theory is one of several quantum chemistry post-Hartree-Fock ab initio methods in the field of computational chemistry. It improves on the Hartree-Fock method by adding electron correlation effects by means of Rayleigh-Schrödinger perturbation theory (RS-PT). [20] The MP-theory is a special application of RS-PT. In RS-PT one considers an unperturbed Hamiltonian operator $\hat{H}_0$ to which a small perturbation $\hat{V}$ is added:

$$\hat{H} = \hat{H}_0 + \lambda\hat{V}\,, \tag{2.1}$$

where λ is a small parameter. In MP-theory the perturbation is the correlation potential. Second (MP2), third (MP3), and fourth (MP4) order Møller-Plesset calculations are standard levels used in calculating small systems and are implemented in many computational chemistry codes. Higher level MP calculations are generally not prefered because of their costs and in many cases increasing the level of pertubation does not improve the results much.[21,22]

Besides the approach employed, the quality of an ab initio calculation also depends on the basis set used for the calculation. [23,24] The decision which basis set should be used is related to the objective of the calculation and the molecules to be studied. It should be kept in mind that even a large basis set is not always a guarantee for agreement with experimental data.[25]

In recent ab initio calculations split-valence basis sets have become quite popular. In these the valence orbital shells are represented by an inner and outer basis function. In this way more flexibility in describing the residence of the electrons has been attained [26]. The split-valence basis sets represent a progress over the STO-3G basis set, and the

3-21G, 4-31G, and 6-31G basis sets are widely used in ab initio calculations. They differ only in the number of Gaussians used in expanding the inner shell and the first contracted valence function [25]. The next level of improvement is the introduction of polarization basis sets. To all non-hydrogen atoms d orbitals are added to allow p orbitals to shift away from the position of the nucleus leading to a deformation (polarization) of the resulting orbitals. This adjustment is particularly important for compounds containing small rings [26]. The polarization basis sets are indicated by a star, e.g. 6-31G*. This basis set uses six Gaussians for the core orbitals, a three/one split for the s and p valence orbitals, and a single set of d functions (indicated by the asterisk or (d)). 6-31G* or 6-31G(d) basis set was also the one used for our quantum calculations for the sulphonate functional group connected to the polyethylene polymer backbone in the ionomer study which we present in chapter 6. A more detailed description of the basis sets is given in books and reviews on this subject [19,25].

Unfortunately there is no rule for choosing an adequate basis set. The level of calculation depends on the desired accuracy and the molecular properties of interest. Actually, usually a geometry optimization of a simple molecule with moderate size can reasonably be performed using a 3-21G basis set. For other problems, however, this degree of sophistication may not be sufficient. If the geometry of the molecule is influenced by polarization effects, electron delocalization or hyperconjugative effects a 6-31G* or higher basis set is necessary to include the d orbitals as already mentioned.

In order to find a suitable level of calculation it is necessary to calibrate the method against experiment or testing the basis sets empirically to yield acceptable results. In our case in chapter 6, we derived dihedral parameter by fitting the potentials obtained

by quantum means to the ones computed by force-field parameters involved in MD. Then, at the end compare the results of the molecular dynamics simulations obtained by the defined force-field parameters with the experimental data.

2.1.2 Monte Carlo

Even though I did not make use of any Monte Carlo (MC) methods for any of the computational study presented in this thesis, they are commonly used in statistical mechanics. To show that integration methods other than MD are also available I will give a brief description of MC methods. For example, MC calculations employ non- dynamic stochastic steps that are based on random movements of the system. This can create more efficient sampling for certain systems. Especially, the Metropolis Monte Carlo technique has been used extensively in liquid simulations. [27,28] In MC, an arbitrary configuration is chosen at the start, and then it is changed at each step with probability exp ($-\Delta U/k_BT$) defined in Boltzmann distribution. This method based on the detailed balance condition in the equilibrium state such as,

$$P_{1\rightarrow 2} \exp(-U_1/k_BT) = P_{2\rightarrow 1} \exp(-U_2/k_BT) \qquad (2.2)$$

where $P_{1\rightarrow 2}$ is a probability to move from a state 1 to the another state 2. The state 1 and 2 differ by the coordinate of one particle, which is taken at a MC step. The probability to accept the move from state 1 to state 2 is $\min(1,\exp(-(U_2- U_1)/k_BT))$ by the Metropolis criteria. In a similar way, the reverse process probability $P_{2\rightarrow 1}$ equals to the $\min(1,\exp(-(U_1- U_2)/k_BT))$. Thus the contributions are the same in both direct and reverse probabilities. With respect to the balance condition, the average number of moves from

state 1 to 2 is the same as the average number of inverse moves from state 2 to 1. When the steps that obey the detailed balance condition are taken in a system of equilibrium, there will be no change in the probability of any conformation and the system will stay in equilibrium.

Among the trial process of several million steps, configurations of the system explored are only the ones that are energetically accessible. Thus, in MC the microscopic states are generated by random steps. The step size is usually tuned so that nearly half of the trial steps are accepted. For instance, for very large steps, the change in energy is also correspondingly too large, thus this attempt will not be accepted. However, for too small steps, the step size will limit the sampling of configuration space. This will lead to slow convergence of computed properties. In addition, since there is no inherent time scale in MC, it is does not acquire suitable information for dynamic properties.

2.1.3 Molecular Dynamics

Molecular dynamics (MD) is a form of computer simulation method, where atoms and molecules move according to the basic laws of classical physics for a period of time under internal and external interactions. Even for molecular systems consist of a vast number of particles it is possible to find the resultant positions and velocities under these physical effects by applying numerical methods. By employing various algorithms, it is possible to investigate the relationship between molecular structure, movement and function. Therefore, MD represents an interface between laboratory experiments and theory, and can be identified as in-silico experiment. In MD, based on statistical mechanics, statistical ensemble averages are equal to time averages of the system. This is

known as the ergodic hypothesis. MD has also been defined as imitating the behavior of particles allowing insight into molecular motion on an atomic scale by numerical solution of statistical mechanics and Newtonian mechanics. [29] Computationally more efficient MD simulations can be obtained with proper selection of algorithms and parameters with improved numerical integration methods available. In the following subsection we will give the basic theory of MD beginning with a classical definition in which we explain how MD is related to Newtonian law of motion. Then we will introduce the parameterization occurring in force fields that describes the potentials. Following that, algorithms for MD to compute the variations of spatial coordinates and velocities by time are given. After then, various computational ways of pressure and temperature coupling methods are explained. At the end tricks to overcome size effects and computational cost of electrostatic interaction calculations are discussed under the subtitles periodic boundary conditions and electrostatic interactions. Reaction field, Ewald summation and particle mesh Ewald are the methods applied for the latter.

2.2. Theory of Molecular Dynamics

2.2.1 Classical Definition

In a classical system of N point particles with masses m_i , the Hamiltonian H depends on the positions set of N Cartesian coordinates $\{\mathbf{r}_i\}$ and their momenta $\{\mathbf{p}_i\}$, of all point masses $i=1,2,...,N$, which results in a phase space with dimension 6N. The classical Hamiltonian H is defined as the sum of the kinetic energy K and potential energy U.

$$\mathrm{H}(\{\mathbf{p}_i,\mathbf{r}_i\}) = K(\mathbf{p}_i) + \mathrm{U}(\mathbf{r}_i) = \sum_{i=1}^{N} \frac{\mathbf{p}_i^2}{2m_i} + U(\{\mathbf{r}_i\}) \tag{2.3}$$

The initial term on the right hand side of eq. 2.3, the kinetic energy contribution to the Hamiltonian relies on momenta $\{\mathbf{p}_i\}$ including particle masses, m_i and velocities, while the potential energy part depends on the coordinates $\{\mathbf{r}_i\}$. This separation in the Hamiltonian that defines kinetic energy as exclusively dependent on the momenta, and potential energy on the coordinates, enables the use of a simple set of equations of motion:

$$\dot{\mathbf{r}}_i = \frac{\partial H}{\partial \mathbf{p}_i} = \frac{\partial K(\{\mathbf{p}_i\})}{\partial \mathbf{p}_i} = \frac{\mathbf{p}_i}{m_i} \quad \text{and} \quad \dot{\mathbf{p}}_i = -\frac{\partial H}{\partial \mathbf{r}_i} = -\frac{\partial U(\{\mathbf{r}_i\})}{\partial \mathbf{r}_i} = \mathbf{f}_i \tag{2.4}$$

where the negative gradient of the potential energy function $U(\{\mathbf{r}_i\})$ with respect to particle coordinate $\mathbf{r}_i$ equals the $\mathbf{f}_i$ is the force acting on particle i. Since molecular dynamics is the time dependent simulation of molecules described by Newton's equation of motion ($\mathbf{f}_i=m_i\mathbf{a}_i$), with a set of initial conditions, these equations can be numerically integrated in discrete time steps in the molecular dynamics simulation using so-called integrators to generate a dynamical trajectory of a system of interacting particles. Numerical integration methods of Newton's equation of motion on a computer to yield particle velocities and positions as a function of time will be discussed in section 2.2.3. The method MD is deterministic in the sense that once the positions and velocities of each atom are known at time t=0, the state of the system can be predicted at any coming time step, but it is not exact. As kinetic energy is just the sum of kinetic energies for all particles, it is the most trivial part of the Hamiltonian. Potential energy is more

complicated constructed out of a combination of pairwise interactive terms, that are described in the molecular force field used, as described in the following section.

2.2.2 Force fields

The energy and geometry of a molecule is evaluated by equations associated with the potential energy part of the Hamiltonian including all interactions between atoms that are covalently bonded (i.e. bond stretching, angle bending, torsional strain) as well as non-bonded interactions between atoms and molecules in molecular systems. Electrons are not considered explicitly. According to the Born-Oppenheimer approximation of the Schrödinger equation, nuclei are much heavier and move much more slowly than electrons, which attain their optimum distribution fast enough to adjust to any movement of the nuclei. We make the approximation that atoms, molecules and their mutual interactions can be described by analytical potential energy functions and their corresponding parameters, called the force field, model the chemistry. The force field must provide a good description of the forces acting within and between the molecules while keeping the calculations within the limits of current computational resources. As discussed in the first subsection of this chapter some of the force field parameters can be obtained from quantum mechanical methods while others are often parameterized to reproduce solid or liquid state properties of the system.

The total potential, mimicked by force fields parametrizations, is composed of bonded ($U_{STRETCH}$, U_{BEND}, $U_{TORSION}$) and non-bonded terms (U_{VDW}, U_{ELEC}):

$$U_{TOTAL} = U_{STRETCH} + U_{BEND} + U_{TORSION} + U_{VDW} + U_{ELEC} \quad (2.5)$$

Bond potentials are described by the force field parameters and treated by simple harmonic potentials: The bond potential characterizes the stretching of covalent bonds between two adjacent atoms (j and k) and is usually described by a harmonic potential.

$$U_{\text{STRETCHING}} = \frac{1}{2} k_{bond} (r_{jk} - r_{jk}^{0})^2 \tag{2.6}$$

In addition, the bond angle vibration between a triplet of atoms (klm) is also given by a harmonic angle potential.

$$U_{\text{BENDING}} = \frac{1}{2} k_{angle} (\theta_{klm} - \theta_{klm}^{0})^2 \tag{2.7}$$

The cosine of the bond angle can also be used in a harmonic potential instead of the angle θ itself in some force field parameterizations as follows;

$$U_{\text{BENDING}}(\theta) = \frac{1}{2} k'_{angle} \left[\cos(\theta) - \cos(\theta_{opt})\right]^2 \tag{2.8}$$

where θ_{opt} is the optimal angle value and k_{angle} is the force constant.

The torsional dihedral potential exists between four atoms h, i, j, and k can alternatively be defined by two types; proper or improper dihedral potentials:

$$U_{\text{TORSION}} = U_{\substack{\text{proper} \\ \text{diheral}}} = k_{\phi} (1 + \cos(n\phi_{hijk} - \phi_{hijk}^{0})) \tag{2.9}$$

or

$$U_{\text{TORSION}} = U_{\substack{\text{improper} \\ \text{diheral}}} = k_{\psi} (\psi - \psi^{0})^2 \tag{2.10}$$

where the angle Φ is the angle between particle h and ijk plane, and ψ is the angle type in improper dihedral case which is the angle between an outer atom and a plane of other tree. In figure 2.1 all these three bonded interactions are depicted except the improper

type dihedral. Improper type is generally used for the cases where there is an aromatic ring in the structure which is easy to visualize.

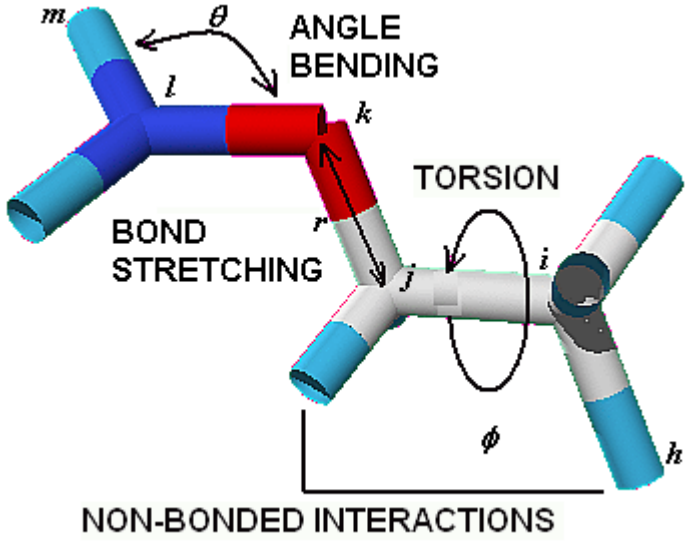

Figure 2.1: Schematic view of interactions involved in force-fields parameterization.

The nonbonded terms in the potential is comprised of electrostatic and dispersion interactions, which will be explained in the following sections.

2.2.2.1 Electrostatics

While regarding charged or polar molecules, electrostatics between a particle i and another one j is given by the electrostatic interaction energy between the two charges q_i and q_j, which is usually described by the Coulomb interaction:

$$U_{ELEC} = U_{Coulomb}(r_{ij}) = \frac{q_i q_j}{4\pi\varepsilon_0 r_{ij}} \qquad (2.11)$$

where ε_0 represents the dielectric permittivity of vacuum and r_{ij} is the distance between the two charged particles. Also, in uncharged molecules allocation of partial charges on atoms representing the dipole and higher order electric moments used to reproduce the electrostatic potential on the molecular surface.

Most of the CPU time is taken by the computation of the forces resulted from electrostatic interactions in MD simulations. Use of rapid but approximate methods reduces the computational expense in systems with a large number of atoms. Accuracy is sacrificed for speed by long-range interactions and electronic polarizability [30]. Electrostatic interactions are long-range forces and truncation, i.e. the use of cut-offs, affects results significantly. [31] Moreover, long MD simulations of proteins without electrostatic cut-offs yield trajectories that looks like known crystallographic structures other than similar simulations with cut-offs.

In MD studies, several approaches have been introduced for the simulation of charged systems to reduce the computational time. [32-35] In some of these, the force of each charge is separated into short- and long-range parts, and use particular methods to deal with the latter. Among them, the inclusion in the calculation of electrostatic forces of a reaction field (RF) term based on the Poison–Boltzman approach has been used in some study of polar and ionic systems by Tironi *et al.* [36]. These special methodologies such as a reaction field and an Ewald summation providing appropriate tricks to treat the electrostatics in simulations will be therefore discussed in more detail in section 2.2.7 where the computational algorithms are given.

2.2.2.2 Dispersion

Induced dipole interactions in a molecule are defined by the dispersion terms in a force field. They are characterized by Lennard-Jones potentials, together with repulsive interactions. A steep repulsion at short separations is caused by Pauli repulsion associated with the overlap of electron clouds belonging to non-bonded atoms or molecules. The Lennard-Jones interaction can either be expressed as a function of radius σ and interaction strength ε, or as Lennard-Jones (LJ) parameters $C^{(6)}$ and $C^{(12)}$.

$$U_{VDW} = U_{LJ}(r_{ij}) = 4\varepsilon\left[\left(\frac{\sigma}{r_{ij}}\right)^{12} - \left(\frac{\sigma}{r_{ij}}\right)^{6}\right] = \frac{C_{ij}^{(12)}}{r_{ij}^{12}} - \frac{C_{ij}^{(6)}}{r_{ij}^{6}} \tag{2.12}$$

It is also possible to modify this LJ potential to obtain unrealistic but useful particle interactions as in the case of the study in chapter 5. There we used modified potentials to create a reference state for a combinatory free energy calculation method, explained extensively in that chapter. Furthermore, when calculating the interaction between different particle types, the interaction potential for this set of particles is needed. In most force fields, this interaction potential is determined by applying a mixing rule on the interaction parameters (interaction strength and optimal distance) of both particle types. The choice of the mixing rule depends on the force field used. For instance, we applied geometric average method for the octadecane made up of simple aliphatic carbons and Lorentz-Bertelot combination rules for the polycarbonate BPA-PC studies to be consistent with the force field. The formulas how to apply these mixing rules are given in the simulation details in chapter 5.

2.2.3 Molecular Dynamics Algorithms

In any computational means of an MD, an algorithm to integrate Newton's equations of motion is the main point. An optimized algorithm means less time expense. Given a set of initial coordinates and (optionally) initial velocities of all particles involved, the interactions, forces, velocities, and updated coordinates in a system are computed from the interaction potentials by means of different integration schemes. In the following figure 2.2, a global flow scheme for MD is given, which is also employed in our simulations. The Gromacs software package used in this thesis [37-39] applies a variation of the Verlet algorithm, and the improved version of it i.e. leap frog algorithm. Forces are calculated from the functions describing the distance-derivative of the interaction potentials (designated as $-\partial V/\partial \mathbf{r}$ **or** $-\partial U/\partial \mathbf{r}$) and time step integration methods applied as explained in the following section.

Furthermore, the simplest form of molecular dynamics describes a system with a constant number of particles, volume and energy (NVE or microcanonical ensemble). However, this ensemble does not resemble standard experimental conditions, therefore alternative algorithms have to be used to sample in different ensembles. For molecular dynamics several methods are available to control temperature and pressure, as will be shown in the following sections.

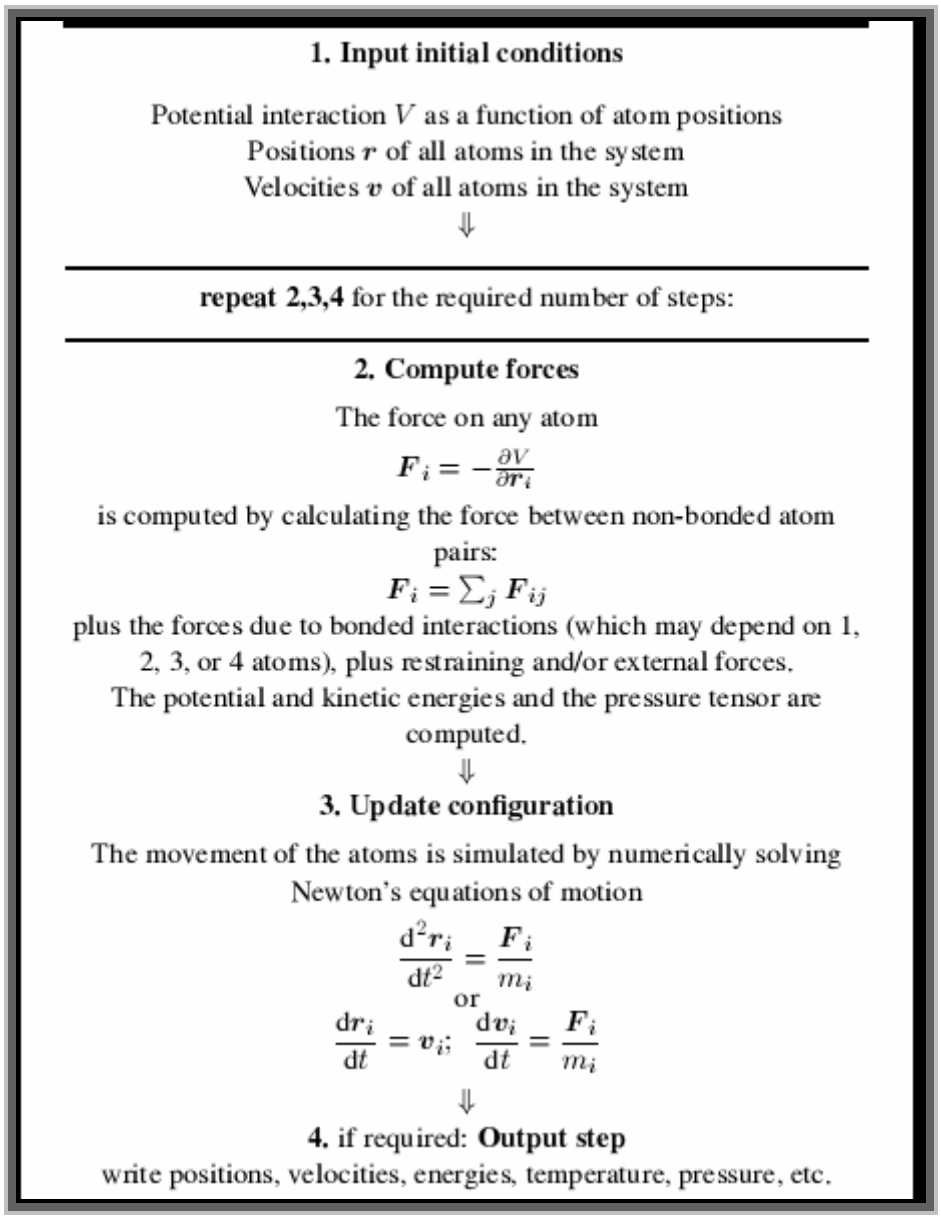

Figure 2.2: The global MD algorithm

2.2.3.1 Equation of Motion Integrations

The fundamental idea behind time step integration is to perform the dynamics incrementally making use of constant time-steps Δt. Continuity and energy-conservation in a simulation can be preserved by infinitely small values of Δt. On the other hand, for

computational efficiency a time step should be chosen as big as possible that can still retain energy-conservation with acceptable accuracy. Initially, the total force on each particle is derived from the interaction potentials with other particles at a certain configuration at time t as a vector sum. Then, the accelerations of the particles are extracted and later on combined with the positions and velocities at time *t* to compute the incoming positions and velocities at a next time step, $t+\Delta t$. To do that we used leap-frog algorithm [40] in our all MD simulations, which has been developed as an improvement to the simple Verlet algorithm [41]. The leap-frog algorithm is simply:

$$v(t+\frac{1}{2}\Delta t) = v(t-\frac{1}{2}\Delta t) + \Delta t a(t) \tag{2.13}$$

$$r(t+\Delta t) = r(t) + \Delta t v(t+\frac{1}{2}\Delta t) \tag{2.14}$$

The velocity at time (t+Δt/2) is obtained from the previous velocity listed at time (t-Δt/2) and the accelerations at time *t*. The positions at time (t+Δt) are then deduced from that obtained velocity knowing the position at time t. As it explicitly includes the velocity, the leap-frog is advantageous over the Verlet algorithm. Yet, it has still the defect that the positions and velocities are not written simultaneously, meaning that it is not possible to compute the kinetic energy contribution to the total energy for the same time step at the positions are known.

The velocity Verlet method [42] has been developed as such;

$$r(t+\Delta t) = r(t) + \Delta t v(t) + \frac{1}{2}\Delta t^2 a(t) \tag{2.15}$$

$$v(t+\Delta t) = v(t) + \frac{1}{2}\Delta t\left[a(t) + a(t+\Delta t)\right] \tag{2.16}$$

giving positions, velocities and accelerations at the same time, and consequently resolving the memory problems in both previous algorithms.

2.2.3.2 Bond and Angle Constraints

At the atomistic level the exact quantum computation of the bond lengths throughout a simulation is not necessary. The SHAKE [43] and the LINCS [44] algorithms in Gromacs software are used to keep the bonds fixed. According to these algorithms all atoms are initially moved in an unconstrained way through the time step integration. Without constraints most bonds will be deviated from their ideal bond lengths. Afterwards, reintroducing the constraints in an iterative way by means of bond potentials, convergence to next coming atomic coordinates is achieved. While using united atom (generally in which hydrogen bonds are omitted) and rigid water models, to increase the computational speed vibrational constraints are avoided.

2.2.4 Thermal Coupling

Molecular dynamic studies are done based on statistical thermodynamics rules, therefore while trying to imitate the dynamics similar to a real world under certain conditions one should obtain the correct corresponding ensemble for the property of interest. In most cases, temperature is a crucial conditional property, which one would like to control, in an experiment and in the same sense in a computational study. Where generation of canonical (NVT) or isotherm-isobar (NPT) ensembles are of interest in the computational case, addition of new degrees of freedom is required to regulate

temperature. However, this should be done without bringing about any results totally unrelated with the property sought. Normally, Berendsen [45] or Nosé Hoover [46,47] thermostats are used to fix the temperature to a certain value through the MD simulations. For the studies discussed in chapter 3, 4 and 6, we also used those according to the feasibility of performance of the chosen method for the property of our interest.

2.2.4.1 Stochastic Langevin Thermostat

Stochastic or velocity Langevin dynamics adds a friction and a noise term to Newton's equations of motion.

$$m_i \frac{d^2 r_i}{dt^2} = -m_i \xi_i \frac{dr_i}{dt} + f_i(r_i) + \overset{o}{r}_i \qquad (2.17)$$

where, ξ_i is a friction term with unit ps^{-1}, and $\overset{\circ}{r}_i(t)$ is a noise process which depends on the absolute temperature and the friction constant. When $1/\xi_i$ is large compared to the time scales present in the system, one could see stochastic dynamics as molecular dynamics with stochastic temperature-coupling. The advantage compared to MD with Berendsen temperature-coupling is that in case of stochastic dynamics (SD) the generated ensemble is known. Therefore, we performed the simulations for the study in chapter 5 with this method, since the ensemble averages were important not the dynamics in that study. On the other hand, when $1/\xi_i$ is small compared to the time scales present in the system, the dynamics will be completely different from MD, but the sampling is still correct. The Langevin thermostat MD method generates an exactly defined canonical, NVT, ensemble, but the random noise does disturb the actual dynamics.

There is also a modified version of the SD thermostat which is the dissipative particle dynamics (DPD) thermostat. DPD is claimed to be applicable as a useful thermostat for both equilibrium and non-equilibrium molecular dynamics simulations particularly for fluids since it has the advantage that it preserves hydrodynamics as the dissipative and random forces are added in a pairwise fashion, which enables the conservation of momentum [48].

2.2.4.2 Berendsen Thermostat

The Berendsen coupling scheme proceeds toward the desired temperature T_0 by scaling the velocities for thermal drift at each step. It was introduced as an alternative to stochastic dynamics which fixes the coupling of temperature to an external heat-bath [45]. The Berendsen temperature coupling applies a variation as dT in temperature for each time step dt to reach the reference temperature T_0.

$$m_i \frac{d^2 r_i}{dt^2} = m_i \gamma \left[\frac{T_0}{T(t)} - 1 \right] \frac{dr_i}{dt} + f_i(r_i) \tag{2.18}$$

$$\left(\frac{\mathrm{dT(t)}}{\mathrm{dt}} \right)_{\mathrm{bath}} = \frac{T_0 - T}{\tau_T} = 2\gamma T_0 - T \tag{2.19}$$

where τ_T is the temperature coupling time constant and γ is a friction term with unit ps^{-1}. A velocity scaling from v to $¢v$ is used to adjust the temperature in the equations of motion. The scaling factor $¢$ is temperature dependent as below:

$$\phi = \left[1 + \frac{\Delta t}{\tau_T} \left(\frac{T_0}{T(t - \frac{1}{2}\Delta t)} - 1 \right) \right]^{1/2} \tag{2.20}$$

2.2.4.3 Nosé-Hoover thermostat

The Nosé-Hoover thermostat introduces an additional degree of freedom as the coupling parameter Q related to the fully dynamic heat bath parameter ξ as such:

$$\left(\frac{\mathrm{d}\xi}{\mathrm{dt}} \right) = \frac{T_0 - T}{Q} \tag{2.21}$$

where T_0 is the desired temperature and T is temperature of the system at time t. The parameter ξ is involved in equation of motion:

$$m_i \frac{d^2 r_i}{dt^2} = -m_i \xi \frac{dr_i}{dt} + f_i(r_i) \tag{2.22}$$

Q parameter is defined to determine the strength of coupling. By that means, kinetic energy oscillations are produced by Nosé-Hoover thermostat between the system and the reservoir. Because of this fluctuating behavior, it takes longer to relax with Nosé-Hoover thermostat than with Berendsen weak coupling. However, an exact constant temperature ensemble can be sustained by Nose Hoover temperature coupling as superior to Berendsen thermostat.

2.2.5 Pressure Coupling

To control the pressure in a MD simulation, the volume of the simulation box is considered as a dynamical variable. In the pressure coupling a “pressure bath” is used

instead of a "heat bath" in the temperature coupling. Either the particle coordinates or velocities set to be varying in the case of Berendsen and Parinello Rahman pressure coupling respectively. Like in the case of temperature coupling, with Berendsen pressure coupling one can reach an equilibration much quicker; however there is the problem that the ensemble generated is not trustable. On the other hand, Parrinello-Rahman introduces longer fluctuations in volume to compute thermodynamic properties, therefore creates a well-defined ensemble.

2.2.5.1 Berendsen

Berendsen pressure coupling rescales both coordinates of a particle **r** and box vectors **b** with a scaling matrix **μ**. [45] During pressure scaling box vectors are adjusted (**b**(t+Δt) = **μb**(t)) for the coming time step while coordinates are scaled by **r**(t+Δt) = **μ**×**r**(t+Δt) after the computation of coordinates. P_x

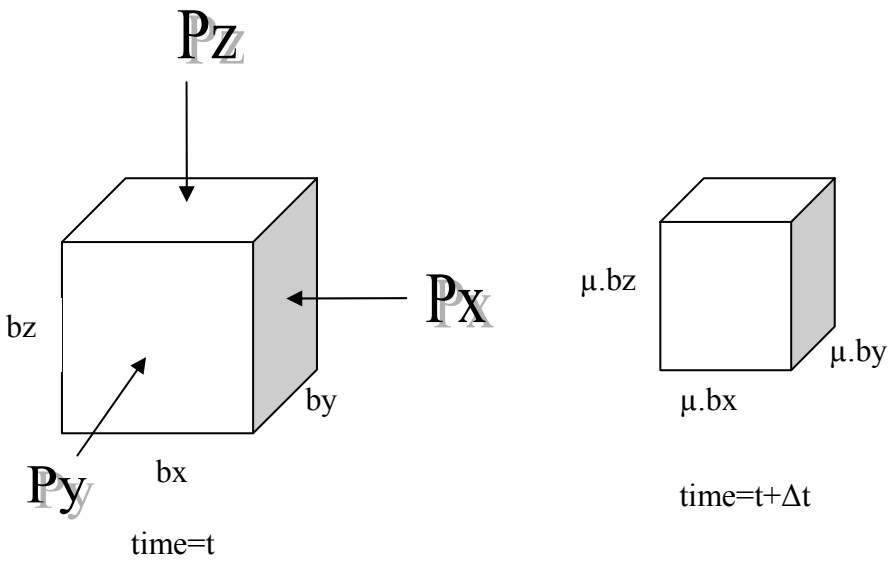

Generally, time dependent pressure has the first-order kinetic relaxation of the pressure towards a reference pressure where P_0 is the desired pressure and P is the instantaneous one at time t:

$$\left(\frac{\mathrm{dP(t)}}{\mathrm{dt}}\right)_{\mathrm{bath}} = \frac{P_0 - P}{\tau_P} \tag{2.23}$$

In the case of isotropic coupling, the scaling factor (μ) is used to perform the pressure coupling which can be described as follows:

$$\mu = \left\{1 - \frac{\kappa_{\mathrm{T}} \Delta t}{\tau_P}(P_0 - P)\right\}^{1/3} \tag{2.24}$$

where τ_P is a relaxation time, κ_T denotes the isothermal compressibility of the system, defined as:

$$\kappa_T = -\frac{1}{V}\left(\frac{dV}{dP}\right)_T \tag{2.25}$$

2.2.5.2 Parrinello-Rahman

Parrinello-Rahman pressure coupling has been developed similar to Nosé-Hoover temperature coupling in order to obtain a correct ensemble. [49,50] In this case, volume and shape of the simulation box responds with pressure tensor, introducing an additional degree of freedom to the equations of motion. This is achieved by introducing a mass

parameter W which is set as the total mass of the system in a simulation box. Mass parameter controls fluctuations on the sample to adjust the pressure to a desired value like a piston used in experiments. The inverse mass parameter matrix W^{-1} employed in Gromacs has the unit of inverse mass and is a function of isothermal compressibility κ_T and time constant τ_P. As it allows for anisotropic coupling it takes the form of a tensor and is defined as $(\mathbf{W}^{-1})_{ij} = (4\pi^2\kappa_{Tij})/(3\tau_P^2 L)$. L denotes the largest box matrix element. Parrinello-Rahman coupling relates the box matrix **b** to volume V, transposed box matrix b^T and $\mathbf{W^{-1}}$.

$$W\frac{db^2}{dt^2} = V\left(b^{-1}\right)^T (P - P_{ref}) \tag{2.26}$$

The scaling matrix **M** is dynamically involved in the equations of motion by the following relation;

$$\frac{d^2 r_i}{dt^2} = \frac{f_i}{m_i} - M\frac{dr_i}{dt} \tag{2.27}$$

as it is described by box matrix b as such:

$$M = b^{-1}\left[b\frac{db^T}{dt} + \frac{db}{dt}b^T\right](b^{-1})^T \tag{2.28}$$

It had been presented that for an efficient equilibration the frequencies of the molecular oscillators and the box volume should be similar so that a very quick energy transfer between them occurs. [51]

2.2.6 Periodic Boundary Conditions

To be able to perform a simulation, a finite number of particles are constructed into a single simulation box. However, a small simulation box will be affected by boundary conditions. In order to prevent that and for a better representation of a realistic system which involves infinitely large number of particles, periodic replicas of the original box are considered at each side surrounding the central one. Under these periodic boundary conditions for each atom in the central periodic box, interaction potentials are computed with the close neighbor atoms which can be either in the same box or in the periodic images of box. In some condensed phase simulations, the effects of periodicity on the forces on the atoms can be significant. Then the simulation box size plays an important role. This kind of size effect will be given in chapter 6.

To improve the computational efficiency, usually, the number of calculations that need to be performed is reduced by only considering interactions within a spherical cut-off radius instead of within the whole simulation box. The cut-off radius should be chosen that a particle in the primary box does not see its own image in surrounding box replicas. To decrease the computational costs atoms within this cut-off are kept in neighbor lists, which are named as Verlet list, and updated at certain time intervals. In addition, special tricks have to be applied to reduce the simulation expenses of long-range electrostatics as will be discussed in the coming sections.

2.2.7 Electrostatic Interactions

The pairwise long range interactions are the computationally most costly part of molecular simulations. The number of calculations for each atom scales with r^3 where r is the spherical cut-off radius. The cutoff radius should be smaller than half box length. To minimize computational expenses short-range cut-offs would be requested. On the other side, too short cut-off radii result in not only unrealistically too high of forces in the system but also spoil the conservation of energy in the system. To resolve the computational cost problem reaction-field electrostatics, summation methods Ewald and improved versions of these are applied.

2.2.7.1 Reaction-field

In the treatment of electrostatics with feasible tricks, the idea is to separate the calculations in short- and long-ranges so that beyond a cut-off radius the computing tricks introduced. By reaction-field method computation of Coulomb interactions can be modified for relatively homogeneous systems, by assuming a constant dielectric environment beyond a cut-off radius r_c.[52,53]

For charged cut off spheres this corresponds to neutralization with a homogeneous background charge. The interaction potential then becomes:

$$U_{ELEC} = U_{RF} = \frac{q_i q_j}{4\pi\varepsilon_0\varepsilon_r}\left[\frac{1}{r_{ij}} + C_1 r_{ij}^2 - C_2\right] \tag{2.29}$$

where ε_r is the relative permittivity with respect to vacuum which equals to unity in explicit solvent applications. In the above equation, the term C_1 is used to ensure the

force becomes zero at the cut-off radius for the energy conservation within the system while C_2 term is used to ensure that the potential of the system is zero at cutoff distance. Then the above equation becomes for a system of zero ionic strength:

$$U_{ELEC} = U_{RF} = \frac{q_i q_j}{4\pi\varepsilon_0}\left[\frac{1}{r_{ij}} + \frac{1}{r_c^3}\left(\frac{\varepsilon_{rf}-1}{(2\varepsilon_{rf}+1)}\right)r_{ij}^2 - \frac{1}{r_c}\frac{3\varepsilon_{rf}}{(2\varepsilon_{rf}+1)}\right] \tag{2.30}$$

where ε_{rf} is the dielectric constant of the medium beyond the cutoff distance. However, the reaction field method is suitable only for homogenous systems where the assumption of constant dielectric environment does not fail. In other cases, Ewald summation method may be an alternative for more accuracy.

2.2.7.2 Ewald summation

The total electrostatic energy in a system of N point charges can be given with the following relation when the system under investigation is periodic:

$$U_{ELEC} = \frac{1}{2}\sum_{|n|=0}\sum_{i,j=1}^{N}\frac{q_i q_j}{\left|r_{ij}+nL\right|} \tag{2.31}$$

However, because of the slow convergence of this electrostatic interaction summation, there are two main contributions in this calculation; an interaction potential within a certain cutoff r_c, that interaction converges to zero far from the cutoff distance, and a slowly varying function at all distances r. In Ewald summation, the idea is to convert one conditionally convergent sum into two absolutely convergent sums. This is achieved by surrounding each discrete charge with a Gaussian charge distribution of opposite sign and equal magnitude. In this way, the interactions are screened so that they are short-ranged

and then the sum of interactions is absolutely convergent. After that, a canceling charge distribution is added so that the overall potential is identical to the original one. Summation of this canceling distribution is performed in a reciprocal space so that it is absolutely convergent. This part is optimized to be represented by a Fourier transformation. Therefore, with the practical application of Fourier transform, the charge interactions can be treated by dividing the potential in three terms, a short range real space interaction $E^{(r)}$, a long range interaction that will be calculated in reciprocal space $E^{(k)}$, and a self interaction correction term $E^{(s)}$, which is constant.

$$U_{ELEC} = U^{(r)} + U^{(k)} + U^{(s)} \tag{2.32}$$

A sum over the set of k-vectors can be used to describe the interactions in reciprocal space which extends infinitely over all periodic images. The treatment of electrostatics with Ewald summation, [54-56] initially developed for the calculation of charges in periodic systems, especially for systems with high periodicity such as crystals [57,58] and nowadays it is widely applied to systems with periodic boundary conditions, however in some cases Particle Mesh Ewald summation methods can be more efficient as explained below.

2.2.7.3 Particle Mesh Ewald summation

In computer simulations, an alternative version of Ewald summation is proposed, Particle Mesh Ewald (PME) especially for large systems [57,59]. Here, the charge distribution of the particles in the system is discretized onto a grid, by that means the potential energy calculations separated into Ewald's direct sum and reciprocal sums. Fast Fourier methods

can be used to equate the potential for this reciprocal sums, after which the resulting potential and force is assigned to each particle by interpolating the potential and force on the surrounding grid points. Consequently, PME reduces the computational cost of Ewald summation with Fourier transform from N^2 orders to NlogN scale with Fast Fourier methods. Considering computational time expenses, PME is suggested to use for large systems, however for small systems Ewald avoiding the expenses in setting up grids and transforms is still better.

2.3. Free Energy in Statistical Mechanics

In the following three chapters we mainly focus on the solution thermodynamics of various additives in systems with different characteristics. During these studies we make use of free energy calculations of solvation and even the individual energetic and entropic contributions in this term to understand the interactions behind. The free energy of solvating a molecule in a liquid equals the reversible work associated with introducing the intermolecular interactions between the solute and the solvent. A negative free energy change indicates that the process proceeds spontaneously.

The process should not be necessarily a solvation, it could be any process, such as the binding of a ligand to a protein or a conformational transition in a molecule in solution. To calculate free energy changes there exist several methods. In this section we will explain three basic ones: the test particle insertion (TPI), thermodynamic integration (TI) and fast-growth TI methodologies. In order to do that, to achieve macroscopic properties we will start with the basic microstates as the beginning of statistical mechanics.

Quantum mechanically, a stationary system can be described by a set of eigenstates Ψ_i with energy E_i. Ψ_i and E_i are solutions of the Schrödinger equation;

$$H\,\Psi_i = E_i\,\Psi_i \tag{2.33}$$

where Hamiltonian H contains the kinetic and potential energy contributions of all particles in the system. At a constant temperature, the occurrence probability p_i to observe the system in microstate Ψ_i is given by the Boltzmann distribution:

$$p_i = \frac{\exp(-E_i / k_B T)}{\sum_i \exp(-E_i / k_B T)} \tag{2.34}$$

where the denominator is the normalization constant named as partition function (Z) equalizing the sum of all probabilities to one. In classical mechanics, the position and momentum variables of a particle can vary continuously, so the set of microstates is actually uncountable. Therefore in classical statistical mechanics, it is inconvenient to express the partition function as a sum of discrete terms, as we have done. The partition function then takes the form of a continuous integral. For instance, the partition function Q of *N* classical particles in a system at constant temperature and volume (so called classical canonical ensemble) is:

$$Q(T,V,N) = \frac{1}{N!h^{3N}} \int L \int dp^N dr^N \exp\left[-\beta H(p^N, r^N)\right] \tag{2.35}$$

where integration is performed over all particle momenta (p^N) and positions (r^N) and $H(p^N,r^N)$ is the *N*-particle Hamiltonian. The *h* is Planck's constant, the variable β equals to $(k_B T)^{-1}$, and the factor N! is used to account for the indistinguishability of the particles. The Hamiltonian can be described by summation of kinetic energy and potential energy terms:

$$H(\mathbf{p}^N, \mathbf{r}^N) = \sum_{i=1}^{N} (\mathbf{p}_i^2 / 2m_i) + U_N(\mathbf{r}^N) \tag{2.36}$$

where $\mathbf{p}_i$ is the momentum vector of the *i*th particle, m_i is the mass of each particle *i*. The $U_N(\mathbf{r}^N)$ is the total potential energy of the system at the specified configuration $\mathbf{r}^N$. Then, the integration over the momenta

$$h^{-3N}\int_{-\infty}^{\infty} dp^N \exp\left[-\beta\sum_{i=1}^{N}(p_i^2/2m)\right] = \left[h^{-1}\int_{-\infty}^{\infty} dp \exp(-\beta p^2/2m)\right]^{3N}$$
$$= \left[h^{-1}(2m/\beta)^{1/2}\int_{-\infty}^{\infty} \exp(-u)^2 du\right]^{3N} \quad (2.37)$$
$$= \left[h^{-1}(2\pi mkT)^{1/2}\right]^{3N} = \Lambda^{-3N}$$

gives Λ^{-3N} is the momentum partition function where Λ is de Broglie wavelength. Furthermore, when the configurational partition function, Z_N, is described as $Z_N = \int dr^N \exp(-\beta U_N(r^N))$, then the canonical partition function becomes:

$$Q(T,V,N) = Z_N/(N!\Lambda^{3N}) \quad (2.38)$$

The free energy F is given in terms of the partition function *Q* by

$$F = -k_B T \ln Q \quad (2.39)$$

2.3.1 Widom test particle insertion

In the test particle insertion (TPI) method, introduced by Widom, the free energy is computed by performing trial insertions in the fluid. The method is useful in case the solute test particle can be readily inserted in transient cavities in the fluid. [60,61] Straight forward application of the TPI method usually is useful only for calculating the

free energy of solvation of relatively small-sized molecules like noble gases or methane. Since it is difficult to observe volume fluctuations within the solvent that create a cavity of appropriate size, insufficient statistical sampling will give inaccurate results for larger solutes.

This method is derived as follows by simply defining the free energy change as the difference between initial state without solute and final state with an additional particle inserted into the N particle solvent system at constant, temperature and volume:

$$\mu = \left(\frac{\partial F}{\partial N}\right)_{V,T} = F(N+1,V,T) - F(N,V,T) \tag{2.40}$$

Obviously, this equation defines the chemical potential μ. For simplicity we shall assume that all N particles are the same, so we restrict our selves to deriving the chemical potential of a pure fluid. The generalization to mixtures is straight forward but will not be given here to keep the notation simple.

Then by insertion of the partition functions into the free energy terms given above, we obtain the free energy change with two contributions:

$$\begin{aligned}
\mu = \left(\frac{\partial F}{\partial N}\right)_{V,T} &= -k_B T \ln\left[\frac{Z_{N+1}}{(N+1)!\Lambda^{3(N+1)}}\right] + k_B T \ln\left[\frac{Z_N}{N!\Lambda^{3N}}\right] \\
&= -k_B T \ln\left[\frac{1}{(N+1)\Lambda^3}\frac{Z_{N+1}}{Z_N}\right] \\
&= k_B T \ln\left[\frac{(N+1)}{V}\Lambda^3\right] - k_B T \ln\left[\frac{1}{V}\frac{Z_{N+1}}{Z_N}\right] \\
&= k_B T \ln\left(\rho\Lambda^3\right) - k_B T \ln\left[\frac{1}{V}\frac{Z_{N+1}}{Z_N}\right]
\end{aligned} \tag{2.41}$$

Since the energy is always expressible as a sum of kinetic (p-dependent) and potential (r-dependent) contributions, the partition function also factorizes into a product of kinetic

(ideal gas) and potential (excess) parts. Thus, in the above equation the first term on the right side represents the ideal part, kinetic energy, of a particle while the second term indicates the excess part which is free energy induced by insertion of an additional particle. Furthermore, the potential energy of a system with *N+1* particles is described by the potential of the N-particle system together with the binding energy B_S of an added one, where B_S equals to the interaction energy of inserted particle (the solute) with all other molecules. Then energy induced by an additional particle insertion is described as $U_{N+1}=U_N+B_S$. Therefore;

$$\begin{aligned} -k_B T \ln\left(\frac{1}{V}\frac{Z_{N+1}}{Z_N}\right) &= -k_B T \ln\left(\frac{1}{V}\frac{\int dr^{N+1} e^{-\beta U_{N+1}(r^{N+1})}}{\int dr^{N} e^{-\beta U_N(r^N)}}\right) \\ &= -k_B T \ln\left(\frac{1}{V}\frac{\int dr^{N+1}\int dr^{N} e^{-\beta U_N(r^N)} e^{-\beta B_S}}{\int dr^{N} e^{-\beta U_N(r^N)}}\right) \\ &= -k_B T \ln\left(\frac{1}{V}\int dr^{N+1}\left\langle e^{-\beta B_S}\right\rangle_N\right) \\ &= -k_B T \ln\left\langle e^{-\beta B_S}\right\rangle_N \end{aligned} \tag{2.42}$$

As a result, the excess free energy change μ^{ex} by the insertion of an additional particle,

$$\mu^{ex} \equiv -k_B T \ln\left\langle e^{-\beta B_S}\right\rangle_{NVT} \tag{2.43}$$

in eq 2.43 $\langle\cdots\rangle_{NVT}$ denotes an N particle ensemble average obtained over pure solvent configurations at constant pressure *V* and temperature *T*. Later on in this thesis we shall

also use the notation ΔF (or at constant pressure, ΔG) for the same quantity. Since the method relies on the statistical accuracy of sampling of solvent configurations that permit the insertion of molecules with low values of the binding energy, B_S, application of TPI is more feasible for small-sized solutes. For larger sized solutes the thermodynamic integration (TI) method can be used to calculate free energy differences. TI is however a more computationally costly calculation methodology.

2.3.2 Thermodynamic integration

Another method for the calculation of free energy changes is thermodynamic integration (TI). In this method, a parameter λ (∈[0,1]) is used that couples the solute with the rest of the system. The free energy change, or coupling work, is obtained by integrating along λ. [62,63]

Suppose potential energy U(λ) so the corresponding free energy will also depend on λ, F(λ) and then;

$$\begin{aligned}\Delta F &= \int_0^1 \frac{\partial F(\lambda)}{\partial \lambda} d\lambda \\ &= -k_B T \int_0^1 \frac{\partial \ln Z(\lambda)}{\partial \lambda} d\lambda \\ &= -k_B T \int_0^1 \frac{1}{Z(\lambda)} \frac{\partial Z(\lambda)}{\partial \lambda} d\lambda\end{aligned} \tag{2.44}$$

substituting into the above equation

$$Z(\lambda) = \int d\mathbf{r}^N e^{-\beta U(\lambda)} \quad \Rightarrow \quad \frac{\partial Z}{\partial \lambda} = -\beta \int d\mathbf{r}^N \frac{\partial U(\lambda)}{\partial \lambda} e^{-\beta U(\lambda)} \tag{2.45}$$

then free energy change becomes

$$\Delta F = \int_0^1 d\lambda \left[\frac{1}{Z(\lambda)} \int d\mathbf{r}^N \frac{\partial U(\lambda)}{\partial \lambda} e^{-\beta U(\lambda)} \right] = \int_0^1 d\lambda \left\langle \frac{\partial U(\lambda)}{\partial \lambda} \right\rangle_\lambda \tag{2.46}$$

U(λ) is the total potential energy and the average is taken over a canonical ensemble with a coupled Hamiltonian H(λ).

For example, in a linear λ dependency scheme potential energy will be;

$$U(\lambda) = \lambda U_B + (1-\lambda) U_A$$
$$\frac{\partial U}{\partial \lambda} = U_B - U_A \tag{2.47}$$

where U scales with $1/r^{12}$ and $1/r^6$ for a hard core LJ particle resulting in singularities. Therefore, form of potential energy should be carefully chosen to avoid any singularity and for relatively smooth differential curves so that the integration is not affected. This is why we have used a soft-core potential function of GROMACS. [37-39] For higher accuracy, the number of λ steps or different initial starting points can be considered at strongly coupled systems. These issues are discussed more in details in chapter 5.

2.3.3. Fast-Growth TI

Fast-Growth TI is an approach based on the non-equilibrium work theorem introduced by Jarzynski. In chapter 5, we will discuss our results from single-step perturbation method by comparing with the data obtained by Jarzynski method in particular with the application to solvation free-energies of additives in polymeric systems. Jarzynski relates the work that is being performed on a system when going from state A to state B along a

coordinate λ with the free energy change, irrespective of the sampling.[64] He finds that the Boltzmann-averaged work of repeated sampling of the path from A to B is equal to the free energy difference between A and B

$$\Delta F_{AB} = -k_B T \ln\left\langle \exp^{-\beta W_{AB}} \right\rangle \tag{2.48}$$

when we consider a finite classical system in contact with a heat reservoir. A central concept in thermodynamics is that of the work performed on such a system, when some external parameters of the system area made to change with time. When the parameters are changed infinitely slowly along some path from an initial point A to a final point B in parameter space, then the total work W performed on the system is equal to the Helmholtz free energy difference ΔF between the initial and the final configurations. $W=\Delta F \equiv F^B - F^A$, where F^A (F^B) refers to the equilibrium free energy of the system, with the parameters held fixed at A (B). By contrast, when the parameters are switched along the same path at a finite rate, then average W will depend on the microscopic initial conditions of the system and reservoir, and will on average exceed ΔF:

$$\langle W \rangle \geq \Delta F. \tag{2.49}$$

The difference ⟨W⟩ - ΔF is just the dissipated work, associated with the increase of entropy during an irreversible process which is stated in the second law of thermodynamics.

Starting from the inequality given above, by contrast Jarzynski derived the equality

$$\left\langle \exp^{-\beta W_{AB}} \right\rangle = \exp^{-\beta \Delta F_{AB}} \tag{2.50}$$

by defining

$$W = \int_0^{t_S} dt \dot{\lambda} \frac{\partial H_\lambda}{\partial \lambda}(z(t)) \tag{2.51}$$

where z denote a point in the phase space of the system and $H_\lambda(z)$ denote the Hamiltonian for the system parameterized by the value of λ.

In the two limiting cases at which switching of the external parameters is infinitely slow ($t_s \to \infty$) and infinitely fast ($t_s \to 0$), the equations for work W takes the form of basic TI and single step perturbation respectively:

$$W = \Delta F = \int_0^1 d\lambda \left\langle \frac{\partial H_\lambda}{\partial \lambda} \right\rangle_\lambda \qquad \text{and} \qquad (2.52)$$

$$W = H_1 - H_0 \equiv \Delta H \Rightarrow \Delta F = -k_B T \ln \left\langle \exp^{-\beta \Delta H} \right\rangle_0$$

Through the applications of this method, polymer microstructure can be considered as a potential landscape as in the following scheme:

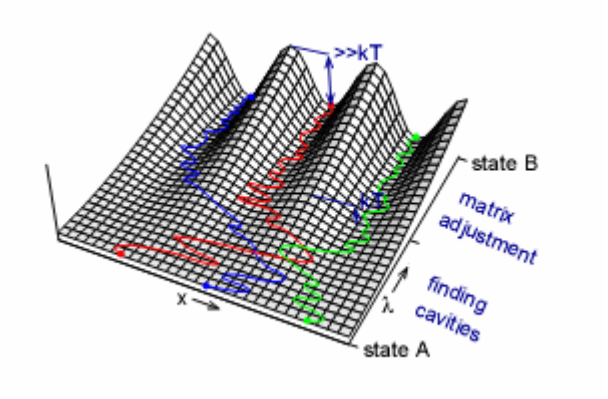

In this context, solvation free energy can be calculated in some cases by performing Fast growth TIs in order to calculate the work requirements to insert the solute in a solvent matrix from sampling the possible coordinates where interaction potentials determines the potential landscape. The application of all the given approaches, methods, and approximations require extensive analysis. In the following chapters we define our cases and discuss the methods that are applicable to these cases.

CHAPTER 3

Preferential solvation of a non-polar solute in DMSO/water mixtures: Energy-entropy compensation

3.1. Introduction

As we discussed in the previous chapter, there are various methodologies used for the free energy calculations based on the knowledge of statistical thermodynamics. It is important to investigate this quantity to understand the thermodynamics and interactions behind a process of interest. The free energy changes related with the addition of molecules in either liquid or polymer systems have great importance not only in chemistry but also in biology fields such as proteins.[65] Even though the free energy change being in most cases the desired quantity determining, *e.g.*, association constants, partition coefficients and solubility, its temperature derivatives (the entropy and heat capacity changes) hold valuable information as well. Yet the latter have received much less attention because they are considerably more expensive to evaluate computationally. Owing to increasing computer power and efficiency of simulation packages this limitation no longer exists. In many applications in the chemical fields, solvation

processes in binary solvents are of special interest. Solutes consisting of functionally different groups interact preferentially with one of the binary solvent components at different concentrations. Because of their selective properties, in some cases they are used as a media for the chemical reactions to control the reaction rates or to preserve stability. Despite their extensive application areas, the atomistic scale mechanisms and their relation with physicochemical properties of the solute and the solvent system are in many cases still incompletely understood.

The first computational study on hydration enthalpies and entropies of molecular solutes was repoted by Gallicchio *et al.*.[66] They applied a solvation shell approximation for the reorganization energy. In this approximation, (constant pressure) enthalpy and entropy changes are considered as local quantities [67] which may therefore be evaluated accounting for only the excess energy of a shell typically containing 20-30 water molecules. [66] They studied hydration enthalpies and entropies of a series of linear, branched and cyclic alkanes using the OPLS-AA force field with the TIP4P water model at 298 K. Paschek [68] studied the temperature dependence of hydration free energies of simple solutes (rare gas atoms, methane), and obtained from that the hydration enthalpies, entropies, and heat capacities. In particular, he reported the performance of various classical water models. Furthermore, for all investigated models and state points he calculated the excess chemical potential for nonpolar molecules (e.g. Xenon) employing the Widom particle insertion technique. In figure 3.1 below, the dynamical hydrogen bond fluctuation in the hydration shell is presented to give a figurative idea on what is happening around a non-polar spherical particle in pure water. This example of

hydrophobic hydration illustrates the merits of splitting up the solvation thermodynamics in solute-solvent and solvent-solvent contributions.

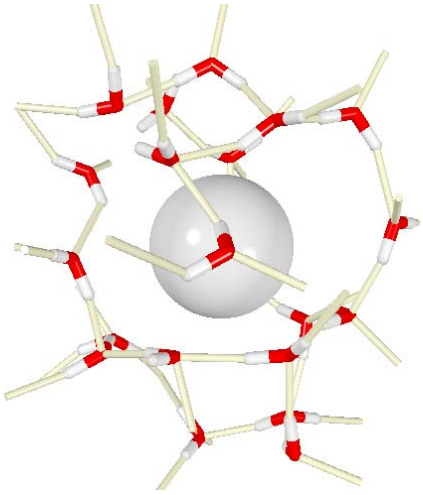

Figure 3.1: Hydration shell of a nonpolar Xenon atom. Grey is Xenon, red is oxygen, and white is hydrogen. [69] The hydration thermodynamics is largely determined by the hydrogen bonding network (solvent-solvent interactions) of the water.

In a related study on hydration of benzene, Schravendijk et al. [70] reported hydration free energies, enthalpies, entropies and heat capacities where they quantified contributions of weak benzene-water hydrogen bonding and water-water interactions to thermodynamic quantities. In a recent work by Lee et al. these concepts were extended to binary solutions to explain the preferential solvation of methane in tertiary butyl alcohol (TBA)-water solvent mixtures.[71] They showed that dissolved (nonpolar) solutes expel

water from alcohol clusters in particular at low concentrations. Figure 3.2 illustrates the preferential solvation of methane below. In that study they performed the simulations with a force field, which they derived from the Kirkwood-buff integrals bringing about consistent results with the experimental data.[72] By the comparison with other force fields they also discuss the effects of parameterization.

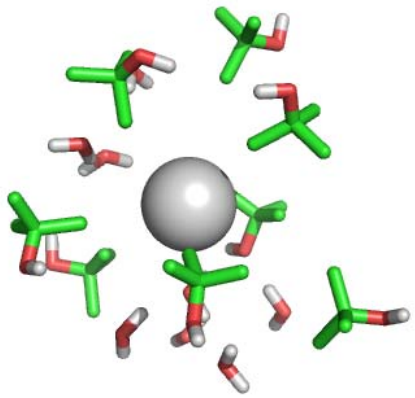

Figure 3.2: Methane solvation snapshot for the LV/SPC. Grey is methane, red is oxygen, and green is carbon and methyl group. Solvent configurations are shown around 6 Å of methane at the 0.1 TBA mole fraction. (Lee et al. [71])

Moreover, Lee et al. also discussed the urea-water binary mixtures by means of potential mean forces (PMF), where they showed that hydrophobic interaction in an aqueous urea solution is one of the major driving forces in protein folding.[73] It is obvious that understanding the interactions behind the solvation processes is quite significant also in biochemistry.

In this chapter, we mainly focus on preferential solvation of methane in dimethyl sulfoxide (DMSO)/water mixtures (298 K, 1 atm). By a simple definition, solvation of

methane is the ability of the methane molecules to transfer from gas phase into solution phase which is DMSO/water binary mixture in our case. The free energy of solvation, ΔG_S, is presented as follows;

$$CH_4(\text{gas}) \overset{K^{eq}}{\longleftrightarrow} CH_4(\text{soln})$$

$$K^{eq} \equiv \frac{C_{CH_4}^{\text{soln}}}{C_{CH_4}^{gas}} = \exp[-\Delta G_s / RT]$$

where K^{eq} is the equilibrium constant which can be obtained by experimental means from the concentrations of methane (CH_4) in gas phase and in solution phase, as $C_{CH_4}^{gas}$ *and* $C_{CH_4}^{So\ln}$ relatively.

The solvation process in dilute case can be considered as a local equilibrium reaction of transformation from pure solvent S(s) and solute in the gas phase X(g) to a phase where solute surrounded by solvent molecules X(s) and solvent molecules exist in the coordination shell of solute S(x). Then, the equilibrium can be written as:

$$X(g) + s_X\, S(s) \rightleftharpoons X(s) + s_X\, S(x)$$

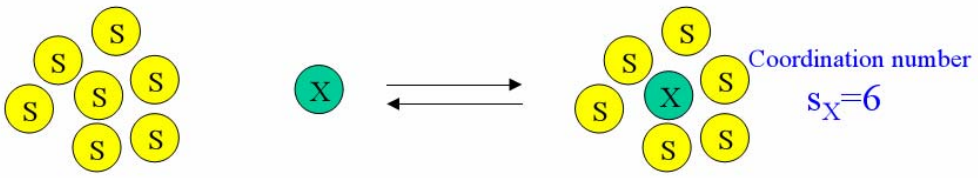

Then, the compensation of enthalpy and entropy in the reorganization of the solvent molecules in the environment can easily be obtained from such schemes by calculating the free energy change with respect to the number of molecules in the coordination shell at equilibrium conditions, as such:

$$G(n_X, n_S, P, T, s_X) = n_X g_{X(s)} + (n_S - n_X s_X) g_{S(s)} + n_X s_X g_{S(x)}$$

$$\left(\frac{\partial G(n_X, n_S, P, T, s_X)}{\partial s_X} \right)_{P,T,n_X,n_S} = 0 \quad \cdots \Rightarrow \quad \Delta G_{env} \equiv g_{S(x)} - g_{S(s)} = 0$$

$$\Delta H_{env} = T\Delta S_{env}$$

In the above decomposition scheme, free energy is defined as a function of independent variables, number of solute and solvent particles in the local environment (respectively n_x, n_s) and pressure and temperature P, T and the number of solvent particles occurring in the solvation shell of the solute s_x. Deriving the differentials at equilibrium where environmental process (env) means the reorganization of molecules in the solvation shell, the enthalpy and entropy compensation has been shown. [74]

We performed molecular simulations to analyze the thermodynamics of this process. The contributions of two sub-processes are studied: (i) introduction of solute-solvent interactions (*primary process*) and (ii) solute-induced disruption of cohesive solvent-solvent interactions (*response*/*secondary process*). The energy and entropy changes of the secondary process always exactly cancel in the free energy (energy-entropy compensation), hence only the primary process is important for understanding changes of the free energy. After discussing the physical significance of the solute-solvent energy and solute-solvent entropy associated with the primary process, in the next chapter we will discuss how to obtain these quantities from experiments combining solvation thermodynamic- and solvent equation of state data.

Herein we evaluate the free energy, enthalpy and entropy change of solvating a single methane solute in DMSO/water mixtures of variable composition by performing test-particle insertions in thermally equilibrated solvent configurations obtained by molecular dynamics (MD) simulations. Our aims are twofold. First, we describe the

solvation entropy in terms of *primary* and *secondary* molecular solvation processes. The primary process is the solute coupling with the solvent. It contributes a solute-solvent excluded volume penalty to the solvation entropy as well as an additional entropy penalty related to how strongly attractive solute-solvent interactions bias the solvation shell composition. The secondary process quantifies solute-induced changes of cohesive solvent-solvent interactions. Loss of solvent-solvent cohesive interaction contributes favourably (positive) to the entropy change while strengthening cohesive interactions tends to reduce the entropy. In studying the primary and secondary processes separately we aim to understand better how much they each contribute to the overall magnitude of the constant pressure solvation entropy. A procedure to obtain the thermodynamic quantities of the primary and secondary processes from experimental sources will also be discussed. Our second aim is to illustrate that, based on our calculations for methane in DMSO/water, a positive change of the entropy relative to solvation in pure water not necessarily means that the entropy drives the process of enhanced methane solvation. We will argue that the solvation entropy and enthalpy share a common contribution – referred to above as the secondary process – that is exactly enthalpy-entropy compensating (cancelling) in the free energy. This exact enthalpy-entropy compensating process has been described in several earlier works [66,70,75-83] but its quantitative evaluation in numerical simulations remains challenging and only few numerical studies have been reported on this subject so far.[66,70,77,79-81]

This chapter is organized as follows: In section 3.2, we start with describing the statistical mechanics basis of the solvation entropy. Next (section 3.3) we describe the

technical aspects of our calculations. In section 3.4 we present and discuss results. The conclusions of this work are summarized in section 3.5.

3.2. The Solvation Entropy

In earlier studies the statistical mechanics derivation of the solvation entropy has been reported.[76,78,80] Hence we will only briefly discuss the essential features here. The solvation entropy (energy) is ensemble dependent different than the free energy.[67,78] The constant-pressure entropy change $(\Delta S)_P$ (as well as the energy $(\Delta E)_P$) will be of interest to us since it probes the local contributions to the solvation thermodynamics that derive strictly from the interactions between the solute and its surrounding solvation shell(s). The constant pressure solvation entropy can be written as; [66,70-81]

$$(\Delta S)_P = \Delta S_{uv} + (\Delta E_{vv})_P / T \qquad (3.1),$$

where ΔS_{uv} is the solute(u)-solvent(v) entropy change and $(\Delta E_{vv})_P$ the constant-pressure solvent(v)-solvent(v) energy change (solvent reorganization energy). The solute-solvent entropy quantifies excluded volume contributions to the constant-pressure solvation entropy. It is determined by the probability of observing density fluctuations in the solvent that produce molecular-sized, empty cavities permitting solute insertion. In mixtures of two solvents, additional excluded volume penalties contribute to ΔS_{uv}; [82,83] the solute (S) may favor (due to stronger Van der Waals or electrostatic

interactions) to be solvated by one of the solvent components, say *A*, but in achieving this it may have to compete with solvent component *B* that also preferably solvates *A*-type molecules. Therefore *S* attracts solvent moiety *A* but excluded volume restrictions interfere with it since moieties *B* have to permit *S* to contact *A*. In the language of solute insertion this is pronounced as insertion in empty cavities is biased by attractive solute-solvent interactions, resulting in a reduction of the entropy. Aliphatic hydrocarbons (*S*) dissolved in DMSO(*A*)/water(*B*) and urea(*A*)/water(*B*) mixtures are a few examples of such systems.[83] The solvent reorganization term $\left(\Delta E_{vv}\right)_P$ in eq (3.1) quantifies the change of the N-solvent-particle potential energy U_N induced by inserting the (N+1)th particle (solute). Hence, $\left(\Delta E_{vv}\right)_P \equiv \left(\left\langle U_N \right\rangle_{N+1} - \left\langle U_N \right\rangle_N\right)$ where $\left\langle \cdots \right\rangle_N$ and $\left\langle \cdots \right\rangle_{N+1}$ denote isothermal-isobaric ensemble averages of the pure solvent and solvent+solute systems, respectively. We re-emphasize that $\left(\Delta E_{vv}\right)_P$ is a local energy change. It quantifies the loss (or gain) of cohesive solvent-solvent interactions in the solute's solvation shell(s), relative to cohesive solvent-solvent interactions in the bulk solution far away from the solute. In response to solvating a solute probe, when cohesive solvent-solvent interactions in the solvation shell become weaker relative to those in the bulk, the resulting increase in configurational freedom of the system is accounted for with a positive entropy contribution $\left(\Delta E_{vv}\right)_P / T$. On the other case, when solvent molecules near the solute engage in a stronger cohesive binding, $\left(\Delta E_{vv}\right)_P / T$ contributes negatively to the entropy.

The constant-pressure solvation enthalpy is given by the sum of the solute binding- and solvent reorganization energy,

$$
\begin{aligned}
\left(\Delta H\right)_P &\simeq \left(\Delta E\right)_P \\
&= \left\langle \psi \right\rangle_{N+1} + \left[\left\langle U_N \right\rangle_{N+1} - \left\langle U_N \right\rangle_N \right] \\
&\equiv \Delta E_{uv} + \left(\Delta E_{vv}\right)_P
\end{aligned}
\qquad (3.2),
$$

where $\Delta E_{uv} \equiv \left\langle \psi \right\rangle_{N+1}$ denotes the average solute (N+1th particle) binding energy (ψ) with all N solvent molecules in a constant pressure-temperature system. ΔE_{uv} is also referred to as the sol*u*te-sol*v*ent energy change. In eq (3.2) we neglected a pressure-volume term $P\Delta V_S^*$ (with ΔV_S^* denoting the solvation volume).[84] In condensed liquid phases the term $P\Delta V_S^*$ usually is 2-3 orders of magnitude smaller than the solvation energy $\left(\Delta E\right)_P$ and can safely be ignored.[84] Note that the solvation entropy (eq 3.1) and solvation enthalpy (eq 3.2) share $\left(\Delta E_{vv}\right)_P$ as a common term. The latter cancels in the free energy. We can thus write the solvation free energy as,

$$
\begin{aligned}
\Delta G &= \left(\Delta H\right)_P - T\left(\Delta S\right)_P \\
&= \Delta E_{uv} - T\Delta S_{uv}
\end{aligned}
\qquad (3.3),
$$

The cancellation of $\left(\Delta E_{vv}\right)_P$ (enthalpy-entropy compensation) should not come as a surprise if one realizes that ΔG is the reversible work of introducing the solute-solvent interactions. The corresponding thermodynamic integration/ thermodynamic

perturbation,[76,80] or particle insertion formulas [77] always depend explicitly on the solute(u)-solvent(v) potential energy functions while the potential energy of solvent-solvent interactions enters implicitly through the ensemble averaging.[76,80] The quantity ΔS_{uv} has been referred to as the solute-solvent entropy,[66,70,76,77,80-83] but different names have also been used in the literature. Sanchez *et al.* refer to it as the *interaction entropy* [69] while Ben-Amotz *et al.* refer to it as the *fluctuation entropy*.[78]

Free energy decomposition schemes may vary and alternative schemes have been used in the literature with corresponding energy-entropy compensating terms different from the compensating solvent-solvent energy defined here.[74,85,86] The usefulness of any of such schemes, including ours, depends on whether the non-compensating terms remaining in the free energy (the solute-solvent terms defined here) can be assigned a well-defined physical meaning. We will show this is indeed the case with the decomposition scheme mentioned above in this chapter. Moreover, as it was recently pointed out by Ben-Amotz *et al.*, [78] the solute-solvent energy and solute-solvent entropy are experimentally accessible under conditions that the constant-volume solvent reorganization energy vanishes. In idealized Van der Waals fluids this is always true, [75,78] while for xenon in *n*-hexane and water at ambient conditions $\left(\Delta E_{vv}\right)_V$ proved to have a magnitude of at most $k_B T$. [78]

The terminology "*primary*" and "*secondary process*" is already introduced above. The introduction of solute-solvent interactions we define as the primary process. The solute-solvent energy ΔE_{uv} and solute-solvent entropy ΔS_{uv} changes are the corresponding thermodynamic quantities. In response to the primary process, solvent-solvent cohesive interactions between molecules vicinal to the introduced solute are

modified. This response process, characterized by the energy change $\left(\Delta E_{vv}\right)_P$, we name as the secondary process. The secondary process is energy-entropy compensating and has therefore no impact on the free energy. It is however important to quantify the magnitude of the secondary process and its relative contribution to the solvation energy and entropy. In case it dominates the solvation energy and entropy, one runs into the danger of interchanging *cause* and *effect*. Attractive Van der Waals interactions could *cause* the free energy to decrease. But these attractive interactions could also induce a large positive change of the solvent-solvent energy $\left(\Delta E_{vv}\right)_P$ with the result (*effect*) that, both, the solvation energy- and entropy change in positive direction. Obviously, concluding that the change of free energy is entropic is untenable in this case.

3.3. Computational Details

3.3.1 DMSO, water and solute models.

We used a rigid, four-site DMSO model developed by Geerke *et al.*[87] In this model, the methyl groups are treated as united atoms. DMSO-DMSO and DMSO-water intermolecular interactions are modeled by a sum of Lennard-Jones (LJ) terms centered on the S, O, and CH_3 interaction sites as well as Coulombic interactions between static partial electronic charges centered on the same sites. The SPC water model [88] was used, which, combined with the above DMSO model, leads to a satisfactory description of most excess thermodynamic properties of DMSO/water mixtures at ambient conditions (298 K, 1 atm).[87] Methane was modeled as a single-site united atom, the LJ parameters of which are reported in ref [82]. Geometric mean mixing rules were used to describe LJ interactions between chemically different atom types/groups.

3.3.2 Simulation details.

All simulations were performed using the GROMACS package.[39] DMSO/water mixtures were studied at DMSO mole fractions x_{DMSO}=0.0, 0.05, 0.10, 0.19, 0.27, 0.35, 0.48, 0.64, 0.81, and 1.00. Details on system sizes are given in Table 2 of ref [82]. Geometries of all molecules were kept rigid by applying constraints to the interatomic distances within the molecules, using the SHAKE algorithm [43] with a relative geometric tolerance of 10^{-4}. A twin-range cutoff scheme with 0.8 and 1.4 nm cutoff radii was applied. The nonbonded interactions in the range between these radii were updated every fifth time step. The equations of motion were integrated using the leap-frog algorithm using a time step of 2 fs. A reaction field approximation was used to account for truncation of electrostatic forces beyond the long range cutoff (1.4 nm). The reaction field relative dielectric permittivities are reported in ref [82]. Constant pressure (1 atm) and temperature (298 K) simulations were performed using the Nose-Hoover thermostat [47,89] and Parrinello-Rahman barostat [46,50] with coupling times τ_T = 1.5 ps and τ_P = 2.5 ps.

3.3.3 Computation of thermodynamic data.

To obtain solvation free energies (ΔG) and solute-solvent energies (ΔE_{uv})the Widom test-particle insertion method is applied [90] by performing at least 1×10^{10} random insertions in 20-50 ns (NPT) simulation trajectories. The solute-solvent entropies (ΔS_{uv}) were obtained by applying eq (3.3). The constant pressure-temperature test-particle-insertion equations for ΔG and ΔE_{uv} are given in refs [81] and [82]. The constant pressure solvation entropy (298 K, 1 atm) was obtained from the finite difference expression

$$\Delta S(T) = -\frac{\Delta G(T+\Delta T) - \Delta G(T-\Delta T)}{2\Delta T} \qquad (3.4),$$

where we used $\Delta T = 25\,\mathrm{K}$. The free energies $\Delta G(T+\Delta T)$ and $\Delta G(T-\Delta T)$ were calculated using test-particle insertions in (NPT) simulation trajectories of at least 50 ns in order to reduce the statistical error in $T\Delta S$ below 0.5 kJ/mol. The solvation enthalpy was calculated as $\Delta H = \Delta G + T\Delta S$ while the solvent reorganization energy was obtained by applying eq (3.2). Besides the finite difference approach (eq 3.4) to obtaining ΔS and ΔH, we calculated ΔH by applying a direct method. In the direct method the average configurational energies of a (solute+solvent) *N+1* particle and (solvent) *N*-particle system are subtracted (accounting for an additional, but usually negligible, $P\Delta V$ term). In addition, a correction needs to be applied to account for the fact that in the direct method the (N+1)th particle has a kinetic energy whereas the solvation enthalpy is defined as the change of the system enthalpy by introducing the solute at an arbitrary but *fixed position* in the system. [84] The effect of the particle's kinetic energy, absent in the solvation process but present in the direct method for computing ΔH, is a system volume increment equal to $k_B T\kappa_T$ (with κ_T the isothermal compressibility of the solvent).[84] As an additonal result also the system's enthalpy increases with a contribution $k_B T\kappa_T\left(\left(\partial U/\partial V\right)_T + P\right) = k_B T^2\alpha_P$ (where $\left(\partial U/\partial V\right)_T$ is the solvent internal pressure and α_P is the solvent isobaric thermal expansion coefficient). Thus, ΔH(direct_method)=ΔH(solvation)+$k_B T^2\alpha_P$. The correction term $k_B T^2\alpha_P$, which we discuss in the next chapter more in detail how to obtain these quantities, is non-negligible

and amounts to 0.6-0.7 kJ/mol for the systems studied in this work. We ran additional 100 ns NPT simulations including five ($x_{DMSO} \leq 0.10$) or ten ($x_{DMSO} > 0.10$) methane molecules at several DMSO/water compositions. We included several methanes, rather than just one, in order to converge the difference between configurational energies within statistical errors of 1 kJ/mol. Below 10% DMSO, including of more than five methane molecules leads to changes in the methane solvation shell composition and deviations of the solvation shell energies with respect to solvating a single methane. In addition to providing an independent means for assessing the accuracy of the finite temperature difference method (eq 3.4), these explicit solute-solvent simulations allow evaluating the solute-solvent energy as well as the solvent reorganization energy including the separate contributions arising from changes of DMSO-DMSO, water-water, and DMSO-water interactions.

3.4. Results and Discussion

3.4.1 Solvation thermodynamics and preferential solute-solvent interactions.

Figure 3.3 shows the methane solvation free energy versus the solvent composition expressed on a mole fraction (x_{DMSO}) scale. Experimentally obtained data [91,92] for the two pure solvents (x_{DMSO}=0.0 and 1.0) are included. The free energy decreases monotonically with x_{DMSO} from 8.6 kJ/mol in water to 4.2 kJ/mol in pure DMSO. The decrease of ΔG with x_{DMSO} is indicative of preferential methane solvation by DMSO molecules at all DMSO/water compositions.[93] The difference in solvation free energy in water (x_{DMSO}=0) and DMSO (x_{DMSO}=1) corresponds to a six-fold increase in methane solubility. The experimental data are ΔG = 8.4 kJ/mol (water) [91] and 5.0 kJ/mol (DMSO) [92] corresponding to a four-fold increase in methane solubility.

Inspection of methane-solvent radial distribution functions in figure 3.4 shows a preferential methane interaction with DMSO methyl groups. The methane's first shell coordination numbers shown in Table 3.1 indicate that the number of water molecules rapidly decreases as x_{DMSO} increases to 0.3. Based on the *excess* first shell- as well as excess coordination numbers up to 10 Å we conclude that methane, in the water-rich regions $x_{DMSO} \leq 0.35$, preferentially attracts DMSO molecules.

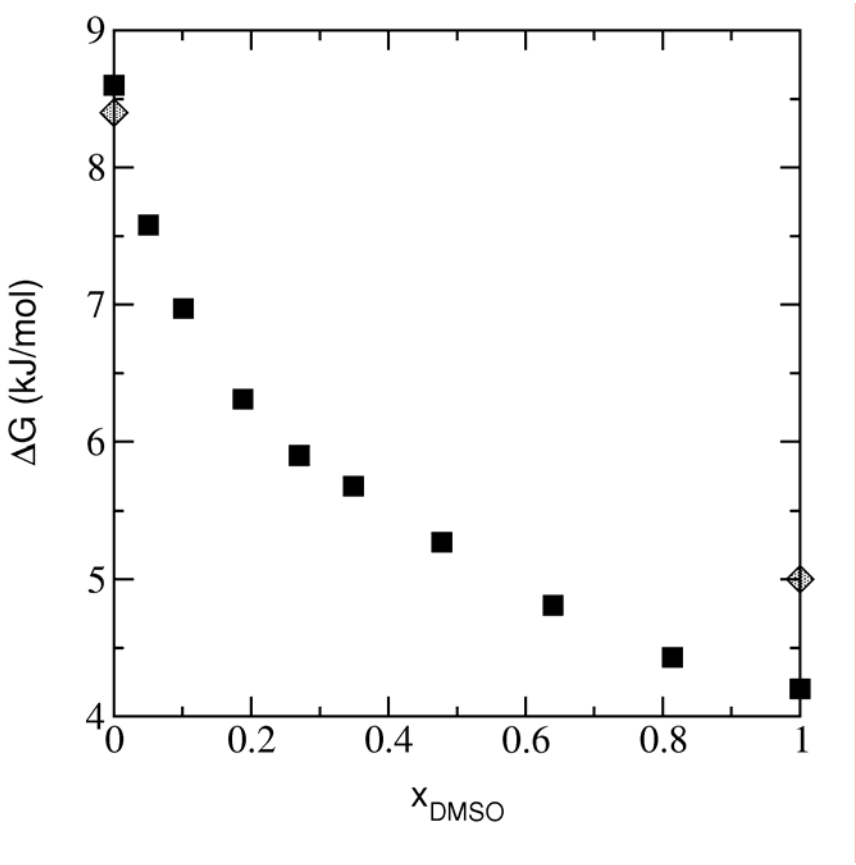

Figure 3.3. Methane solvation free energy in DMSO/water mixtures (298 K, 1 atm) computed using test-particle insertions (squares). Experimental values for methane solvation in pure water [91] and pure DMSO [92] are included (diamonds).

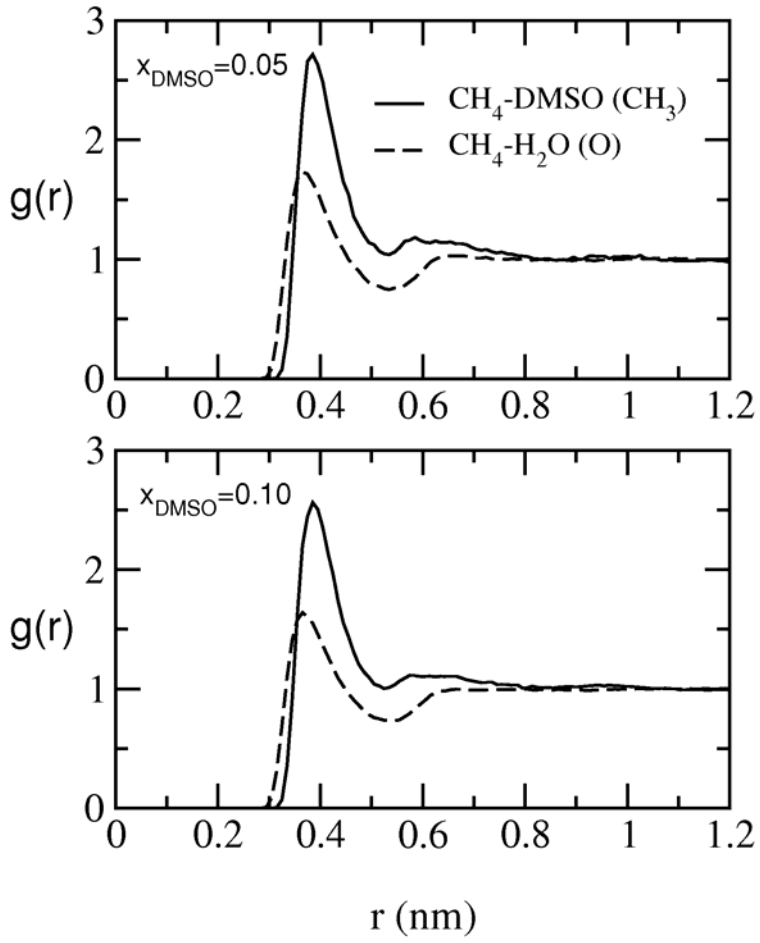

Figure 3.4. Methane-solvent radial distribution functions for x_{DMSO}=0.05 (top panel) and x_{DMSO}=0.10 (bottom panel). Shown are CH_4-CH_3 (methane-DMSO) and CH_4-O (methane-water) correlations with full- and dashed line, respectively.

Table 3.1. Methane 1st shell coordination numbers (N_{Rmax}), excess 1st shell coordination numbers (N_{Rmax}[ex]) and excess coordination numbers up to 10 Å. R_{max} is the upper distance defining the spatial extension of the first shell. (Excess) coordination numbers are based on the oxygen positions for water and the methyl group positions for DMSO. Excess coordination numbers are obtained by subtracting the statistically expected number of solvent species.

	H_2O				DMSO			
x_{DMSO}	N_{Rmax}	N_{Rmax}[ex]	R_{max}(Å)	$N_{10Å}$[ex]	N_{Rmax}	N_{Rmax}[ex]	R_{max}(Å)	$N_{10Å}$[ex]
0.00	19.3	–1.6	5.39	–1.9	–	–	–	–
0.05	14.9	–2.2	5.35	–3.6	2.2	0.4	5.35	0.9
0.10	11.9	–2.4	5.35	–4.3	3.5	0.5	5.26	1.2
0.19	8.4	–1.9	5.26	–3.7	5.1	0.4	5.25	0.9
0.27	5.5	–1.6	5.36	–2.2	4.9	0.2	5.26	0.3
0.35	5.4	–1.4	5.35	–1.8	7.1	0.1	5.30	0.1
0.48	3.6	–1.0	5.35	–1.2	7.9	0.0	5.25	–0.1
0.64	1.8	–0.6	5.15	–0.8	8.9	–0.2	5.30	–0.2
0.81	0.8	–0.3	5.24	–0.4	9.3	–0.3	5.25	–0.3
1.00	–	–	–	–	9.6	–0.4	5.25	–0.4

Table 3.2. Methane solvation free energy ΔG, constant pressure solvation energy $(\Delta E)_P$ and entropy $T(\Delta S)_P$ in DMSO/water mixtures at 298 K and 1 atm. Units are kJ/mol.

x_{DMSO}	ΔG	$(\Delta E)_P$	$T(\Delta S)_P$
0.00	8.6	–2.6	–11.2
0.05	7.6	–0.5	–8.1
0.10	7.0	0.9	–6.1
0.19	6.3	2.1	–4.2
0.27	5.9	3.2	–2.7
0.35	5.7	2.9	–2.8
0.48	5.3	2.5	–2.8
0.64	4.8	2.3	–2.5
0.81	4.4	1.8	–2.6
1.00	4.2	1.0	–3.2

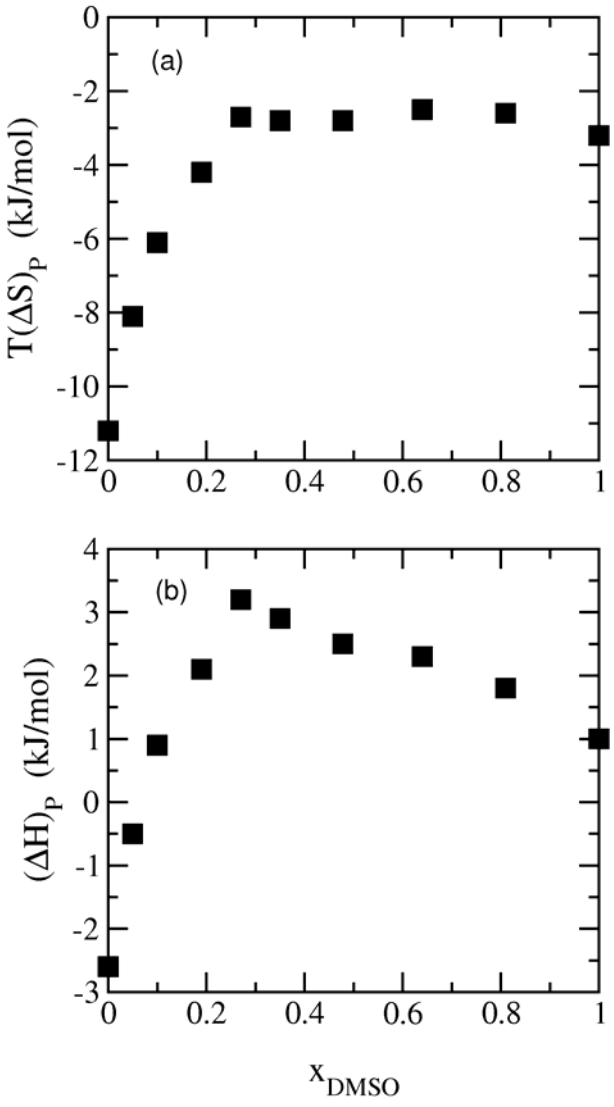

Figure 3.5. (a) Methane solvation entropy $T\left(\Delta S\right)_P$ calculated from finite temperature differences (cf. eq 3.4). (b) Methane solvation enthalpy $\left(\Delta H\right)_P$ obtained from $\left(\Delta H\right)_P = \Delta G + T\left(\Delta S\right)_P$. T=298 K, P=1 atm.

In pure water (at 298 K), the methane hydration shell has a low enthalpy and entropy since first shell water molecules avoid wasting hydrogen bonds and form hydrogen bonded cage structures.[94] These low entropy (enthalpy) water structures are disrupted by DMSO molecules, therefore one expects that the methane solvation entropy (enthalpy) increases with increasing x_{DMSO}. Figures 3.5a and 3.5b show the solvation entropy and enthalpy, respectively. The data are summarized in Table 3.2. In the water-rich region ($x_{DMSO}<0.30$), the methane solvation entropy rapidly increases as the DMSO mole fraction of solution increases, whereas it stays essentially unchanged at higher DMSO mole fractions ($0.30\leq x_{DMSO}\leq 1.0$). The enthalpy rapidly increases also for DMSO mole fractions smaller than 0.3, but then reaches a maximum value, and next decreases. Symons reported identical trends in an experimental study of hydrogen gas solubility in the DMSO-water system.[95] The maximum in the hydrogen solvation enthalpy found by Symons appears in the 25-35 mol% DMSO range.[95] Based on the data in Figs 3.3 and 3.5 and the commonly used expression $\Delta G = \Delta H - T\Delta S$ we tentatively conclude that the downward trend of the solvation free energy with x_{DMSO} (increase of methane solubility) is entropic in the water-rich region (<30 mol% DMSO) while it is enthalpic at higher DMSO content. Below, where we account for enthalpy-entropy compensation, we will show that this conclusion is unjustified and the molecular driving force of preferential methane-DMSO interaction *never* is the entropy change.

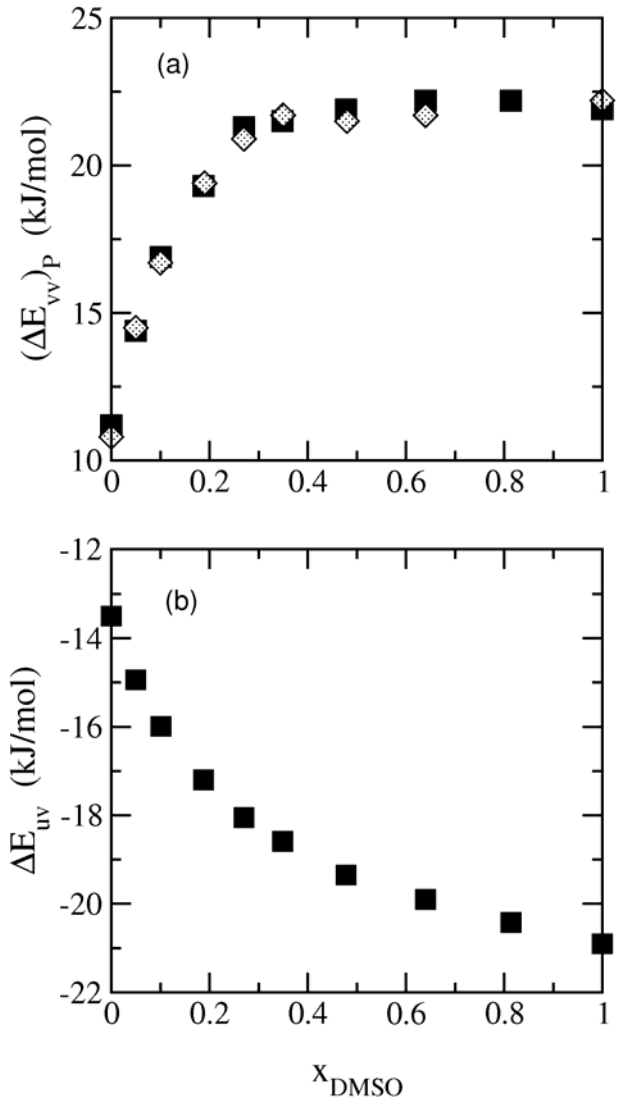

Figure 3.6. (a) Constant pressure solvent reorganization energy (squares) obtained from the data in figure 3.5(b) by subtracting the solute-solvent energy (eq 3.2). Solvent reorganization energies obtained by direct subtraction of the configurational energies of a (N+1)- and N-particle system $\left[\langle U_N \rangle_{N+1} - \langle U_N \rangle_N\right]$ are also included (diamonds). (b) Solute-solvent interaction energies.

3.4.2 Solute-solvent and solvent-solvent energy changes.

In section 3.2 we classified the solute-solvent and solvent-solvent energy changes as energetic measures of the primary and secondary processes, respectively. The energy of the secondary process is exactly enthalpy-entropy compensating and does not impact the free energy. Figures 3.6a and 3.6b show the solvent-solvent energy change and solute-solvent binding energy, respectively. The solvent-solvent energy change is smallest in pure water, strongly increases with DMSO mole fraction (with approximately a factor 2) and settles at a constant value of approximately 22 kJ/mol around 30 mol% DMSO. In addition to the solvent-solvent energies obtained from the temperature dependence of the free energy (squares in fig 3.6a) we included in the same figure the solvent-solvent energies obtained by taking differences of the configurational energies (diamonds) sampled in the (N+1)-particle and N-particle systems (see section 3.3). The comparison is very satisfactory. The methane-solvent binding energy (Fig 3.6) decreases monotonically with DMSO ratio in the mixture. This trend is explained by methane-DMSO dispersion interactions being stronger than methane-water dispersion interactions. Note that the methane binding energy and solvent reorganization energy are of comparable magnitude but have opposite sign. There are a number of additional comments we can now make regarding the methane solvation enthalpy in fig 3.5b. Below 30% DMSO the methane solvation enthalpy increases with x_{DMSO} and changes sign. In water the solvation process is exothermic due to comparably small solvent reorganization energy. Above 5 mol% DMSO the solvation process becomes endothermic, which it remains up to $x_{DMSO}=1$. Below $x_{DMSO}=0.30$ the reorganization energy overcompensates

the methane binding energy and the solvation enthalpy follows the trend of the solvent reorganization energy.

Table 3.3. Methane constant pressure solvation energy $(\Delta E)_P$, solvent reorganization energy $(\Delta E_{vv})_P$ and contributions of water-water, DMSO-DMSO and DMSO-water interactions to the solvent reorganization energy. $(\Delta E)_P$ and $(\Delta E_{vv})_P$ were obtained from the temperature dependence of the free energy (see text). The values denoted in parentheses were obtained by taking differences between configurational energies of solute-solvent and pure solvent systems and correcting those values with a term $k_B T^2 \alpha_P$ (see text). The individual solvent-solvent contributions were obtained also by taking differences between configurational energies of solute-solvent and pure solvent systems. $(\Delta E_{vv})_P + k_B T^2 \alpha_P = (\Delta E_{H_2O-H_2O})_P + (\Delta E_{DMSO-DMSO})_P + (\Delta E_{DMSO-H_2O})_P$. T=298 K, P= 1 atm. Units are kJ/mol.

x_{DMSO}	$(\Delta E)_P$	$(\Delta E_{vv})_P$	$(\Delta E_{H_2O-H_2O})_P$	$(\Delta E_{DMSO-DMSO})_P$	$(\Delta E_{DMSO-H_2O})_P$
0.00	–2.6	11.2 (10.8)	11.5	–	–
0.05	–0.5	14.4 (14.5)	8.1	–0.1	7.1
0.10	0.9	16.9 (16.7)	6.0	2.1	9.3
0.19	2.1	19.3 (19.4)	2.2	4.0	13.9
0.27	3.2	21.3 (20.9)	1.6	7.5	12.5
0.35	2.9	21.5 (21.7)	1.9	10.8	9.7
0.48	2.5	21.9 (21.5)	2.0	15.1	5.1
0.64	2.3	22.2 (21.7)	–0.4	17.7	5.1
0.81	1.8	22.2 (22.7)	–0.2	20.7	2.2
1.00	1.0	21.9 (22.2)	–	22.9	–

The maximum in the methane solvation enthalpy in fig 3.5b happens because the solvent reorganization energy stays at a constant value after reaching x_{DMSO}=0.30 while the methane binding energy continues to decrease with increasing x_{DMSO} owing to favorable dispersion interactions with the large DMSO molecule.

3.4.3 Contributions to the entropy.

The solvent reorganization energy in Fig 3.6a contributes to the solvation entropy $\left(\Delta S\right)_P = \Delta S_{uv} + \left(\Delta E_{vv}\right)_P / T$ (eq 3.1). The solvation entropy in Fig 3.5a reaches a constant value exactly where also the reorganization energy becomes constant (x_{DMSO}~0.30). The striking similarity between Figs 3.5a and 3.6a indicates that solvent reorganization provides a substantial, if not the most prominent, contribution to the overall solvation entropy. This observation has far-reaching implications: based on the shape of the entropy curve (Fig 3.5a) in section 3.4.1 we concluded that the observed larger methane solubility for larger x_{DMSO} is entropy-driven. Here we however find that the increase of the methane solvation entropy at x_{DMSO}<0.30 is caused by an energy-entropy compensating solvent reorganization process. Due to this compensation, the conclusion of section 3.4.1 is unjustified i.e. it is not true to say that the preferential methane solubility is entropy-driven. Before we analyze the solute-solvent contributions pertinent in the free energy $\Delta G = \Delta E_{uv} - T\Delta S_{uv}$ (eq 3.3), we look at contributions to the solvent reorganization energy $\left(\Delta E_{vv}\right)_P$ and the implications on $\left(\Delta H\right)_P$ and $\left(\Delta S\right)_P$. Table 3.3 shows the changes of the potential energy of DMSO-DMSO, water-water, and DMSO-water interactions contributing to the constant pressure solvent reorganization energy. The sum of these contributions minus $k_B T^2 \alpha_P$ equals the overall solvent reorganization energy presented in Table 3.3 and Fig 3.6a. With increasing DMSO concentration of the

solution, the water-water reorganization energy steadily decreases while the DMSO-DMSO reorganization energy steadily increases, as expected. The DMSO-water reorganization energy passes through a maximum, however not at x_{DMSO}=0.5, but at x_{DMSO}=0.19. The major contribution to the overall solvent reorganization energy at solution compositions x_{DMSO}<0.30 stems from loss of DMSO-water cohesive interactions. For DMSO concentrations x_{DMSO}<0.30, the excess number of DMSO molecules in the methane's first shell is positive (table 3.1) indicating that methane attracts the DMSO molecules from the bulk into its solvation shell(s). In that process, DMSO molecules are forced to sacrifice strong cohesive (polar) interactions with water molecules which are then left behind in the bulk. Eventually it is this "release" of DMSO hydration water that contributes to the increase of the entropy observed in Fig 3.5a.

In a previous study by Van der Vegt and Van Gunsteren the methane solute-solvent entropy has been extensively studied in solutions of NaCl/water, acetone/water and DMSO/water.[82] At sufficiently high concentrations of salt ions or cosolvents that strongly bind water molecules density fluctuations required to produce (empty) molecular sized cavities large enough to host a solute are suppressed. As a result the solute-solvent entropy becomes stronger negative the more salt or cosolvent is present in solution. In NaCl/water ion hydration waters are bound strongly to the ion so that most cavities can form only far outside the ion hydration shells. This causes less waters being available to hydrate the methane at higher salt content, $k_B \ln P_{ins}$ to decrease and the methane being "salted-out". Also in DMSO/water the formation of transient cavities is suppressed due to strongly polar DMSO-water interactions.[82,87] Thus, $k_B \ln P_{ins}$ decreases with x_{DMSO} as is shown in Fig 3.7b.

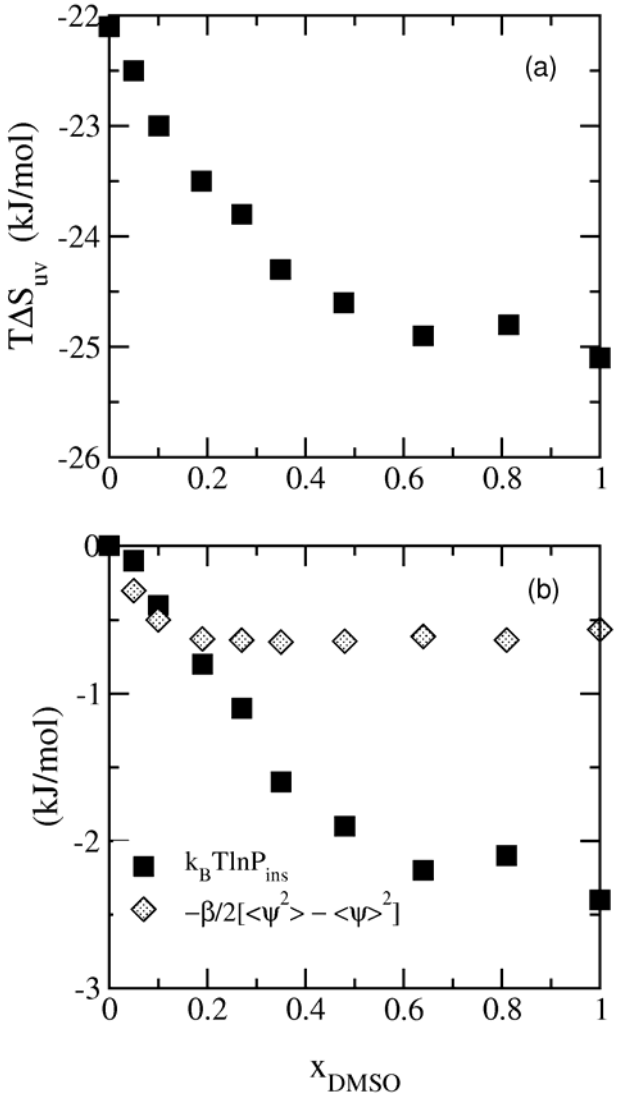

Figure 3.7. (a) Solute-solvent entropy change $T\Delta S_{uv}$ (eq 3.1). (b) Contributions to the solute-solvent entropy change (eq 3.5) arising from the insertion probability that a methane particle in a pure DMSO/water solvent system has zero or negative binding energy (squares) and fluctuations of the binding energy that cause a biasing of cavity occupation (triangles). The data are presented relative to the values in pure water. For (SPC) water these are: $k_B T \ln P_{ins} = -20.1$ kJ/mol, $-\beta/2\left[\left\langle \psi^2 \right\rangle - \left\langle \psi \right\rangle^2\right] = -2.0$ kJ/mol.

For $x_{DMSO}<0.20$, the second term in eq (3.5) causes an additional reduction of the entropy (Fig 3.7b). This term, proportional to the fluctuations of the solute-solvent interaction energy, measures the extent to which attractive solute-solvent interactions (indicated by subscript 'a') bias the solvent configuration space. [75] Since methane-DMSO dispersion interactions are stronger than methane-water dispersion interactions, fluctuations of the solute-solvent interaction energy are indeed expected because the solute will not only occupy cavities solvated mostly by DMSOs but also occasionally occupy hydrated cavities. The methane-DMSO attractive interaction however puts a stronger bias on occupying those transient cavities mostly solvated by DMSO molecules. This biasing process leads to a selected, non-random solvation shell structure and a lowering of entropy.

We have shown that methane preferentially interacts with DMSO molecules (*cf.* Fig. 3.4, Table 3.1) causing methane solvation free energies to be lower in DMSO/water mixtures with larger DMSO concentration (Fig. 3.3). What is the molecular driving force for this preferential interaction? One can straightforwardly argue that the methane dispersion interaction with the larger (polarizable) DMSO molecule is stronger than with the smaller water molecule but it is non-trivial that this energetically stronger interaction should be the pertinent driving force. [83] In condensed phases, the entropy of the solvent usually plays a role which is equally important role as the energy. However it is often unclear how to link entropy changes to molecular-scale processes and to what extent energy and entropy changes of such processes are compensating in the free energy. In this chapter the energy and entropy of the *primary process* are emphasized and based on

that the molecular driving force has proven to be energetic (the entropy of the primary process opposes methane-DMSO interaction). Experimentally, however, one cannot distinguish between primary and secondary sub-processes and only the overall solvation energy and entropy are being measured. Based on the trends observed in the experimental solvation enthalpies and entropies one would easily conclude that the molecular driving force for preferential methane-DMSO interaction (in the water-rich regime) is the entropy. The example discussed in this work, therefore, shows the risk of proclaiming a process being energetic or entropic when not properly accounting for compensating terms.

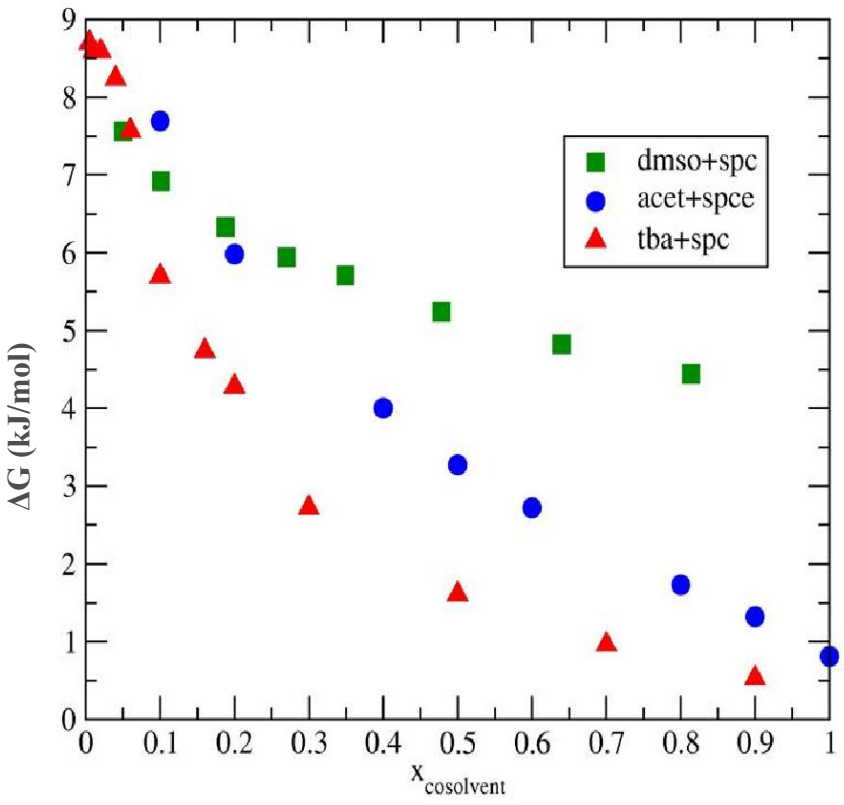

Figure 3.8: Methane solvation free energy in water mixtures with cosolvents DMSO, acetone, and TBA (298 K, 1 atm)

In this chapter, preferential methane solvation in DMSO/water mixtures was discussed in terms of the solvation free energy, enthalpy and entropy. To understand preferential solvation in binary mixtures, the energy contributions were considered by splitting the contributions of solute-solvent and solvent-solvent interactions. A decomposition of free energy into its energetic and entropic components provides useful insights in atomic-scale solvation mechanisms. When we compare the solvation free energies of methane in different binary solvent systems of DMSO, acetone, and TBA with the data taken also from other studies of Lee and Van der Vegt mentioned in the introduction part, as shown in Figure 3.8, we observe that in all cases there is a preferential solvation with the increasing solvent content. The TBA-water binary mixture performs better than mixtures of water with the both cosolvents acetone and DMSO. In case of methane insertion in TBA/water mixtures, the solvent-solvent energy changes significantly whereas the solute-solvent energy remains constant as the TBA mole fraction is changed. There the solvent reorganization energy is a dominant contribution to the methane solvation as well. However, since the solvent reorganization process is enthalpy-entropy compensating in the free energy, entropy change by itself cannot explain the preferential interaction of methane. The enthalpy-entropy compensation becomes larger in the order urea, dimethyl sulfoxide and acetone. Moreover, it is helpful in understanding solvation thermodynamics of hydrophobic interactions in liquid mixtures. In particular, it is important to know the exact enthalpy-entropy compensation in the free energy.

3.5. Conclusions.

It is common practice to ask whether a preferential interaction in a liquid solution environment is driven by the enthalpy or entropy. This question, however, often is inappropriate because enthalpy and entropy changes may contain significant contributions that cancel out in the free energy (enthalpy-entropy compensation). In this chapter we investigated methane solvation in DMSO/water mixtures where preferential methane-DMSO interactions cause a reduction of the methane solvation free energy with the DMSO concentration. The solvation free energy is determined only by the solute-solvent coupling interactions (*primary interactions*) whereas all changes of the enthalpy and entropy occurring in response to modifying cohesive solvent-solvent interactions (*secondary interactions*) are always enthalpy-entropy compensating. We have shown that loss of solvent-solvent cohesive interactions fully determines the methane solvation enthalpy and entropy: methane is preferentially solvated by DMSO molecules; however, DMSO molecules in the methane solvation shell release hydration waters thereby increasing the enthalpy and the entropy. As a result, a process that does not influence the free energy dominates the enthalpy and entropy differences.

CHAPTER 4

Solvent Reorganization in Solute Transfer Thermodynamics Derived from Solvent Equation of State

4.1. Introduction

In all chemical processes in the fluid phase the concept of solvation is of central importance. Intimately related to aspects of solvation, to understand the molecular driving forces and interactions behind the processes like permeability of membranes and stability of folded proteins an urgent requirement exists. Therefore, to understand the solvation phenomena from an atomistic point of view, we tried to give the relations between preferential interactions and basic thermodynamic quantities and statistically derived contributions in previous chapter, Chapter 3.

In chapter 3, we have shown that there is a solvent reorganization term compensating in the free energy, on the other hand dominating in the enthalpy and entropy quantities. There, we discussed the thermodynamics of methane solvation in dimethyl sulfoxide (DMSO)/water mixtures in terms of free energy, enthalpy and entropy

by performing molecular simulations. In order to do that, we investigate the two contributions from (1) solute-solvent interactions (primary contribution) and (2) solute-induced modifications of solvent-solvent interactions (solvent reorganization) (secondary contribution). Moreover, we showed that the solvation entropy and enthalpy share a common contribution – referred to chapter 3 as the secondary process – that is exactly enthalpy-entropy compensating (canceling) in the free energy. We concluded that even though the secondary process fully cancels out without any contribution to the solvation free energy, it dominates the changes of the methane solvation entropy and enthalpy. For example, below 30 mole percent DMSO in the mixture, methane – due to more favorable dispersion interactions with DMSO molecules – preferentially attracts DMSO molecules which in response release water molecules into the bulk causing an increase of the entropy. Furthermore, this large energy-entropy compensating process easily causes a confusion of *the cause for* and *the effect of* preferred methane-DMSO interactions. Procedures that infer thermodynamic driving forces from analyses of the solvation entropies and enthalpies should therefore be used with caution. Here, methane-DMSO dispersion interactions are the cause, the entropy change is the effect. This exact enthalpy-entropy compensating process has been described in several earlier works [66,70,75-83] but its quantitative evaluation in numerical simulations remains challenging and only few numerical studies have been reported on this subject so far.[66,70,77,79-81] In chapter 3, we explained the physical significance of and quantitative ways to obtain the solute-solvent energy and solute-solvent entropy associated with the primary process. From now on we will discuss how to potentially estimate these quantities from experiments combining solvation thermodynamic- and

solvent equation of state data. In this chapter we want to discuss an approach to obtain these individual terms from bulk properties of solvents so that it would be available to compare and improve the parameters involved in the simulations. The question is whether a recipe is available to improve or check the accuracy of the force field parameters from easily obtainable experimental data, such as the compressibility or expansion coefficient of the fluid.

Hummer, Pratt, and co-workers [66-68,70,75,76] have shown in their studies of hydrophobic effects how the temperature dependence of aqueous solubilities of nonpolar solutes can quantitatively be described using molecular theory, while at a more qualitative level it can be understood from the bulk solvent equation of state. Although descriptions of this as well as other hydrophobic effects [75] in terms of bulk solvent properties (i.e., the isothermal compressibility) are approximate, they have been very successful in providing semiquantitative explanations of isotope effects on hydrophobic hydration [75] and entropy convergence.[67]

Moreover, as it was recently pointed out by Ben-Amotz *et al.*, [78] the solute-solvent energy and solute-solvent entropy are experimentally accessible under conditions that the constant-volume solvent reorganization energy vanishes. In idealized Van der Waals fluids this is always true, [75,78] while for xenon in *n*-hexane and water at ambient conditions $\left(\Delta E_{vv}\right)_V$ proved to have a magnitude of at most $k_B T$. [78]

Although the real molecular driving forces in a solvation process are the solute-solvent energy and solute-solvent entropy as it is discussed in the previous chapter, these quantities are easily derived from computer simulations, but are sensitive to details of the empirical force field. Therefore, comparison with experimental estimates of the solute-

solvent energy- and entropy is necessary. We will in particular be interested in the *solvation enthalpy*, which is not only determined by direct interactions of the solute with the solvent but also by changes in cohesive solvent-solvent interactions resulting from structural solvent rearrangements around the solute. We will show that we can estimate the solvent reorganization energy of methane solvation in DMSO within an accuracy of k_BT based on information on the solvent thermodynamic equation of state (α_P, κ_T, or $\left(\partial U / \partial V\right)_T$) at the appropriate state point (P,T) allowing for experimental assessment of the solute-solvent energy and solute-solvent entropy. In addition to the solvent equation of state data, the latter procedure requires the solvation free energy, solvation enthalpy, and solvation volume from experimental sources. Not only are experimental estimates of solute-solvent binding interactions and solute-solvent entropies of interest per se (*e.g.* to better understand molecular driving forces of specific interactions), but also development of empirical force fields can benefit from it.

4.2. Theoretical Background

4.2.1. Solvent Reorganization term in Solvation Enthalpy and Entropy

In the previous chapter, we explained how to compute from the simulations all various contributions appearing in the basic quantities of solvation thermodynamics. Depending on the assumption that the Hamiltonian of a solute/solvent system can be formally split into solute-solvent (denoted by the subscript uv) and solvent-solvent (vv) interactions (where the latter refers to the pure solvent-solvent interactions, evaluated as if no solute were present). On the basis of this splitting, the constant-pressure solvation enthalpy, ΔH_P, is given by the sum of the solute binding- and solvent reorganization energy;

$$
\begin{aligned}
\left(\Delta H\right)_P &\simeq \left(\Delta E\right)_P \\
&= \left\langle \psi \right\rangle_{N+1} + \left[\left\langle U_N \right\rangle_{N+1} - \left\langle U_N \right\rangle_N \right] \\
&\equiv \Delta E_{uv} + \left(\Delta E_{vv}\right)_P
\end{aligned}
\qquad (4.1),
$$

where $\Delta E_{uv} \equiv \left\langle \psi \right\rangle_{N+1}$ denotes the average solute (N+1th particle) binding energy (ψ) with all N solvent molecules in a constant pressure-temperature system. ΔE_{uv} is also referred to as the sol*u*te-sol*v*ent energy change.

For the constant-pressure entropy change $\left(\Delta S\right)_P$, which probes the *local* contributions to the solvation thermodynamics, the splitting into solute-solvent and solvent-solvent terms results in two contributions: where ΔS_{uv} is the solute(u)-solvent(v) entropy change and $\left(\Delta E_{vv}\right)_P$ the constant-pressure solvent(v)-solvent(v) energy change (solvent reorganization energy):

$$
\left(\Delta S\right)_P = \Delta S_{uv} + \left(\Delta E_{vv}\right)_P / T \qquad (4.2),
$$

As we emphasized before, the solvation enthalpy (eq 4.1) and solvation entropy (eq 4.2) share $\left(\Delta E_{vv}\right)_P$ as a common term cancelling out (exact enthalpy-entropy compensation) in the free energy:

$$
\Delta G_S = (\Delta H)_P - T(\Delta S)_P = \Delta E_{UV} - T\Delta S_{UV} \qquad (4.3)
$$

Of course, this does not mean that solvent-solvent interactions play no role in ΔG; their contribution is indirect in that the ensemble averages (refer to eqns 3.1 and 3.2) have the total potential energy in the exponential weighting factor. Whereas the thermodynamic quantities on the left-hand sides of eqs 4.1 and 4.2 can be obtained experimentally,

evaluation of the corresponding statistical mechanics quantities all discussed in the chapter 3, however, on the right-hand sides of these equations requires, in addition, approximate theories and/or computer simulations. Due to the exact enthalpy-entropy compensation of the solvent reorganization enthalpy $(\Delta H_{vv})_P$ in the free energy of solvation, only the solute-solvent energy and the fluctuation contribution to the entropy directly contribute to solvation phenomena. It should be noted however that the solvent reorganization enthalpy can be particularly large such that it overrides the solute-solvent energy and solute-solvent entropy in the experimentally accessible thermodynamic quantities $(\Delta H)_P$ and $(\Delta S)_P$ which may be misleading in the interpretation of these data. Although exactly compensating parts could not be quantified at that time, Roseman and Jencks more than three decades ago already stated that it is potentially misleading and even unjustified to reach "conclusions regarding the driving forces and mechanism for interactions... from observed enthalpies and entropies of interaction" due to "mutually compensating changes in enthalpy and entropy".[87] This is what we have achieved to prove recently by means of numerical results and discussed so far. For that reason, it is a requirement to obtain individual contributions from solute-solvent interactions so called primary process. By means of molecular simulations, nowadays this is not so difficult. However, all the computational methods depend on the force field parameterizations of which the accuracy should be checked. Experimentally it is not possible to obtain solute-solvent interactions on a numerical basis. On the other hand, if one can achieve to obtain quantitatively solvent-solvent contribution, $(\Delta H_{vv})_P$, from experimental ways also as well as computational means, by moving back-steps it will also be possible to understand the solute-solvent interactions and improve the force-fields accordingly.

4.2.2. Solvent reorganization energies derived from pure solvent data.

The primary thermodynamic quantities (solute binding energy, solute-solvent entropy) characterize the atomic scale driving forces but cannot be obtained directly from experiments. By virtue of the relation $\left(\Delta E_{vv}\right)_P = \left(\Delta E_{vv}\right)_V + \left(T\alpha_P / \kappa_T\right)\Delta V_S^*$ Ben-Amotz *et al.* however showed that indirect experimental ways to obtain the solute-solvent binding energy and solute-solvent entropy exist in case the constant-volume solvent reorganization energy $\left(\Delta E_{vv}\right)_V$ vanishes.[78] In that case the constant pressure solvent reorganization energy $\left(\Delta E_{vv}\right)_P$ equals the volume expansion term $(T\alpha_P / \kappa_T)\Delta V_S^*$ with α_P the isobaric thermal expansion coefficient of the solvent, κ_T the solvent isothermal compressibility and ΔV_S^* the solvation volume of solute *S*. Ben-Amotz *et al.* could show that the constant-volume solvent reorganization energy for solvating xenon in water and *n*-hexane at 298.15 K approaches zero within an accuracy of $\sim k_B T$.[78] Hence, experimental data on $\left(\Delta E\right)_P$, α_P, κ_T and ΔV_S^* suffice to estimate the xenon binding energy (*cf.* eq 4.1) with room temperature water and with *n*-hexane within an accuracy of $k_B T$. Having obtained that information, additional experimental information on ΔG allows one to obtain the solute-solvent entropy change by means of eq (4.3). The experimentally obtained binding energy and solute-solvent entropy obviously are of huge benefit in the validation of empirical force fields.

Here we first provide a heuristic derivation of Ben-Amotz's result (*i.e.* $\left(\Delta E_{vv}\right)_P \simeq (T\alpha_P / \kappa_T)\Delta V_S^*$) starting from the test-particle insertion equations for the enthalpy of solvent reorganization and the solvation volume. The derivation makes clear

under what conditions/assumptions the above result can be expected to hold. Equations (4.4) and (4.5) denote the (exact) test-particle insertion formulas for the solvent reorganization enthalpy and the solvation volume, respectively.[77,81,82]

$$\left(\Delta H_{vv}\right)_P = \frac{\left\langle \delta H_{N,i} B_i \right\rangle_{NPT}}{\left\langle B_i \right\rangle_{NPT}} \qquad (4.4),$$

$$\Delta V_S^* = \frac{\left\langle \delta V_i \, B_i \right\rangle_{NPT}}{\left\langle B_i \right\rangle_{NPT}} \qquad (4.5).$$

In eq (4.4) and (4.5), $\delta H_{N,i} = H_{N,i} - \left\langle H_N \right\rangle_{NPT}$ denotes the instantaneous fluctuation of the N-particle solvent-solvent enthalpy ($H_{N,i} = U_{N,i} + PV_i$) corresponding to a given configuration i of solvent particle coordinates, $\delta V_i = V_i - \left\langle V \right\rangle_{NPT}$ the corresponding instantaneous volume fluctuation. Instantaneous fluctuations allowing the creation of free volumes which are necessary for the insertion of solutes can be shown schematically as such:

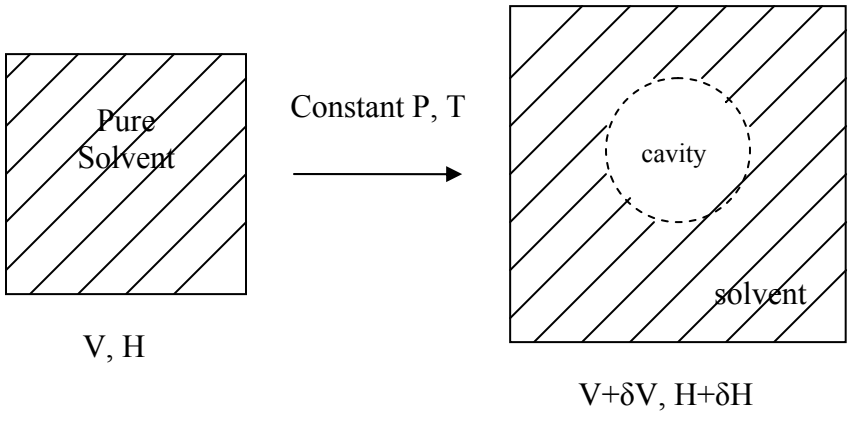

$B_i = \overline{e^{-\beta\psi_k}}$ the solute insertion factor where the horizontal bar indicates an averaging over many random locations in solvent configuration i (ψ_k denotes the solute-solvent binding energy at a randomly chosen kth location in solvent configuration i). The exponential factor $\exp[-\beta\psi_k]$ vanishes whenever the randomly chosen location produces solute-solvent overlaps. Whenever the location is that of an empty cavity suitably large to host the solute, $\exp[-\beta\psi_k]$ is non-vanishing and contributes to B_i. To arrive at an expression with the solvent reorganization enthalpy being proportional to the volume change we combine eqs (4.4) and (4.5) to obtain,

$$\begin{aligned}\left(\Delta H_{vv}\right)_P &= \frac{\left\langle \delta H_{N,i} B_i \right\rangle_{NPT}}{\left\langle \delta V_i \, B_i \right\rangle_{NPT}} \Delta V_S^* \\ &= \frac{\left\langle \delta H_{N,i} \delta B_i \right\rangle_{NPT}}{\left\langle \delta V_i \, \delta B_i \right\rangle_{NPT}} \Delta V_S^*\end{aligned} \qquad (4.6).$$

So far the result is still exact. We now assume that (attractive) solute-solvent interactions do not affect the way solvent molecules reorganize vicinal to the inserted solute. This assumption obviously does not hold for polar solutes dissolved in water (or other polar solvents), where water molecules orient H-bonds towards the solute, but for nonpolar solutes interacting with the solvent through dispersion forces this assumption should be reasonable. The solute, then, merely occupies space and fluctuations of the insertion factor δB_i correlate with the volume fluctuations δV_i; *i.e.* $\delta B_i \sim \delta V_i$. Using this assumption in eq (4.6) yields,

$$\left(\Delta H_{vv}\right)_P \simeq \frac{\left\langle \delta H_{N,i}\delta V_i \right\rangle_{NPT}}{\left\langle \delta V_i^2 \right\rangle_{NPT}} \Delta V_S^* = \frac{T\alpha_P}{\kappa_T}\Delta V_S^* = \left[\left(\frac{\partial U}{\partial V}\right)_T + P\right]\Delta V_S^* \quad (4.7),$$

where we used the NPT-ensemble fluctuation formulas $\left\langle \delta H \delta V \right\rangle_{NPT} = k_B T^2 \alpha_P \left\langle V \right\rangle_{NPT}$ and $\left\langle \delta V^2 \right\rangle_{NPT} = k_B T \kappa_T \left\langle V \right\rangle_{NPT}$. In eq (4.7), $\left(\partial U / \partial V\right)_T$ is the solvent internal pressure, which in terms of state variables P, V, and T reads $\left(\partial U / \partial V\right)_T = T\left(\partial P / \partial T\right)_V - P$ (the thermodynamic equation of state). Finally we recall that in the liquid state the term $P\Delta V_S^*$ is usually small and therefore $\left(\Delta H_{vv}\right)_P \simeq \left(\Delta E_{vv}\right)_P$. We note that in a somewhat different context the significance of the thermodynamic equation of state of water has been emphasized in understanding hydrophobic hydration and hydrophobic interactions.[96,97]

4.3. Computation of thermodynamic data

For the analysis explained in this chapter mainly the trajectories obtained from the simulations performed in the previous study (chapter 3) were used. Besides these to obtain some other necessary quantities, such as isothermal compressibility further simulations performed with the same molecule models as mentioned in the last chapter. In the previous chapter, the determination of constant pressure solvent reorganization energy was done from the simulations by statistical thermodynamic formulations both by subtracting the solute-solvent energy from the total enthalpy and also by direct subtraction of the configurational energies of a (N+1)- and N-particle system $\left[\left\langle U_N \right\rangle_{N+1} - \left\langle U_N \right\rangle_N\right]$. In addition to having provided an independent means for assessing

the accuracy of the finite temperature difference method, these explicit solute-solvent simulations allowed to evaluate the solute-solvent energy as well as the solvent reorganization energy including the separate contributions arising from changes of DMSO-DMSO, water-water, and DMSO-water interactions.

For the determination of constant pressure $(\Delta H_{VV})_p$ from the bulk equation of state, the basic properties such as κ_T the isothermal compressibility of the solvent, α_P the solvent isobaric thermal expansion coefficient and $\left(\partial U/\partial V\right)_T$ the solvent internal pressure are required. These are the bulk properties which can be obtained easily from the experiments as well as by computational means. We calculated α_P, κ_T and $\left(\partial U/\partial V\right)_T$ of all DMSO/water mixtures at 298 K and 1 atm. To obtain κ_T and $\left(\partial U/\partial V\right)_T$ two additional 1 ns NVT runs were performed in which the density was changed by ±2% relative to the state point of interest (298 K, 1 atm). The isothermal compressibility was obtained by monitoring the average pressures in the two runs; *i.e.* $\kappa_T \simeq \left(\ln\left[\rho_2/\rho_1\right]/\left[P_2-P_1\right]\right)_T$ where ρ_1 and ρ_2 are the densities and P_1 and P_2 the pressures. From the same NVT runs the internal pressure was calculated as $\left(\partial U/\partial V\right)_T \simeq \left[\left(U_2-U_1\right)/\left(V_2-V_1\right)\right]_T$ where U_1 and U_2 are the average potential energies of nonbonded interactions and V_1 and V_2 the volumes. The isobaric thermal expansion coefficient was obtained by performing two additional 1 ns NPT simulations in which the temperature was changed ±10 K and the volume response was monitored; *i.e.* $\alpha_P \simeq \left(\ln\left[\rho_1/\rho_2\right]/\left[T_2-T_1\right]\right)_P$.

4.4. Results and Discussion

We tested the validity of eq (4.7) for our system at the various DMSO/water ratios. Table 4.1 presents α_P, κ_T and $\left(\partial U / \partial V\right)_T$ for DMSO/water mixtures at 298 K and 1 atm as predicted by our classical force field.[87] We note that $\left(\partial U / \partial V\right)_T$ was evaluated directly from the nonbonded interactions (see section 3.3 in chapter 3), rather than obtaining it from the computed values of α_P and κ_T, because the latter approach introduces larger errors. Experimental values [98] for $\left(\partial U / \partial V\right)_T$ are included in Table 4.1 as well.

Comparison of the experimental and force-field-predicted internal pressures shows that the model performs quite well between 19% and 64% DMSO. In pure DMSO the model prediction is 10% too high, while in pure (SPC) water the model prediction is 150% too high. The large discrepancy between SPC- and real water happens owing to a significantly too large thermal expansion coefficient of the SPC water model.

Table 4.1. Thermal expansion coefficient (α_P), isothermal compressibility (κ_T) and internal pressure of DMSO/water mixtures at 298 K and 1 atm. Experimental data are denoted within parentheses: (a) ref [98] (b) ref [99] (c) ref [100]

x_{DMSO}	$10^{-4}\,\alpha_P$ (K^{-1})	$10^{-6}\kappa_T$ (bar^{-1})	$\left[\left(\partial U/\partial V\right)_T + P\right]$ (kJ/cm^3)
0.00	7.6 (2.57) [(b)]	54.4 (45.2) [(b)]	0.41 (0.169) [(a)]
0.05	8.7	52.6	0.47
0.10	9.1	51.3	0.48 (0.397) [(a)]
0.19	9.7	51.3	0.57
0.20			(0.550) [(a)]
0.27	9.8	49.4	0.60
0.30			(0.604) [(a)]
0.35	9.7	49.8	0.62
0.40			(0.611) [(a)]
0.48	9.7	48.6	0.60
0.60			(0.565) [(a)]
0.64	9.0	49.4	0.60
0.80			(0.526) [(a)]
0.81	8.9	49.0	0.56
1.00	8.9 (9.3) [(c)]	48.5 (53.2) [(c)]	0.57 (0.510) [(a)]

In Table 4.2 the methane partial molar volumes, solvation volumes and volume expansion terms $\left[\left(\partial U/\partial V\right)_T + P\right]\Delta V^*_{CH_4}$ (eq 4.7) are listed. Comparison of the latter quantity with $\left(\Delta E_{vv}\right)_P$ in Table 3.3 (in the previous chapter) shows that both ways to obtain $\left(\Delta E_{vv}\right)_P$ agree within an accuracy of k_BT on average.

Table 4.2. Methane partial molar volumes ΔV_{CH_4}, methane solvation volumes $\Delta V^*_{CH_4} = \Delta V_{CH_4} - k_B T \kappa_T$ and volume expansion contribution $\left[\left(\partial U / \partial V\right)_T + P\right]\Delta V^*_{CH_4}$ to the constant pressure solvation energies in Table 3.3. The partial molar volumes were obtained from finite volume differences of solute-solvent- and pure solvent constant pressure simulations (see text).

x_{DMSO}	ΔV_{CH_4} (cm^3/mol)	$\Delta V^*_{CH_4}$ (cm^3/mol)	$\left[\left(\partial U / \partial V\right)_T + P\right]\Delta V^*_{CH_4}$ (kJ/mol)
0.00	37.3	35.9	14.7
0.05	37.7	36.4	17.1
0.10	38.6	37.3	17.9
0.19	39.6	38.4	21.9
0.27	40.2	39.0	23.4
0.35	40.7	39.5	24.5
0.48	41.0	39.8	23.7
0.64	41.4	40.2	24.1
0.81	41.8	40.6	22.8
1.00	41.9	40.7	23.2

Note that $\left(\Delta E_{vv}\right)_P$ predicted by eq (4.7) is however systematically larger than $\left(\Delta E_{vv}\right)_P$ obtained directly from the simulations (refer to the Table 3.3 in the previous chapter). We were proposing that this overestimation (rather than an underestimation) could be because of that in writing eq (4.7) the correlation between attractive solute-solvent interactions and solvent-solvent enthalpy fluctuations (present in eq 4.6) is lost so that comparatively large enthalpy- and volume fluctuations therefore contribute in eq

(4.7) with a too high weight because methane-solvent dispersion interactions bias the denser states in which the methane-solvent binding energy is more favorable and of which the instantaneous enthalpy- and volume fluctuations are smaller. However, after the present study, by means of a more recent systematic study of Peter and Van der Vegt [1] we realized that the reason was not related with the solute-solvent but with the solvent-solvent interactions mainly.

In their study Peter et al. discussed whether this is a general result that for all systems the volume relaxation enthalpy provides an accurate estimate of the solvent reorganization enthalpy, i.e., $(\Delta H_{vv})_P \approx T(\alpha_P/\kappa_T)\Delta V_S$, or whether it is limited to small, nonpolar solutes only. The purpose of their study is to examine the range of validity of the above estimate for the solvent reorganization enthalpy. For that reason they studied the solvation of a series of molecular solutes of increasing size in hexane and DMSO pure solvents under ambient conditions. They obtained the changes in solvent-solvent interactions directly from these simulations and compared them to the volume relaxation enthalpy. They discussed the deviations observed due to solute and solvent molecular properties. Furthermore, they investigated the linear dependence of $(\Delta H_{vv})_P$ and ΔV_S and we showed the Figure taken from this work for a better understanding of linear dependence in our system.

For the solvation of various solutes in pure solvents hexane and DMSO, they found a negative deviation of the slope from $T(\alpha_P/\kappa_T)$ showing that $(\Delta E_{vv})_V$ is negative and linearly dependent on the solvation volume. The observation $(\Delta E_{vv})_V \sim \Delta V_S$ indicates that both the hexane and DMSO systems behave in a way in which the nature of the

solvent-solvent interactions cause the cavity. The negative slope deviation from the ideal behavior should therefore be explained in terms of only the pure solvent properties. If, alternatively, solute-solvent perturbative interactions would cause the negative deviation by somehow biasing solvent molecules to adopt (solute-specific) spatial and orientational arrangements in addition to those arrangements imposed by the solute's excluded volume radius, it would be unlikely to obtain the almost perfect linear dependence in ΔV_S as depicted in Figure 4.1. If, however, only the above excluded volume restriction needs to be satisfied, changes of solvent-solvent interactions should somehow grow proportionally to the solute size which in turn is proportional to ΔV_S.

It was surprising that we got so accurate results, even though there was a negative deviation from the ideal behavior for the pure DMSO case. It was also indicating that the assumptions we made for our system worked well. The reason was that in the limit, $\Delta V_S \rightarrow 0$ the solute diameter reduces to a size which is comparable to (or smaller than) the typical free volume in the solvent which is determined by the "packing" of solvent particles, so that the solvent does not need to reorganize to make space for a solute-sized cavity. Therefore, in the limit $\Delta V_S \rightarrow 0$, $(\Delta E_{vv})_V$ should smoothly approach zero, which was actually the assumption we have started with.

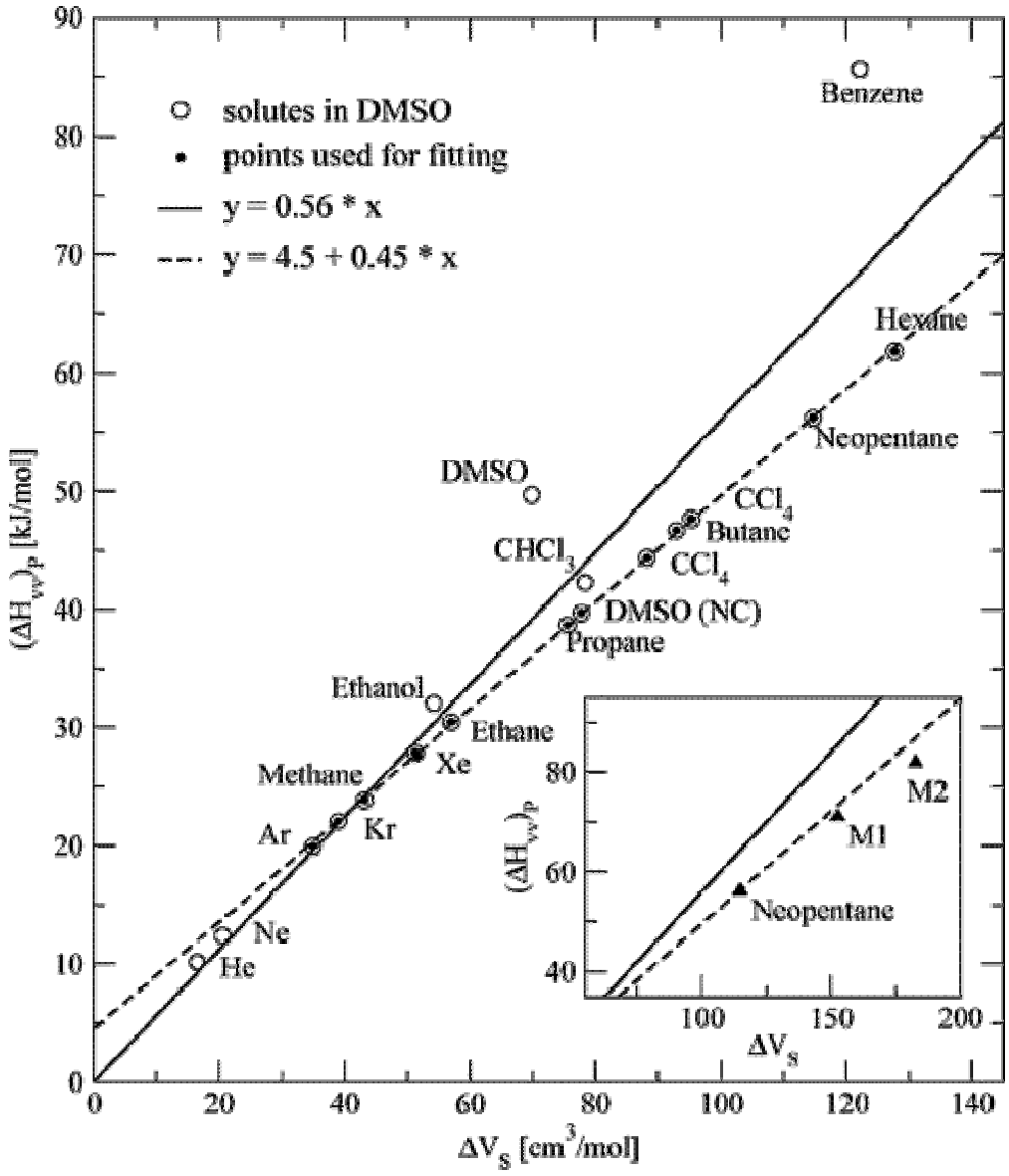

Figure 4.1: Solvent reorganization enthalpy $(\Delta H_{vv})_P$ vs solvation volume of the solute (ΔV_S) for various solutes in DMSO (T = 298.15 K and P = 1 bar): (empty circles) all solutes; (solid line) y = 0.56x = $T(\alpha_p/\kappa_T)x$; (dashed line) linear fit through solutes represented by filled circles ($y = 0.45x + 4.5$); special solutes, (DMSO (NC)) DMSO with partial charges turned off; (M1 and M2 in small panel) *neo*-pentane with modified Lennard-Jones interactions.[1]

This is in agreement with the observation that for solutes smaller than methane (helium, neon, etc. in Figure 4.1), the relation between $(\Delta H_{vv})_P$ and ΔV_S follows the ideal behavior without any deviation.

The accuracy of eq (4.7) opens new avenues not only for obtaining solvent reorganization energies of nonpolar solvation from experimental sources, but also for obtaining (from the same sources) estimates of solute binding interactions with the solution as well as the solute-solvent entropies. Having available the experimental estimates of solute binding interactions should also be of benefit for parameterizing empirical force fields, which, in the case of solvated molecules or liquid mixtures, are often parameterized against thermodynamic properties such as solvation free energies, heats of mixing and solution densities. We take as an example methane hydration in water (298 K, 1 atm). The required experimental data are: $\alpha_P = 2.57\times10^{-4}$ K^{-1}, [99] $\kappa_T = 45.2\times10^{-6}$ bar^{-1} ($T\alpha_P/\kappa_T = 0.169$ kJ/cm^3), [99] $\Delta V_{CH_4} = 37.3$ cm^3/mol,[101] $(\Delta H)_P = -11.5$ kJ/mol.[91] Hence we find $T(\alpha_P/\kappa_T)\Delta V^*_{CH_4} = 6.1$ kJ/mol, and, through eq (4.2), $\Delta E_{uv} = -17.6$ kJ/mol. Our force-field-predicted value is $\Delta E_{uv} = -13.5$ kJ/mol. Using the experimental hydration free energy $\Delta G = 8.4$ kJ/mol, [91] we find the experimental estimate of the solute-solvent entropy: $T\Delta S_{uv} = \Delta E_{uv} - \Delta G = -26.0$ kJ/mol which compares to −22.1 kJ/mol from the simulation. Even though our experimental estimate of the water reorganization energy is an upper bound and the real value is likely to be smaller (by about k_BT), from the experimental estimate of ΔE_{uv} it seems that the methane-water dispersion interaction used in the simulation is slightly too weak. The methane solvation enthalpy in SPC water $(\Delta H)_P = -2.6$ kJ/mol is significantly too high,

however this discrepancy cannot be explained with a too weak methane-water dispersion energy. This deviation clearly is due to a too high internal pressure of SPC water causing a significant overestimation of the water-water reorganization energy. Paschek [68] who, based on the liquid density and structural features, concluded that the SPC model corresponds structurally to water at increased temperature, made similar observations. For a detailed study on water-model dependencies of nonpolar gas hydration enthalpies and entropies we refer to the work of Paschek.[68,102]

4.5. Conclusions.

A procedure to obtain the thermodynamic quantities of the primary and secondary processes from experimental sources discussed so far suggested that these contributions can, under certain conditions, be estimated with additional experimental data on thermodynamic response functions of the pure solvent (coefficient of thermal expansion, isothermal compressibility) and the solute solvation volume. The statistical mechanical quantities defined in the previous section can all be obtained from experimentally accessible solvation data if the constant-volume solvent reorganization energy vanishes, as has been illustrated for the solvation of methane in DMSO/water binary solvents.

By means of this study of solvation thermodynamics, we have shown that quantitative estimates of solvent reorganization enthalpies of the methane solvation in DMSO/water binary mixtures can be obtained from bulk solvent properties. The enthalpy contribution of structural solvent reorganization, $(\Delta H_{vv})_P$, to the constant-pressure solvation enthalpy of methane could be predicted almost quantitatively (within an accuracy of $k_B T$) provided that the solvent thermal expansion coefficient (α_P), isothermal

compressibility (κ_T), and the solute solvation volumes (ΔV_S) are known. In cases where the constant-volume solvent reorganization energy, $(\Delta E_{vv})_V$, vanishes, it is then possible to determine $(\Delta H_{vv})_P$, which is related to its constant-volume analog according to $(\Delta H_{vv})_P = (\Delta E_{vv})_V + T(\alpha_P/\kappa_T)\Delta V_S$, only by the second-the volume relaxation-term. In the last two chapters, we calculated the constant-pressure solvent reorganization enthalpy, solvation volume, and thermodynamic response quantities of the solvent all directly from computer simulations. Studying methane dissolved in DMSO, water, and mixtures of DMSO with water under ambient conditions, we found that for all systems the volume relaxation enthalpy provides an accurate estimate of the solvent reorganization enthalpy, i.e., $(\Delta H_{vv})_P \approx T(\alpha_P/\kappa_T)\Delta V_S$. However, application of the linear correlation approximations we mentioned above requires some caution. For example, for the cases such as a polar solute in a polar solvent (e.g., self-solvation of DMSO in DMSO, and-to weaker extent-$CHCl_3$ and ethanol in DMSO) where due to orientational polarization of the solvent molecules surrounding the solute, the solvent ensemble of the mixture differs from the pure solvent. In such cases where the solute-solvent potential induces a significant change in the solvent configurational entropy in which case first-order thermodynamic perturbation theory fails and the models described by Ben-Amotz [77] are not applicable.

As a conclusion, the real molecular driving force is not the entropy itself but the solute-solvent terms energy and entropy, furthermore these quantities are easily derived from computer simulations but are sensitive to details of the empirical force field. Therefore, comparison with experimental estimates of the solute-solvent energy- and entropy is required instead of free energy or entropy of whole system for development of force fields. We have shown that information on the solvent thermodynamic equation of

state (α_P, κ_T, or $\left(\partial U / \partial V\right)_T$) at the appropriate state point (*P,T*) suffices to estimate solvent reorganization energies within an accuracy of k_BT allowing for experimental assessment of the solute-solvent energy and solute-solvent entropy. In addition to the solvent equation of state data, the latter procedure requires the solvation free energy, solvation enthalpy, and solvation volume from experimental sources. Not only are experimental estimates of solute-solvent binding interactions and solute-solvent entropies of interest per se (*e.g.* to better understand molecular driving forces of specific interactions), but also this will be beneficial for construction or improvement of empirical force fields.

CHAPTER 5

Modeling Solubilities of Additives in Polymer Microstructures: Single Step Perturbation Method based on a Soft Cavity Reference State

5.1. Introduction

We have introduced the basic methods used for free energy calculations to determine solubilities in the methodology chapter. Furthermore, in chapter 3 and 4 we applied these basic approaches to investigate the thermodynamics of preferential solvation of methane in low molecular weight liquid mixtures. In this chapter, we would like to present an advanced methodology to compute via molecular simulations the solubilities of additive molecules whose molecular sizes exceed the typical dimensions of free volume cavities pre-existing in amorphous polymers. We tried to depict this by a

case study on the computation of solubilities of additives based on a single simulation trajectory of a soft cavity embedded in bisphenol-A-polycarbonate microstructure.

Several methods exist already for the calculation of chemical potentials of solute molecules in dense polymer microstructures using computer simulation methods [103]. In particular the test-particle-insertion method by Widom [60] has frequently been applied to gas molecules, [8,81,104-110] because these solutes typically are small (diameters smaller than ~ 4Å) and can readily be inserted in empty cavities pre-existing in all amorphous polymers. However, the case is different for larger solutes. These solutes, which at ambient temperatures usually are in a liquid or (unsaturated) vapor phase, represent a substantially larger perturbation and, unlike in the Widom particle insertion method, usually cannot be inserted "at once". Widom insertion methods combined with excluded volume map sampling (EVMS) [111] and/or Configurational Bias Monte Carlo (CBMC) [112] sampling have been used to compute chemical potentials of larger solutes in polymer microstructures. [107,109,113-115] Even though CBMC has proven to work very well for flexible solutes (*e.g.* alkanes) in low-T_G (rubbery) polymer matrices, both EVMS and CBMC insertion-based methods fail in case the reference ensemble (solute-free polymer matrix) is rigid and does not sample the required cavity spaces needed for solute insertion during a finite length simulation.

Alternatively, one can resort to methods in which the solute coupling with the polymer microstructure is introduced in small steps, thus allowing the solute to enforce its required cavity space and the chain environment to locally adjust to the solute. Thermodynamic coupling parameter integration [116] (TI) or free energy perturbation (FEP) [117] methods are common techniques that can be employed for this purpose.

Although these techniques are seemingly more suitable for larger solutes in rigid polymers, they lack the advantage of insertion-based methods where volume averaging over the entire microstructure is achieved by performing insertions at randomly chosen locations. This becomes particularly problematic in molecular dynamics (MD) simulations of (slow diffusing) polymeric systems where the solute particle, on time scales of nanoseconds, stays trapped inside a local cavity and explores only very small distance scales. Then, several independent TI calculations would have to be performed. This can be done using fast-growth TI [118] and employing Jarzynski's equality [64] for the free energy change as has recently been discussed elsewhere. [119] Alternative to TI and FEP, a staged-particle-deletion scheme (that is based on the inverse-Widom scheme) has been developed [120,121] which can be combined with MD simulations.[122] The idea is to introduce an intermediate stage in the calculation where the solute particle to be removed is substituted by a hard particle. This method, however, faces similar problems as the TI and FEP method in slow diffusing systems.

The above discussion makes clear that alternative free energy calculation methods are needed that alleviate the above sampling problems. In one approach, [123] studied already some time ago, expanded ensemble molecular dynamics (EEMD) simulations were used in which the coupling of the test particle with the rest of the system is continuously changing thereby offering the advantage of sampling the complete simulation cell in relatively short (~ 500 picosecond) MD runs. Although this method turned out being superior in comparison to TI, it requires an umbrella potential that eliminates free energy barriers that may exist at various values of the coupling parameter.

In this chapter we propose and examine an alternative technique that combines the advantages of the thermodynamic integration and particle insertion methods. The new method capitalizes on a judicious choice of a *soft-cavity* reference state, [124] which is defined by the polymeric microstructure in which a soft-core particle has been introduced. By virtue of its optimized softness, the soft-core particle explores the simulated volume on time scales of nanoseconds while at the same time creating the space requirements for insertion of large and rigid solutes. The applicability of this method will be tested in liquid octadecane as well as in a bisphenol-A-polycarbonate (BPA-PC) microstructure. [119,125]

5.2. Methods

Before we introduce the general concept of the method used in this work, we briefly summarize some aspects of the TI and FEP methods used in this chapter.

5.2.1 TI and FEP

5.2.1.1. Thermodynamic Integration (TI). The TI expression for the free energy change of introducing nonbonded interactions between solute and matrix reads [116]

$$\Delta F^{TI} = \int_0^1 \left\langle \frac{\partial V_{sc}(\lambda)}{\partial \lambda} \right\rangle_\lambda d\lambda \qquad (5.1),$$

where

$$V_{sc}(r,\lambda) = (1-\lambda)V\left(\left[\alpha\sigma^6\lambda^p + r^6\right]^{(1/6)}\right) \qquad (5.2),$$

is a soft-core pair potential and $V(r)$ the normal, hard-core, pair potential, which usually includes Lennard-Jones (LJ) and, for polar solutes with partial atomic charges, Coulombic terms. In Eq. (5.2), σ is the LJ size parameter of the atom pair, and $\lambda = 0$ and $\lambda = 1$ correspond to the fully coupled and uncoupled states, respectively. In our calculations, we used a λ-power p=1 and soft-core parameter α=0.7. Because the integration process involves the coupling of a single particle with the remainder of the system, Eq. (5.1) provides the solute excess chemical potential, *i.e.* $\Delta F^{TI} = \mu_{ex}$.

The relation between μ_{ex} and the solute solubility, S, is given by [81], $S = (T_0 / P_0 T)\exp(-\mu_{ex} / RT)$ with commonly reported units $\mathrm{cm}^3(\mathrm{STP})/\mathrm{cm}^3\,\mathrm{bar}$. In this relation, T_0, P_0, R and T are the standard temperature (273.15 K), standard pressure (1 atm.), gas constant and the absolute temperature, respectively.

5.2.1.2 Free energy Perturbation (FEP). The free energy perturbation formula for the free energy difference between two systems *A* and *B* is given by [117]

$$\Delta F_{A\to B}^{FEP} = F_B - F_A = -k_B T \ln\left\langle e^{-\beta(U_B - U_A)}\right\rangle_A \qquad (5.3),$$

where $\beta = 1/k_B T$, with k_B Boltzmann's constant and *T* the absolute temperature, and *U* is the configurational energy with subscripts *A* and *B* referring to the two systems of interest. The angle brackets indicate an ensemble average performed on the *A* system which we call the *reference* (the *B* system is the target). In the calculation of an excess chemical potential by one-step FEP, the *A* system represents the polymer matrix

containing N_S solutes and the *B* system represents the polymer matrix containing $N_S + 1$ solutes. In this chapter we shall be concerned with the case $N_S = 0$.

5.2.2. FEP and TI using a soft-cavity reference state

5.2.2.1. General concept. Fig. 5.1 shows a thermodynamic cycle summarizing the approach examined in this chapter. The horizontal arrow represents the process of introducing nonbonded interactions between the solute molecule and the polymeric microstructure. The solute excess chemical potential amounts to the free energy difference ΔF between the two states connected by this process.

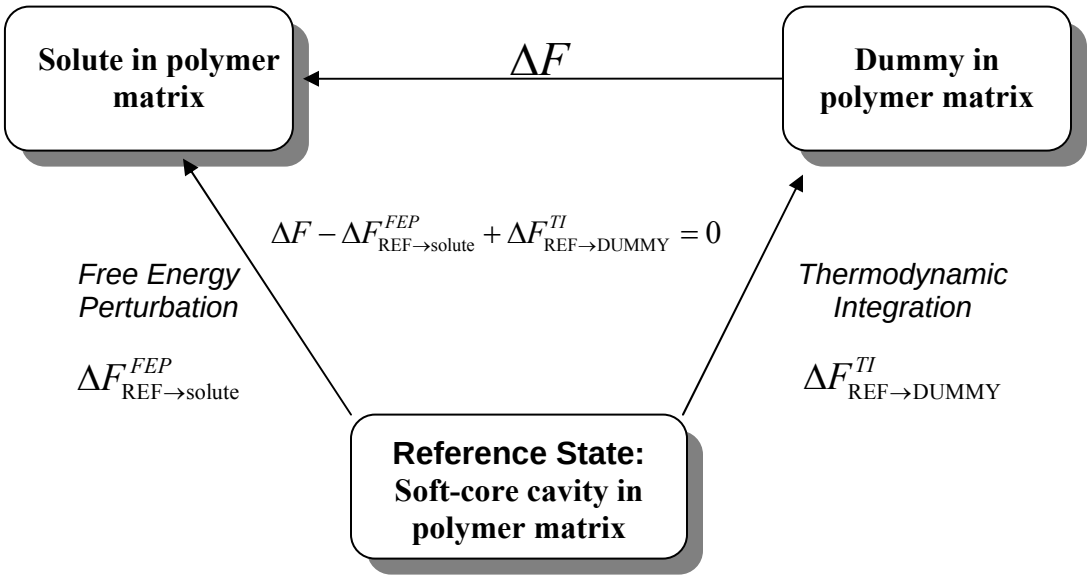

Figure 5.1: Thermodynamic cycle for calculating the free energy change of solvation (ΔF).

TI or FEP can in principle be used to compute this quantity but in practice face severe sampling problems in slow diffusing systems with large-sized solutes. As was mentioned

before, TI suffers from poor sampling over the volume of the amorphous microstructure (diffusion problem); FEP suffers from insertion problems usually encountered in dense systems. Both methods can however be combined in a way that alleviates the sampling problems encountered in either of the two methods. The idea is to introduce a "soft" reference state [124] (Fig. 5.1) corresponding to a soft-core Lennard-Jones particle (defined by Eq.(5.2)) embedded in the matrix. Because diffusion barriers for the motions of the soft-core particle are small, the box volume and relevant cavity spaces can be sampled in a short MD run. The chemical potentials of the solute (Fig. 5.1, upper left corner) and non-interacting dummy (upper right corner) – relative to the soft-core reference – can readily be obtained by FEP and TI, respectively. In the FEP step (*cf.* Eq.(5.3)), the soft-core reference ensemble ("*A*") is used and the perturbation energy $\Delta U = U_B - U_A$ is defined as the potential energy U_B of the system with the real solute (located at the position of the soft particle) relative to the potential energy U_A of the soft-cavity reference system. In the TI step, the soft-core particle is gradually changed into a dummy. Both, the FEP and the TI steps do not suffer from inadequately sampling the volume of the simulation cell. Because the free energy change of the closed cycle is zero, the excess chemical potential is obtained from the difference between FEP and TI free energies relative to the reference state.

5.2.2.2 Choice of the reference state. The above concept introduces an optimization problem that I briefly discuss here and treat in greater detail lateron while discussing the detailed calculations. On the one hand the soft-core reference must to some extent retain the hard-core repulsive nature of the intermolecular potential of any real solute in order to keep the perturbation energy ΔU small. Only then, the configuration spaces of the final

and reference systems have sufficient overlap and the traditional insertion problem can be circumvented. The soft-core particle must on the other hand be significantly softer than real solutes in order to sample overall system volume and the cavity spaces in the microstructure efficiently.

Table 5.1: Parameters for the Reference state Lennard-Jones particles (Eq. 5.2): The A and B references apply to octadecane, the C and D references apply to BPA-PC. $V_{SC}(r=0;\lambda,\alpha,p)$ denotes the maximum of the soft particle – matrix atom potential at full particle overlap. For octadecane $V_{SC}(r=0;\lambda,\alpha,p)$ refers to CH_2 units; for BPA-PC, the aromatic carbons are chosen (the values in parentheses denote the maximum soft particle interaction with carbonyl oxygens). C_{12A} and C_{6A} are the mixed parameters indicating full interaction as state A.

Reference	λ	V_{SC}(r=0;λ,α,p) (kJ/mol)	ε_{SC} (kJ/mol)	σ_{SC} (nm)	C_{12A} (kJ.nm^{12}/mol)	C_{6A} (kJ.nm^{6}/mol)	α	p
A1	0.65	2.6	1.2532	0.8	$3.42058*10^{-3}$	0.099066	0.7	1
A2	0.55	5.4						
A3	0.50	7.6						
B1	0.65	2.6	1.2532	0.6	$6.08790*10^{-4}$	0.041793		
B2	0.55	5.4						
B3	0.50	7.6						
C1	0.80	0.7 (1.1)	1.2532	0.8	$3.34093*10^{-3}$ ($2.89509*10^{-3}$)	0.090065 (0.104589)		
C2	0.60	3.2 (5.0)						
C3	0.55	4.5 (7.1)						
C4	0.45	9.2 (14.4)						
D2	0.65	2.2 (3.5)	1.2532	0.7	$1.12697*10^{-3}$ ($9.22466*10^{-4}$)	0.0523093 (0.0590378)		
D3	0.60	3.2 (5.0)						

We model the soft reference ensemble by running a MD simulation of a softened LJ particle in the polymeric microstructure. The size and softness of this particle is determined through the choice of the parameters λ, α, σ, ε and p in Eq. (5.2). The LJ size and energy parameters σ and ε depend on the atom pair considered and are defined as $\sigma = (\sigma_{SC} \times \sigma_{atom}^{matrix})^{1/2}$ and $\varepsilon = (\varepsilon_{SC} \times \varepsilon_{atom}^{matrix})^{1/2}$ for the octadecane systems. Lorentz-Berthelot combination rules ($\sigma = (\sigma_{SC} + \sigma_{atom}^{matrix})/2$ and $\varepsilon = (\varepsilon_{SC} \times \varepsilon_{atom}^{matrix})^{1/2}$) have been used for BPA-PC to be consistent with the BPA-PC force-field.[126] Because α (=0.7) and p (=1) are kept fixed, the softness is determined by the choice of λ (we refer to this choice as λ^*), which is made based on two criteria: (i) the soft-core pair potential with any of the matrix atoms at full overlap ($r = 0$) should be of the order of the thermal energy $k_B T$ and (ii) $\partial \Delta F / \partial \lambda = \langle \partial U_{sc} / \partial \lambda \rangle$ in the interval $\lambda \in [\lambda^*, 1]$ must be a precisely sampled, ideally monotonic function of λ, because that permits using TI to calculate $\Delta F_{\mathrm{REF} \to \mathrm{DUMMY}}^{TI}$ (see Fig. 5.1) with high accuracy.

Fig. 5.2 (top) shows a "TI-curve" ($\partial \Delta F / \partial \lambda$ versus λ) corresponding to a LJ particle (corresponding to reference state A in Table 5.1) in liquid octadecane. Arrows are included at three values of λ and the corresponding soft-core potentials are shown in the fig5.2 (bottom). The maximum values of the potentials (at $r = 0$) are $k_B T$, $2k_B T$, and $3k_B T$ for potentials A1, A2 and A3, respectively. Although it is clear that $\Delta F_{\mathrm{REF} \to \mathrm{DUMMY}}^{TI}$ will be obtained most accurately with soft-core reference state A1, it is unclear if the corresponding, small barrier height is sufficient to successfully perform the FEP calculation. For this reason three choices are taken for the soft-core reference.

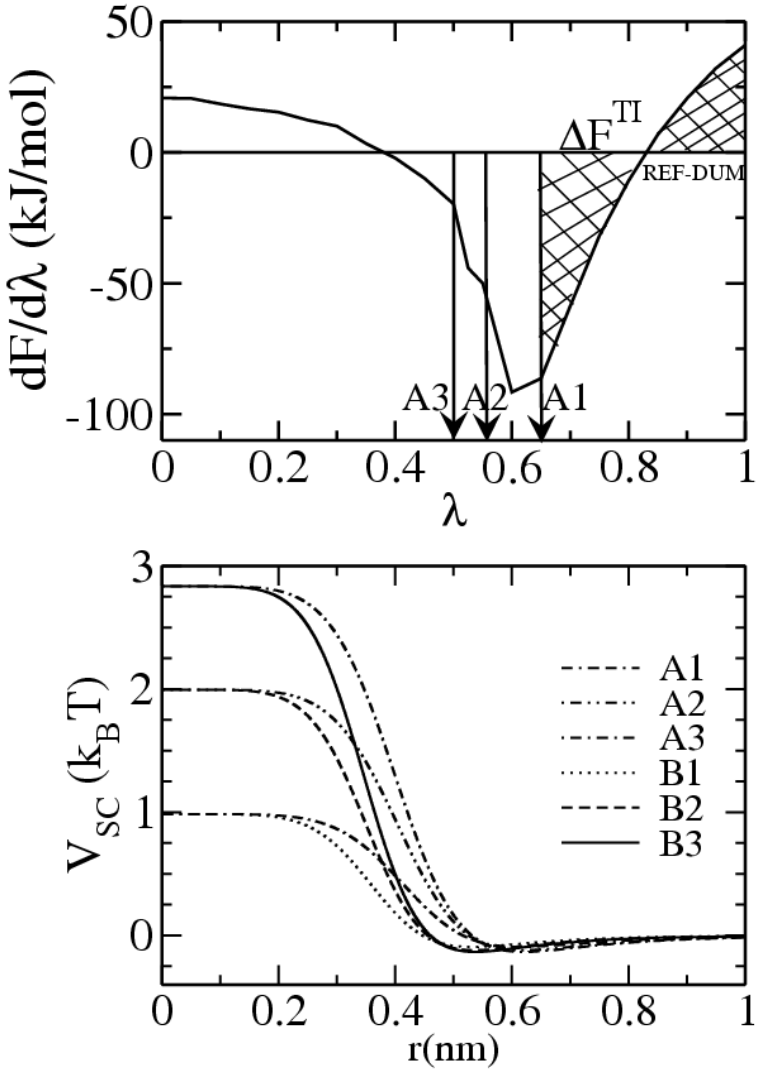

Figure 5.2: top) Region (shaded) depicted for the calculation of $\Delta F^{TI}_{REF \rightarrow DUM}$ for a reference soft core particle A1 from a full thermodynamic integration curve in liquid octadecane matrix with 1ns equilibrium and 1ns run time. References A2 and A3 positions are also shown with arrows with respect to lambda points they correspond. **bottom)** Soft-core potential energy functions $V_{SC}(r;\lambda,\alpha,p)$ of some chosen reference states with the liquid octadecane matrix carbons at 323K.

The parameters describing the soft core Lennard Jones reference states are summarized in Table 5.1. The "A" and "B" reference states are used for the liquid octadecane systems, the "C" and "D" reference states are used for BPA-PC.

5.3. Simulation Details

MD simulations of liquid octadecane were performed with a system containing 200 molecules in a periodic cubic box. The temperature was set at 323 K (corresponding k_BT = 2.7 kJ/mol). The GROMOS 45A3 united atom potential was applied. [127] After including the soft Lennard-Jones particles, all systems were equilibrated for 2 ns followed by 10 ns runs for sampling the soft-cavity reference ensembles. To calculate $\Delta F^{FEP}_{\mathrm{REF}\rightarrow\mathrm{SOLUTE}}$ (see Fig. 5.1), first a back insertion of the soft cavity into its original coordinates in the trajectory was done followed by particle insertion of the real solute. A total of 10^5 insertions of the propane, chloroform and DMSO molecules were performed in each snapshot of the trajectory stored every 1 ps. Solutes were inserted with random orientations, allowing their center of mass positions to fall within a radius of 0.05 nm from the center of the soft cavity. Slow growth TI was used to calculate the excess chemical potentials of the solutes in octadecane. At each λ point, 1 ns equilibration and 1 ns sampling was performed. In total, 22 λ points were used equally divided between 0 and 1. In addition to liquid octadecane, in which the free energy landscape of the solute is very smooth, we modeled a "polymeric" analogue (with a more rugged energy landscape) by increasing the torsion barrier by a factor of 3.5. With the increased torsion barrier, a (volumetric) glass transition temperature was observed of 300 ± 10 K. By simulating this

system at 323 K we model a highly viscous short chain "polymer melt"; we will refer to this system as "viscous octadecane".

In addition to liquid and viscous octadecane, a polymer matrix of BPA-PC was simulated. BPA-PC simulations were performed at 480 K (k_BT = 4.0 kJ/mol). The pressure was 1 atm in all simulations. The BPA-PC simulation box [119,125] contained 50 chains of five monomeric repeat units corresponding to a total number of 9550 atoms. Force field parameters of the BPA-PC all atom model were taken from Ref. [126]. For BPA-PC the simulations were performed with twin-range 0.9/1.4 nm reaction-field electrostatics. The bond lengths in the matrix as well as the internal geometries of the additives were kept by SHAKE algorithm.[43] For the Lennard-Jones interaction a twin-range 0.9/1.4 nm and 1.0/1.4 were used for BPA-PC and octadecane, respectively. To obtain a canonical distribution when the additive is nearly decoupled from the polymer matrix, a local thermostat is required. We chose to use Langevin dynamics with a friction coefficient of 1 ps^{-1}. A Berendsen barostat [45] was used for 1 atm with a coupling time of 5 ps. All simulations were performed by GROMACS software package [39] and for the insertion calculations a version of the package modified by Hess was used.

5.4. Results and Discussion

The single-step perturbation method described in section 5.2 has been applied to liquid octadecane, viscous octadecane and bisphenol-A-polycarbonate. In all systems, the excess chemical potentials of propane, chloroform and dimethyl sulfoxide have been calculated. Because a single TI run for each of the above solutes provides the excess chemical potential with sufficiently high accuracy in liquid octadecane, this system was

chosen as a benchmark for optimizing the parameters characterizing the soft reference state.

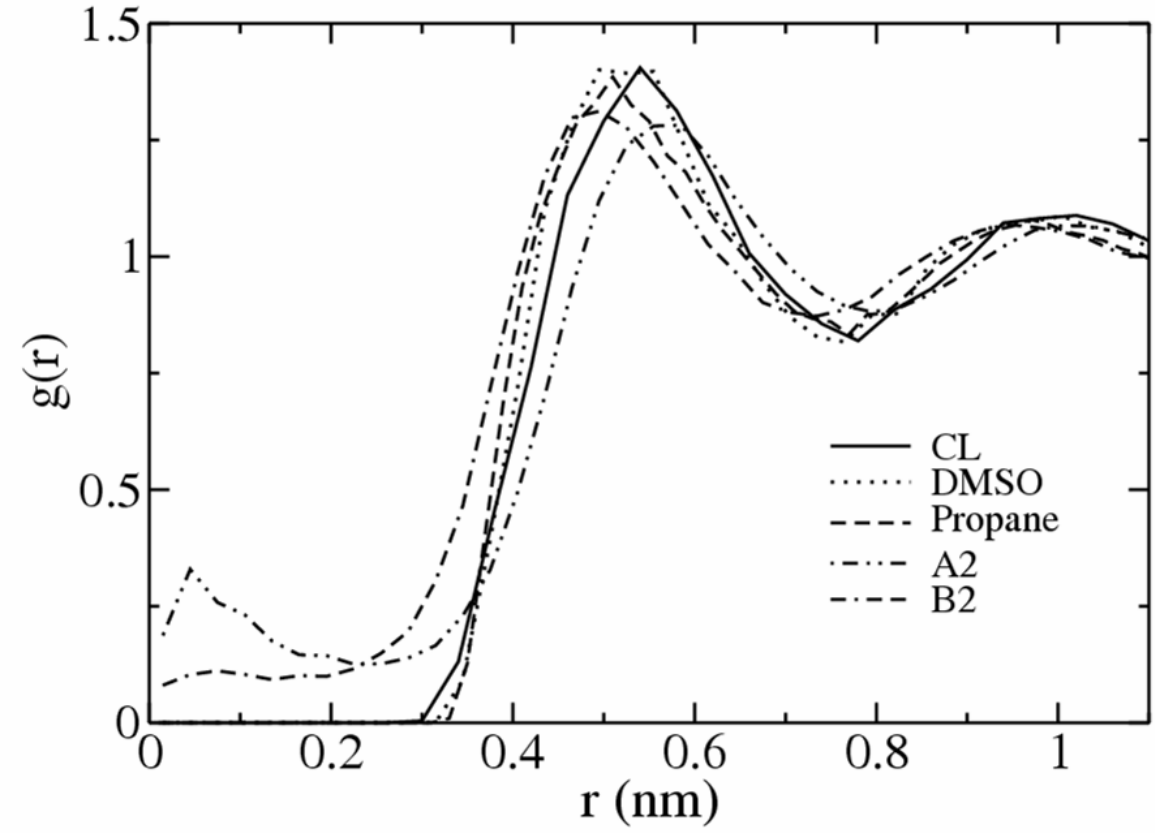

Figure 5.3: Radial distribution functions g(r) of various solutes (chloroform, DMSO, and propane) and some soft-core cavities (A2 and B2) with respect to the distance r(nm) to backbone carbons of liquid octadecane matrix.

Octadecane Fig. 5.3 shows the solute-solvent radial distribution functions (RDFs) together with soft cavity-solvent radial distribution functions in octadecane. The soft-cavity size parameter σ fixes the location of the first maximum of the soft cavity-solvent

RDF, while the potential maximum $V_{sc}(r=0)$ determines the value of the RDF at r=0. While with reference A2 (see Table 5.1) the location of the first maximum is at slightly larger distance than the three solutes, with reference B2 the location of the first maximum is at slightly smaller distance. The overall match between the locations of the first maxima of the solutes and soft-particles is however reasonably good, based on which we decided to use σ=0.6 nm and σ=0.8 nm for the soft-core reference potentials in octadecane (see table 5.1).

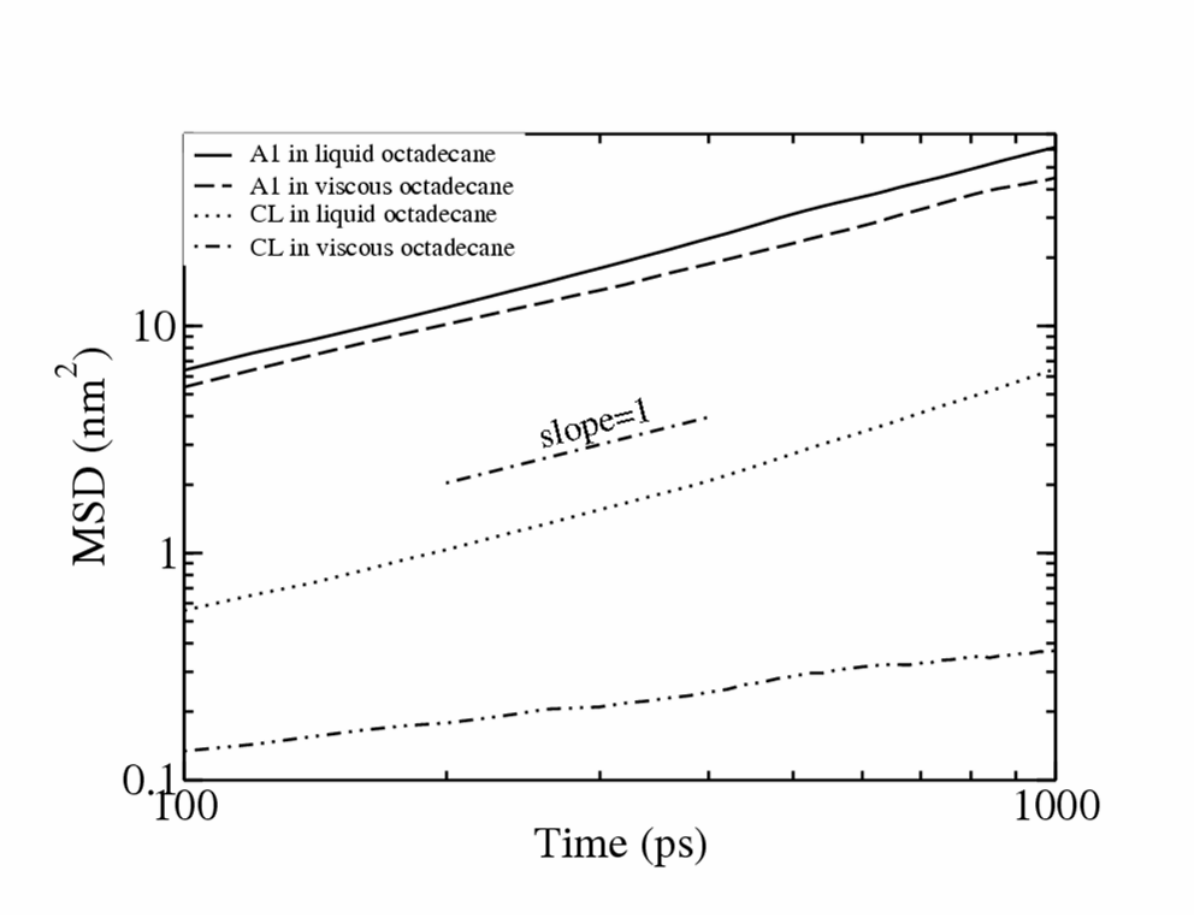

Figure 5.4: Log-log scale Mean Square Displacement curves of various species a real solute chloroform (CL) and a reference core (A1) in liquid and viscous octadecane matrices.

Table 5.2: Free energy changes in octadecane by FEP and TI with long runs of 10 ns and 1ns at each λ, respectively for two methods. Errors (obtained by block averaging) are given in parentheses.

Free Energy Changes in kJ/mol						
Polymer		Reference	$\Delta F^{FEP}_{\text{REF}\rightarrow\text{SOLUTE}}$	$\Delta F^{TI}_{\text{REF}\rightarrow\text{DUMMY}}$	ΔF^{FEP}	ΔF^{TI} (slow growth)
			Chloroform			
Octadecane	Liquid	A1	–16.0 (0.3)	–3.2 (0.3)	–12.8	–14.5
		A2	–25.1 (0.2)	–11.2 (0.9)	–13.8	
		A3	–27.2 (0.3)	–13.2 (1.1)	–14.0	
		B1	–14.3 (0.5)	–1.7 (0.2)	–12.6	
		B2	–20.6 (0.4)	–6.4 (0.6)	–14.2	
		B3	–22.7 (0.4)	–7.8 (0.7)	–14.9	
	Viscous	A1	–15.9 (0.4)	–3.1 (0.3)	–12.7	–14.4
		A2	–26.0 (0.3)	–11.3 (1.9)	–14.7	
		A3	–27.0 (0.5)	–13.1 (2.3)	–13.9	
			DMSO			
Octadecane	Liquid	A1	–18.9 (0.4)	–3.2 (0.3)	–15.6	–16.9
		A2	–27.4 (0.2)	–11.2 (0.9)	–16.1	
		A3	–29.8 (0.3)	–13.2 (1.1)	–16.6	
		B1	–17.3 (0.5)	–1.7 (0.2)	–15.6	
		B2	–23.2 (0.5)	–6.4 (0.6)	–16.8	
		B3	–25.2 (0.4)	–7.8 (0.7)	–17.4	
	Viscous	A1	–18.3 (0.6)	–3.1 (0.3)	–15.2	–17.2
		A2	–28.2 (0.3)	–11.3 (1.9)	–16.9	
		A3	–29.3 (0.4)	–13.1 (2.3)	–16.2	
			Propane			
Octadecane	Liquid	A1	–8.2 (0.4)	–3.2 (0.3)	–4.9	-6.01
		A2	–16.8 (0.2)	–11.2 (0.9)	–5.6	
		A3	–19.2 (0.3)	–13.2 (1.1)	–6.0	
		B1	–6.3 (0.4)	–1.7 (0.2)	–4.6	
		B2	–12.4 (0.4)	–6.4 (0.6)	–6.0	
		B3	–14.8 (0.5)	–7.8 (0.7)	–6.9	
	Viscous	A1	–7.8 (0.5)	–3.1 (0.3)	–4.7	-5.5
		A2	–17.4 (0.2)	–11.3 (1.9)	–6.1	
		A3	–18.9 (0.4)	–13.1 (2.3)	–5.8	

To measure the extent by which the solutes and soft reference particles explore the volume of the simulation box, we examine their diffusion. Fig. 5.4 shows the mean square displacements of chloroform and the soft reference particle A1 in liquid and viscous octadecane. On the presented time scale (1 ns), chloroform in viscous octadecane does not move beyond 0.5 nm. This distance corresponds to the location of the first peak in Fig. 5.4 and indicates that chloroform does not escape its cage formed by first neighbor carbon atoms. Calculation of the chloroform excess chemical potential in this system (using sampling times on the order of nanoseconds) by TI provides the free energy in the local cage rather than a volume-averaged result. The soft-particle (A1) in viscous octadecane performs diffusional motion on this time scale with a mean-square displacement only slightly smaller than in liquid octadecane.

The free energies of propane, chloroform and dimethyl sulfoxide in liquid and viscous octadecane obtained by single-step FEP with the various soft reference states are summarized in Table 5.2. Free energies obtained by TI are included in the last column. The soft cavity FEP data presented for the three solutes are based on a single 10 ns MD run of the soft reference state. The free energies obtained by TI in the last column of table 5.2 however required 44 ns of simulation time for each of the three solutes. Also when taking into account equilibration times and the calculation of the remaining TI contribution $\Delta F^{TI}_{\mathrm{REF}\rightarrow\mathrm{DUMMY}}$ (see Fig. 5.1), the soft cavity FEP method saves considerable computer time in comparison to performing normal TI. The comparison between the soft reference FEP free energies ($\Delta F^{FEP} = \Delta F^{FEP}_{\mathrm{REF}\rightarrow\mathrm{solute}} - \Delta F^{TI}_{\mathrm{REF}\rightarrow\mathrm{DUMMY}}$) and TI free energies ($\Delta F^{TI}$) is very good irrespective of the soft cavity reference state. To investigate the accuracy of the FEP step ($\Delta F^{FEP}_{\mathrm{REF}\rightarrow\mathrm{solute}}$) we present in Fig. 5.5a the probability density

distribution $\rho(\Delta U_{\mathrm{REF}\to\mathrm{DMSO}})$ obtained from the simulation of liquid octadecane. The energies $\Delta U_{\mathrm{REF}\to\mathrm{DMSO}}$ have been Boltzmann weighted over all DMSO insertion attempts per simulation snapshot of the soft reference trajectory before accumulating the histogram. In Fig. 5.5b the quantity $\rho(\Delta U_{\mathrm{REF}\to\mathrm{DMSO}})\exp\left[-\beta\Delta U_{\mathrm{REF}\to\mathrm{DMSO}}\right]$ is presented. This quantity must be sampled well over the maximum down to low energies in order to obtain an accurate estimate of the free energy $\Delta F^{FEP}_{\mathrm{REF}\to\mathrm{DMSO}}$.[128] Comparison of Figs. 5.5a and 5.5b illustrates the importance of sampling the low energy tail of $\rho(\Delta U_{\mathrm{REF}\to\mathrm{DMSO}})$.

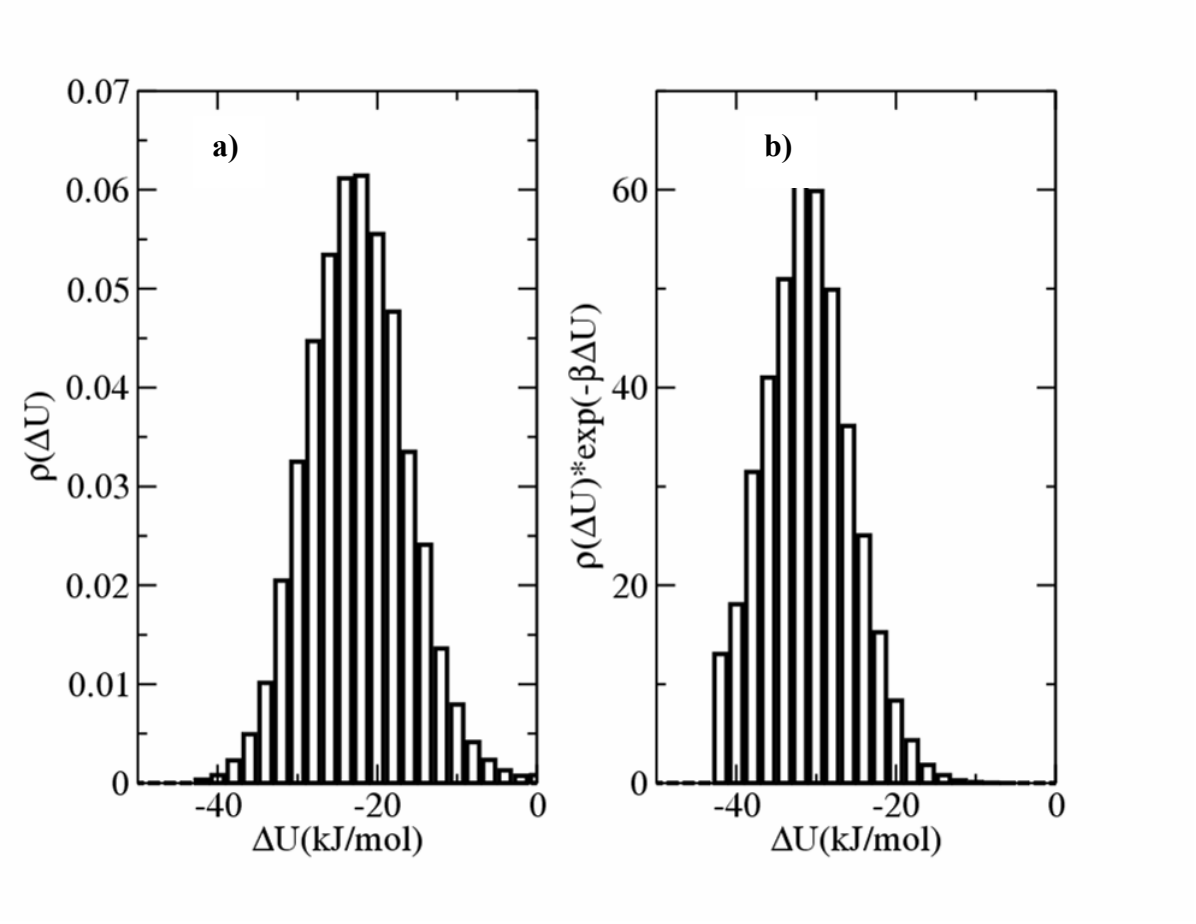

Figure 5.5: a) Probability distribution function ρ(ΔU) and **b)** its exponentially weighted plot ρ(ΔU)*exp(-βΔU) of DMSO perturbation of a reference in liquid octadecane matrix.

Despite solutes being trapped in local cages in the viscous octadecane matrix, the free energies ΔF^{TI} are not significantly different from those in the liquid (Table 5.2). This most probably reflects the chemical homogeneity of the matrix in which the solute-solvent interaction is governed completely by Van der Waals interactions with CH_2 and CH_3 groups.

Bisphenol-A-polycarbonate. The same methodology has been applied to a melt of 50 BPA-PC 5-mers at T=480 K. The chemical structure of BPA-PC includes polar units (carbonate) as well as nonpolar units (isopropylidene) and therefore the solute interactions with the polymer backbone include Van der Waals as well as electrostatic contributions potentially resulting in much greater differences in the free energies of propane (nonpolar), chloroform (slightly polar), and DMSO (highly polar). In contrast to the octadecane system, slow growth TI calculations of solute free energies in BPA-PC produced unreliable data. For example, we performed two TI calculations (23 λ-points, 1 ns sampling per λ-point) decoupling chloroform from the BPA-PC matrix starting off with the chloroform molecule at two different initial locations in the matrix. The resulting free energies were 11.9 and 5.5 kJ/mol. Similar differences were obtained with DMSO and propane. To resolve this problem we performed a large number of fast-growth TIs [118] and used averaging of exponential of the resulting work distributions to obtain accurate solute free energies in BPA-PC. We discuss this fast growth TI approach in greater detail elsewhere. [119] The statistical errors on the free energies obtained from fast growth TI are 0.6 (propane), 1.0 (DMSO) and 1.2 kJ/mol (chloroform). The fast growth TI free energies (ΔF^{TI}) are summarized in Table 5.3 together with the free

energies obtained by free energy perturbation (ΔF^{FEP}) based on the various soft cavity reference states.

Table 5.3: Free energy changes computed for BPA-PC by FEP and TI, with long runs of 10ns and 1ns at each λ, respectively for these two methods. Data for various reference states are given for comparison and the criteria for a good choice of a reference state is discussed in the chapter. Errors (obtained by block averaging) are given in parentheses.

Free Energy Changes in kJ/mol					
Polymer	Reference	$\Delta F^{FEP}_{\text{REF}\rightarrow\text{SOLUTE}}$	$\Delta F^{TI}_{\text{REF}\rightarrow\text{DUMMY}}$	ΔF^{FEP}	ΔF^{TI} (fast growth)
		Chloroform			
BPA-PC	C2	–19.3 (0.7)	–11.3 (2.1)	–8.0	–8.8
	C3	–23.0 (0.3)	–16.2 (2.9)	–6.8	
	C4	–32.8 (1.9)	–16.9 (4.1)	–15.9	
	D2	–13.7 (1.6)	–3.2 (0.6)	–10.5	
	D3	–17.2 (0.8)	–8.1 (1.1)	–9.1	
		DMSO			
	C2	–26.1 (0.5)	–11.3 (2.1)	–14.8	–18.2
	C3	–30.4 (0.4)	–16.2 (2.9)	–14.2	
	C4	–39.1 (0.9)	–16.9 (4.1)	–22.2	
	D2	–20.1 (2.2)	–3.2 (0.6)	–16.9	
	D3	–24.4 (0.5)	–8.1 (1.1)	–16.3	
		Propane			
	C2	–11.0 (0.7)	–11.3 (2.1)	0.3	–0.6
	C3	–14.9 (0.3)	–16.2 (2.9)	1.3	
	C4	–23.9 (1.9)	–16.9 (4.1)	–7	
	D2	–5.2 (1.6)	–3.2 (0.6)	–2	
	D3	–9.1 (0.8)	–8.1 (1.1)	–1	

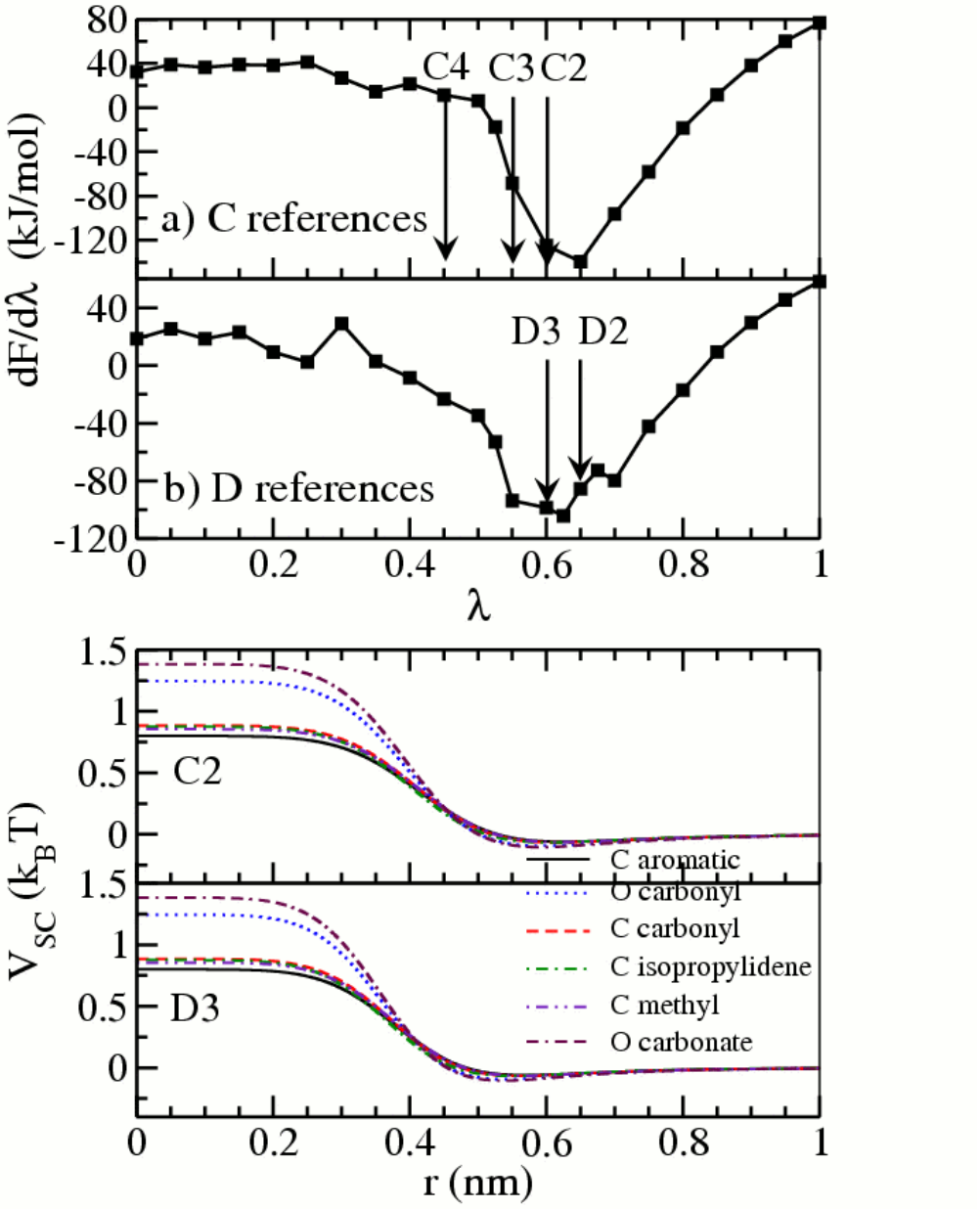

Figure 5.6: top) Thermodynamic Integration curves for the C and D references in BPA_PC with 1ns equilibrium and 1ns run time.

bottom) Soft-core potential energy functions $V_{SC}(r;\lambda,\alpha,p)$ of the references C2 and D3 with the various atom types of the BPA-PC backbone at 480 K.

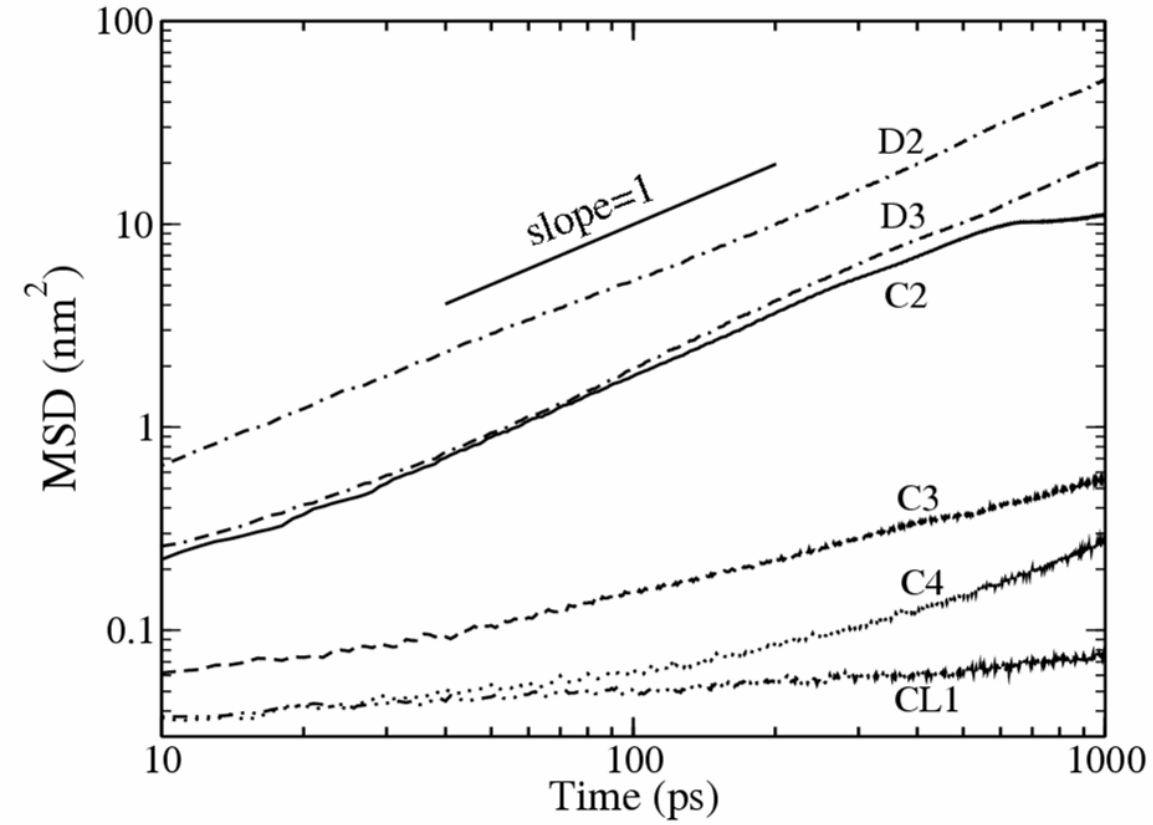

Figure 5.7: Log-log scale Mean Square Displacement curves of various species; a real solute Chloroform(CL1) and references C2, C3, C4, D2,and D3, in BPA-PC.

Fig. 5.6 (upper panel) shows $\partial \Delta F / \partial \lambda$ versus λ for LJ particles C and D (see Table 5.1) in the BPA-PC microstructure. The choices of the λ-values used to define the soft reference states are indicated with the arrows; the corresponding soft-particle potentials for C2 and D3, where only σ differs as a parameter in the potential, are shown in the lower panel. Since BPA-PC contains various atom types, the potentials between soft-cores and these atom types are plotted separately. Fig. 5.7 shows the MSDs of C2, C3, C4, D2, D3 and chloroform in the BPA-PC matrix. In 1 ns simulation time, it is seen

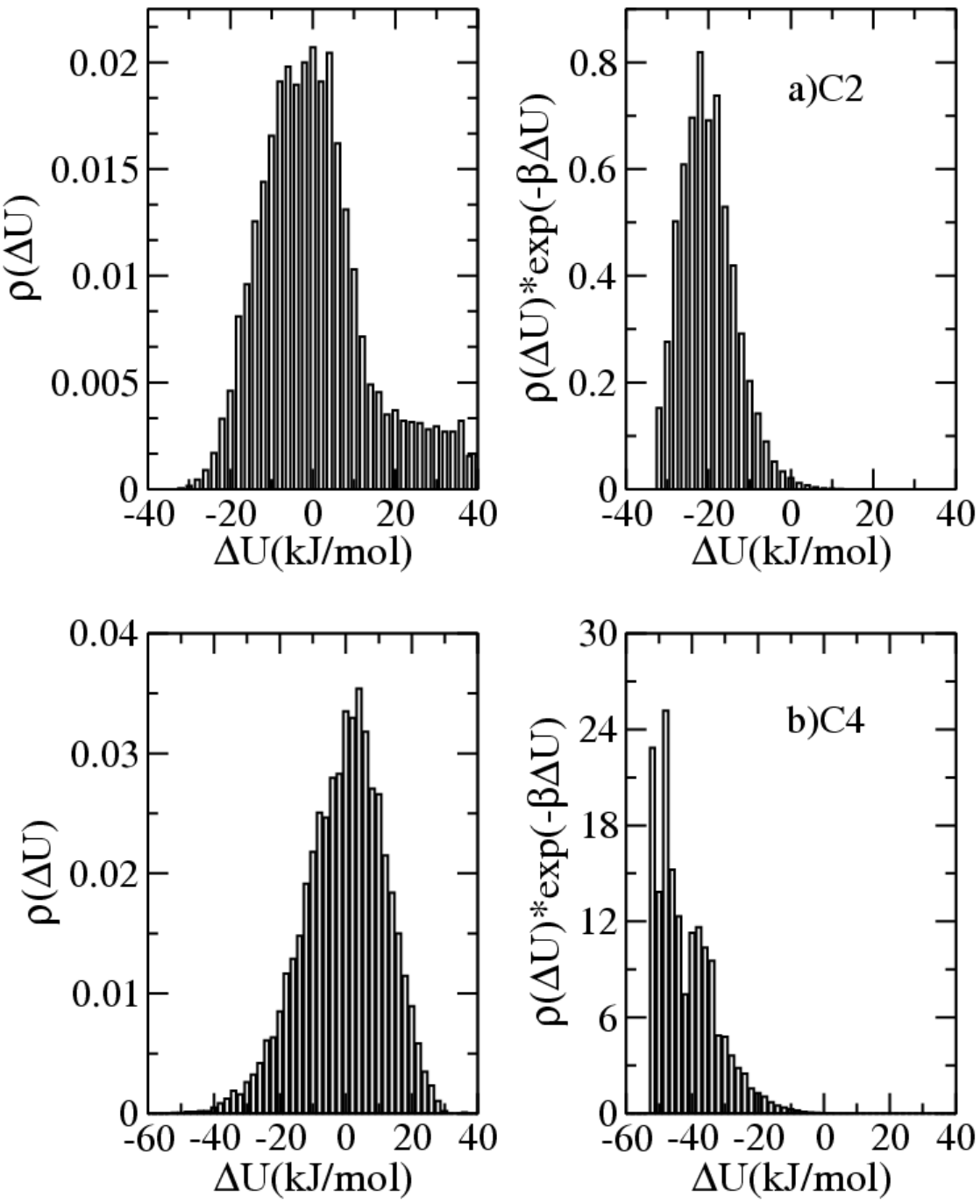

Figure 5.8: left) Probability distribution function ρ(ΔU) and **right)** its exponentially weighted plot ρ(ΔU)*exp(-βΔU) of propane perturbation of a) a good reference C2 and b) a bad reference C4 in BPA-PC matrix.

that C2, D2, and D3 move diffusively and explore most of the simulation volume (the box size is 4.87 nm). C3 and C4 only move over distances up to 0.5-0.7 nm indicating that these reference states are too hard causing the soft particle to stay close to its initial position in the matrix (the BPA-PC monomer size defined through the carbonate-carbonate distance along the backbone equals 1.1 nm). On the other hand, chloroform does not move at all on this time scale. This clearly illustrates that the free energy changes obtained by means of (slow growth) TI using nanosecond simulation times cannot provide reliable results as volume-averaged sampling over the various low energy cavities in the matrix is lacking.

Fig. 5.8 shows the energy distributions $\rho(\Delta U_{\mathrm{REF}\to\mathrm{PROPANE}})$ and the reweighted distributions $\rho(\Delta U_{\mathrm{REF}\to\mathrm{PROPANE}})\exp\left[-\beta\Delta U_{\mathrm{REF}\to\mathrm{PROPANE}}\right]$ obtained with the C2 (upper panel) and C4 (lower panel) reference ensembles. The reweighted distribution based on the C2 reference is sampled with reasonable accuracy unlike the corresponding distribution obtained by sampling the C4 reference state. A similar difference between C2 and C4 emerges with the chloroform and DMSO solutes (not shown). In Fig. 5.9 the running average value of ΔF^{FEP} is shown for chloroform, DMSO and propane. The lines represent the different soft cavity reference states. Based on the 10 ns reference trajectories convergence is achieved with the C2, C3 and D3 reference states. D2 and, in particular, C4 are not converged, which explain negative deviation of ΔF^{FEP} with respect to ΔF^{TI} for D2 and C4 in Table 5.3.

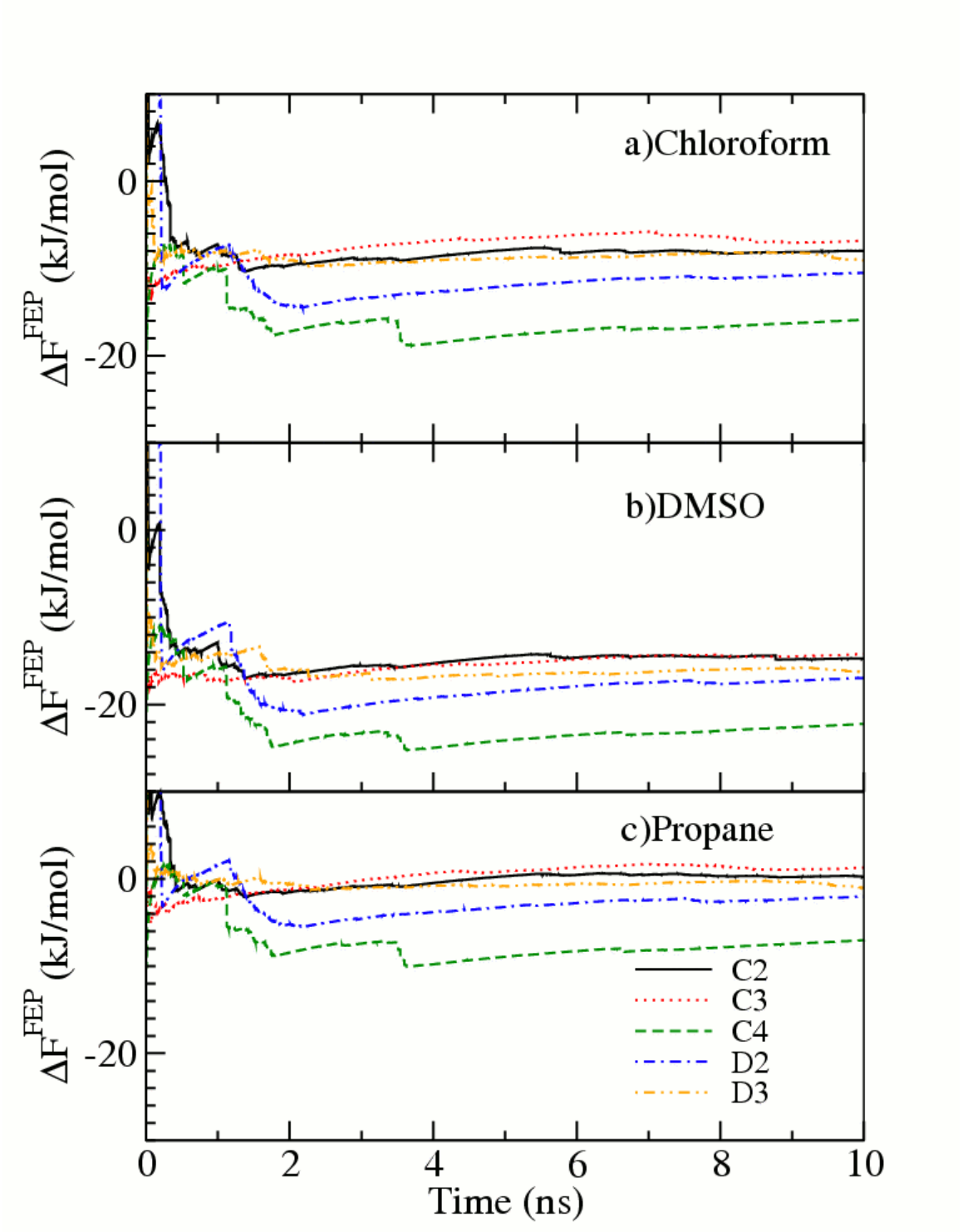

Figure 5.9: Time Running average curves of the Free Energy changes of solvation, ΔF^{FEP}, for the solutes a)Chloroform, b) DMSO and c) propane obtained from the perturbation using various reference states (C2, C3, C4, D2,and D3) in BPA_PC.

5.5. Conclusions

By the help of methodologies explained in the previous chapters, solubility of small gaseous penetrants in polymer microstructures is accessible via molecular simulations. On the other hand, solubilities of large-sized penetrants cannot easily be calculated owing to the complexity of the typical free energy surfaces in dense polymer microstructures. Solubilities of large and internally rigid solute molecules are particularly difficult to obtain since these molecules can neither be inserted at once (by Widom test-particle-insertion) nor be inserted step-wise (in the latter case configurational biasing MC methods [112,113,115] offer advantages with flexible solutes). Because the free energy barriers separating the low energy minima ("cavities") are typically much larger than k_BT, fully coupled, large molecules are moreover prevented from sampling all possible minima during finite time molecular dynamics simulation, which causes slow growth thermodynamic (coupling parameter) integration (TI) methods to be computationally inefficient. In this chapter, slow growth TI is used to introduce a Lennard-Jones particle, which is coupled to the matrix up to a value of the coupling parameter where the particle is still sufficiently "soft" to explore all cavity spaces of the matrix. Based on this system, a long "soft cavity reference-state" trajectory has been generated from which the excess chemical potentials of several solutes have been calculated using a thermodynamic perturbation analysis. This single step perturbation method [124] offers a useful route to calculating solubilities of "bulky" additive molecules inside polymeric microstructures, achieving efficient averaging over the microstructure volume on nanosecond time scales.

In this chapter the method has been applied to liquid octadecane and a bisphenol-A-polycarbonate (BPA-PC) microstructure. The solute excess chemical potentials (free

energies) of propane, chloroform and dimethyl sulfoxide have been calculated and (for BPA-PC) compared with results obtained by an alternative – equally well applicable – fast growth thermodynamic integration method.[119] The comparison illustrates good agreement for soft cavity references in which the soft-core – matrix atom (repulsive) interaction does not appreciably exceed a value of k_BT. Because a *single* simulation of an appropriate reference state potentially provides information for many different solutes, the method is particularly useful for calculating solubility ratios of large-sized penetrant pairs whose relative sizes are comparable.

CHAPTER 6

A Structural and Dynamics Study of an Ionomer

6.1. Introduction

As we have mentioned in the introduction chapter there are two main ingredients to permeation of small molecules in polymer microstructures: solubility and diffusivity. After investigating aspects of molecular solubility in the previous three chapters, here we present the calculation of water tracer diffusion coefficients in a water-swollen ionomer via atomistic MD.

Ionic polymers are composed of linear or branched chains with certain fraction of charged monomers distributed either randomly or regularly in the form of ionic blocks. The ionic polymers with high ion fractions present in dilute solution of a polar solvent such as water are referred to as polyelectrolytes, whereas the ones with low ion fractions (<20%) are called ionomers. In these kinds of systems oppositely charged counterions ensure overall charge neutrality. In an ionomer case, when the energetic cost related with counter ion release is high, these ions are closely coupled to the polymer backbones. When the solvent is water a microphase separation may occur by means of hydrophilic and hydrophobic distribution of the polymer backbone and the ionic charges by means of

electrostatic interactions between the ions and the counterions. This phase separation occurs such that the chains are bridged by ionic species resulting in a transient polymer network formation. According to the distance between ionic groups and amount of solvent, since the nonfunctional part of polymer backbone is apolar, ionomers are capable of absorbing substantial amounts of water in hydrophilic channels. As the hydrophilic and hydrophobic chain parts are well separated, water-swollen ionomers exhibit an interesting micro morphology characterized by hydrophilic domains and channels containing mostly the water embedded in a nonpolar matrix. Structural details in these kind of systems affect the diffusion dynamics of the solvent molecules (which is water in our case) and the ions with a strong dependence on the defree of solvent swelling.

Understanding the spatial arrangement of the components in these systems and the resulting transport behaviour within ionomers is important in various application fields including; proton exchange membranes, biomedical materials, coatings.[129] For studies on the structure formation and related dynamic properties MD simulations offer microscopic insights. In the past, several studies were done to investigate local structures and solvent dynamics in solvent-swollen simple polymers such as polyvinyl alcohol or polystyrene without any ionogenic groups. [130-132] There were also MD studies of polymer/water systems where ions are involved. [113-138] However, in those studies there are either just one long polymer or multiple polymers of short chain lengths. Urata et al. mentioned the significance of chain length in a simulation of Nafion, which is a similar system consisting hydrophobic and hydrophilic regions.[137] Thus, to model the morphology of a water-swollen ionomer one requires many long chains. In addition, periodic boundary conditions may bring about some artifacts in the results. As mentioned

in some previous studies, the morphology of the microphase may be distorted by periodic boundary conditions. [139] For that reason, for the simulation of the diffusion of water in ionomeric materials size effects should be carefully considered. Moreover, in the case of solvent-swollen polymer systems when the polymer concentration is high, different states of solvent molecules were mentioned before [140]. Therefore, for the calculation of diffusivity coefficients in the less water swollen matrices, extra care should be given. The simulations done before had sampling times in the order of 10 to 10^3 ps. This means that either the systems investigated were not too complex or only very fast dynamical processes could be studied with sufficient accuracy. Simulation of these kinds of systems is computationally demanding because of their size and their slow dynamics. Sometimes several computational approaches are used to handle these big systems. For example, generic bead-spring models were used to study structure formation during a microphase separation in ionic copolymers. [139] Also in some cases for computational simplicity, motion of bead-rod chain representing a linear ionomer molecule was calculated just in two dimensions [141]

As mentioned above, there are some nontrivial aspects for the investigation of the dynamics in such systems at the atomistic scale. In this chapter we will discuss these issues, such as the construction of the initial configuration including force field parameterization, effects resulted from the simulation box size, and structural equilibration.

In this study, we performed molecular dynamics simulations of water-swollen sulphonated polyethylene (SPE) system neutralized by sodium ions at the atomistic scale as it is depicted in the following scheme:

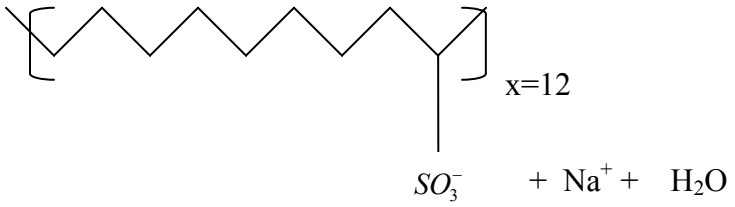

Recently, the most widely used and tested polymer electrolyte membranes are the perfluorinated sulfonated polymers.[142] Among these the mostly simulated one is Nafion, but we have chosen SPE. The reason that we have chosen the SPE system is that it is possible to discuss the simulation constraints with a system similar to, but simpler than Nafion. Also there are some experimental data on SPE related to the transport properties that we aim to reproduce.[143,144] We focused on sodium-neutralized SPE with sulphonation degree of 20% with varying degrees of water swelling as was in the case of the experimental study. [143,144]

The aim of this chapter is to investigate based on an all-atom force field description of a water-swollen sodium-SPE microstructure whether we are capable of (i) achieving full equilibration of hydrophilic/hydrophobic microphase-segregated structure, and consequently (ii) achieving quantitative prediction of water tracer diffusion coefficients and their temperature dependence. The various measures that are evaluated in this study are depicted by configuration snapshots, pair correlation functions, mean square displacements, Arrhenius plots and van Hove correlation functions as well as the xy-projection of water motion through the system.

6.2. System and Initial Structure preparation

To construct an initial model for a SPE chain, statistically independent PE chain conformations representative for melt polyethylene were used. The SO_3^- groups were introduced in these polyethylene conformations according to the above scheme that puts a SO_3^- group on each 10^{th} carbon. Obviously this creates rather arbitrary initial configurations and it remains to be validated if the final system including water molecules and counter ions could be equilibrated with MD. During initial structure preparation, energy minimization in MD were done based on the knowledge of the intra- and intermolecular interactions between the atoms provided by the Gromos 45a3 force field parameters [145]. United atom models were used for CH, CH_2, and CH_3 groups. The water model used in this study was simple point charge (SPC) model.[88] For the insertion of water molecules into the system some of the initially prepared SPE chains were taken out randomly and water molecules were inserted to the possible empty spaces created. After energy minimization, an appropriate number of water molecules were replaced with sodium ions depending on the water ratio desired and the system size. Then they were energy minimized again.

For the force field parameterization of the SO_3^- group, quantum chemical (QC) geometry optimization of the connection unit, i.e. isopropyl sulphonate, was done. QC calculations were performed at Hartree Fock level with 6-31G(d) basis sets by using the Gaussian Software package.[146] Electronic energies at certain geometries were obtained at the MP2 level and point charges were obtained from electron surface potential (ESP) fit using the Merz Kollman method. [147] The minimum energy configuration is shown in Figure 6.1.

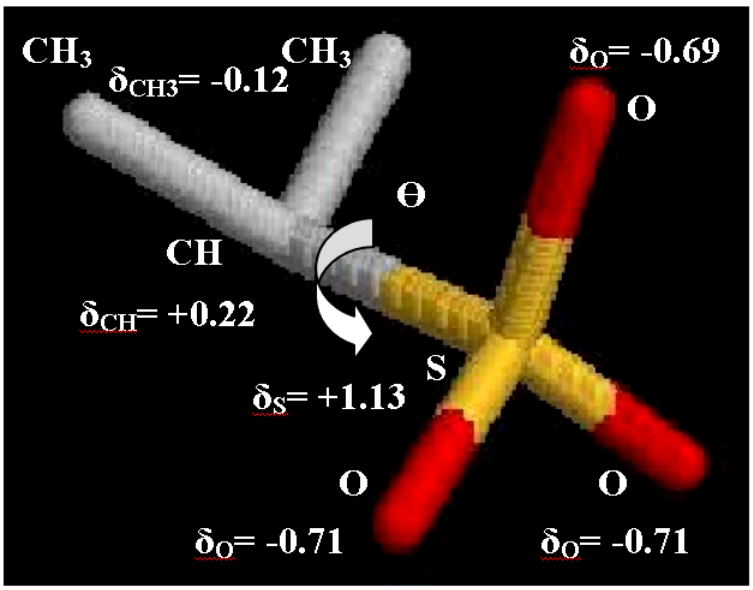

Figure 6.1. The minimum energy configuration of $C_3H_7SO_3^-$ obtained by QC (MP2) energy minimization. Point charges obtained from ESP fit by using Merz Kolmann (MK) method are included. Partial charges on CH_3 and CH united atoms are the added contributions of the carbon and hydrogen atoms obtained from the MK method. θ is the dihedral angle (or the rotation angle of the upper oxygen atom) and the conformation at θ=0 is the one in this figure whose potential energy surface has been determined as minimum . Colors indicate atoms: gray, carbonyls; yellow, sulphur; red, oxygens.

Parameterization of the partial charges on the atomic site positions of the SO_3^- group was done via comparison of the QC derived charges with the charges of the same group in similar polymers simulated before.[136] Thus, in our simulations two different charge parameter sets were used for the SO_3^- group. In addition, two different parameter sets

were used for the sodium ions, Na^+. Combination of the parameters for SO_3^- and Na^+, three parameter sets were used as given in table 6.1.

Table 6.1. Three different types of parameter sets used for the MD simulation of the systems.

Type / Parameter	Type I QC derived SO_3^-	Type II modified SO_3^-	Type III KB Na^+
q_S /e	1.1	1.1	1.1
q_O /e	-0.7	-0.64	-0.7
q_{CH} /e	0	-0.18	0
Na^+ parameters	Gromos[a]	Gromos[a]	KB Na^+ [b]

[a] Berendsen, Straatsma, J. Chem. Phys. (1988), 89, 5876
[b] S.Weerasinghe, P.E.Smith, J. Chem. Phys. (2003), 119 (21), 11342-11349

Type I parameter set include the quantum chemically (QC) derived charges for the sulphonic group connection unit and the Gromos [148] force field parameters for the sodium cation. In type I parameters, only sulphur and oxygen atoms of the connection unit was taken as having partial charges whereas there was no charge on carbon atoms of the connection unit. The type II parameter set consists of modified charges for the connection part $CH\,SO_3^-$ and again the same Gromos force field parameters for sodium ion. In the type II, for a better representation, also the CH carbon atom of the connection unit was considered to carry a charge since ESP depends on the geometry of the molecule considered and the ESP for $C_3H_7\,SO_3^-$ does not necessarily represent that of SPE. Therefore, reference [136] which performed similar QM calculations on SO_3^- connected

to a longer aliphatic chain was used for type II parameters. The type III parameter set has Kirkwood-Buff (KB) sodium parameters [149] while keeping the QC derived charges for the sulphonate group.

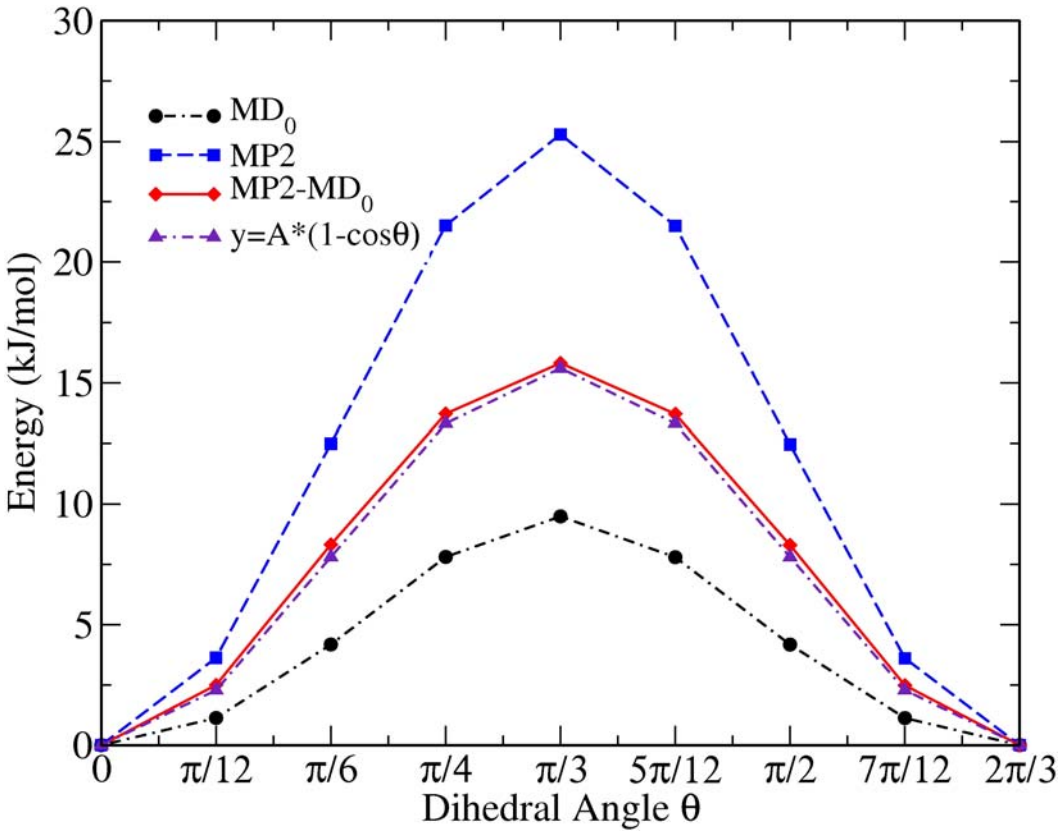

Figure 6.2. The dihedral constant determination for the SO_3^- group by fitting QC (MP2) derived potential energies and the minimized energy with MD parameters (where MD_0 is computed without dihedral parameters). Graphs show the energy variation scanning through the dihedral angle step by step.

The dihedral force constant at the connection unit was determined by fitting QC calculated potentials (MP2) to the potentials obtained by energy minimizations ($MD_0^{/}$) force field parameters:

$$\text{MP2} = MD_0^{/} = MD_0 + y \qquad \text{and} \qquad y = A(1-\cos\Theta)$$

where MD_0 is minimized energy by MD simulation parameters without the dihedral parameter and $MD_0^{/}$ is with the dihedral parameter included. 'y' is the dihedral potential and the dihedral force field parameter A was calculated as A=7.2 kJ/mol. In order to obtain this constant, MP2 ab-initio calculations were performed with 6-31G(d) basis sets by scanning step by step for the dihedral angle Θ. Then, dihedral force constant was fitted by matching the total classical potential energies for this degree of freedom as shown in figure 6.2.

Throughout the simulations, the sulphonation degree was kept fixed at 20%, which means 20% of the repeat units [-(CH_2-CH_2)$_n$-] carry a charged group. This corresponds to a high ionic capacity of 4.41 meq/g PE mentioned in the experimental study [143, 144] referred in the section 6.1. The initially constructed system consists of 10 SPE chains. Each of the chains were 120 C long corresponding to a polymerization degree n=60. The sulphonic groups (SO_3^-) were connected to either each 9th or 10th C atom of a 10C unit in a random fashion. Then, for the systems consisting 80 or 270 chains of SPE, in each direction 2 or 3 times replicated simulation boxes were used respectively. Therefore, in our studies there exist systems with three different sizes at ratio 7.0 and various middle-sized simulation boxes with different water ratios. The systems investigated are tabulated in table 6.2.

Table 6.2. The properties of the systems simulated and the simulation temperatures.

H_2O/ SO_3^- Ratio	Temperature (K)	Parameter Type	Box size (nm)	Number of atoms
2.5	298	I	7.22	Total=21600
	298	II	7.23	OW=2400
	315	II	7.25	Na=S=960
	330	I	7.25	
	330	II	7.27	
5.1	298	I	7.64	Total=29088
	298	II	7.67	OW=4896
	315	II	7.70	Na=S=960
	330	I	7.69	
	330	II	7.72	
7 (small)	298	I	3.97	Total=4245 OW=815 Na=S=120
7 (smallx8)	298	I	7.93	Total=34680
	298	II	7.96	OW=6760
	298	III	7.95	Na=S=960
	315	II	8.00	
	330	I	8.00	
	330	II	8.02	
	330	III	8.01	
7 (smallx27)	298	II	11.95	Total=117045 OW=22815 Na=S=3240
10	298	II	8.38	Total=43200
	315	II	8.42	OW=9600
	330	II	8.45	Na=S=960

In this study, we prepared initial configurations of ionomer systems by including number of sulphonated polyethylene (SPE) chains, water and counter ions. Initially, for the determination of proper simulation box size, three different systems with 10, 80 and 270 SPE chains were prepared at water to sulphonic group (SO_3^-) ratio 7. To investigate the swelling behaviour, also simulation boxes with different water amounts were prepared. The number of water molecules in each simulation box was determined depending on the water to sulphonic group ratio of interest. Thus, they contained 2.5, 5.1, 7 and 10 water molecules per SO_3^- group of the SPE chains. Therefore, from now on the amount of swollen water will be expressed as the ratio of water molecules per SO_3^- group.

6.3. Computational Details:

The simulations were performed with the molecular dynamics simulation software package GROMACS 3.3. [39,40] After the energy minimizations, 20 ns equilibrations were done. Then, molecular dynamics runs of 100 ns were performed using the isobaric and isothermal (NPT) ensemble and then used for the analysis. Temperature and isotropic pressure (1 atm) were regulated according to Berendsen's method [45] with coupling times of 0.2 and 1 ps, respectively. The simulations were done for each system at three different temperatures, 298, 315 and 330 K. The time step was 4 fs. For the non-bonded interactions Lennard-Jones potentials a twin-range cut-off 0.9/1.4 nm and for the long range electrostatics Particle Mesh Ewald (PME) method a real-space cut-off 0.9 nm were used. [57,59]

6.4. Results and Discussion

In this work our aim was to examine the structural and dynamical properties of hydrated SPE. For a systematic modelling scheme, we will consider the system size, structural equilibration by time, swelling behaviour and calculation of diffusion coefficients together with a comparison to experimental values.

6.4.1. System Size:

For the determination of the diffusivity behaviour, possible size effects that might have resulted from the periodic boundary conditions during the simulations should be overcome. To observe the size effects on diffusivity, we simulated three different system sizes with the same water ratio 7 and the same chemical properties. The first, smallest system had 10 chains of 120-carbon long and the second one was created by replicating the smallest system once in x, y, and z direction so that it was 8 times bigger. The third, i.e. the biggest system, was 27 times of the smallest system. As a result, there were 3 systems with 10, 80 and 270 SPE chains. In figure 6.3, mean square displacement (MSD) of water molecules versus time plots were shown for these systems with three different sizes. It can be seen that the size effect disappeared with the second middle sized system, in other words with the system having 80 chains convergence in MSDs with respect to size was observed.

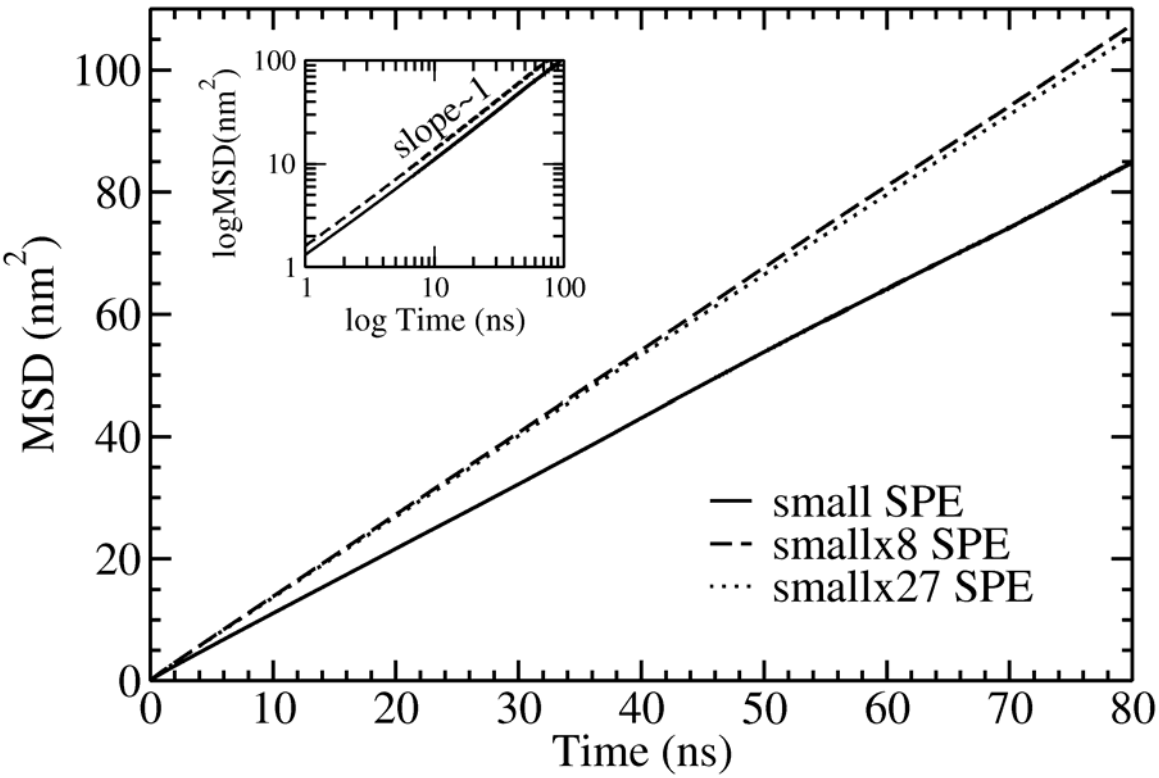

Figure 6.3. Mean square displacement (in 100 ns) versus time plots for three different sized boxes; small box, 8 times, and 27 times the dimension of the small box with H_2O/SO_3^- ratio 7. On log-log scale slope ~ 1.

6.4.2. Structural Equilibration:

The spatial distribution was studied by plotting the pair correlation curves as a function of the separation distance r. Radial distribution function g(r) of carbon to carbon is plotted in Figure 6.4 at different time intervals for middle sized system of ratio 7 with parameter type II. In the g(r) plots, up to three bonds the carbon-carbon correlations were excluded. The peak positions P1, P2 and P3 refer to the high C density regions corresponding to polymer strands. Between P2 and P3 there exists hydrophilic water domains. Since the water domains develop in time the minimum in the C-C RDF between P2 and P3 becomes gradually deeper. When the characteristic peaks P1, P2 and P3 were

investigated, heights of these remain constant after a certain simulation time. As a result, it can be seen from the graphs that convergence was obtained at around 20ns.

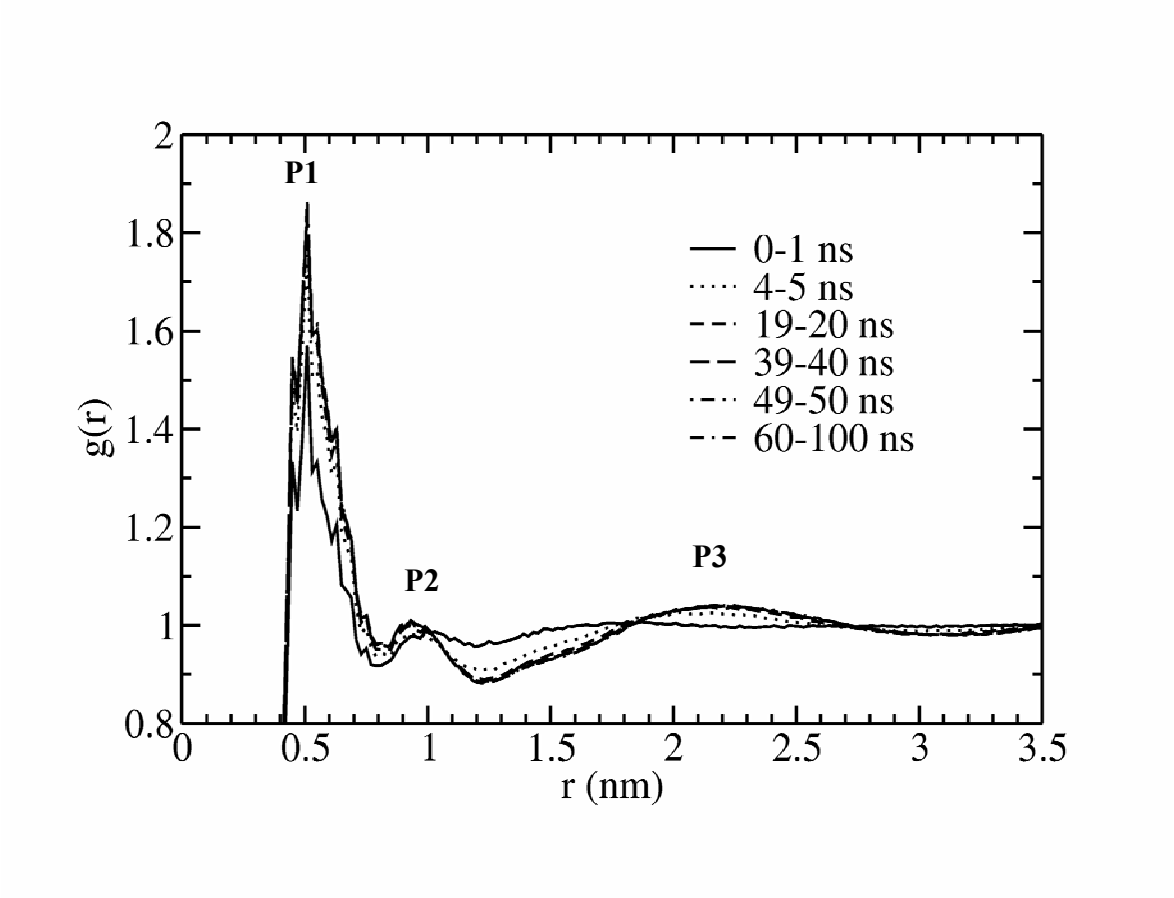

Figure 6.4. Carbon to carbon radial distribution functions at distance r at different time periods in middle-sized ratio 7 type II system at 298K. P1, P2 and P3 are indicated to represent the peaks.

In addition to the g(r)s, were an equilibrated snapshot of a hydrated SPE system is shown in Fig. 6.5. Here, this view is a snapshot of typical time and size converged system with water to SO_3^- ratio of 7 where 80 chains are involved.

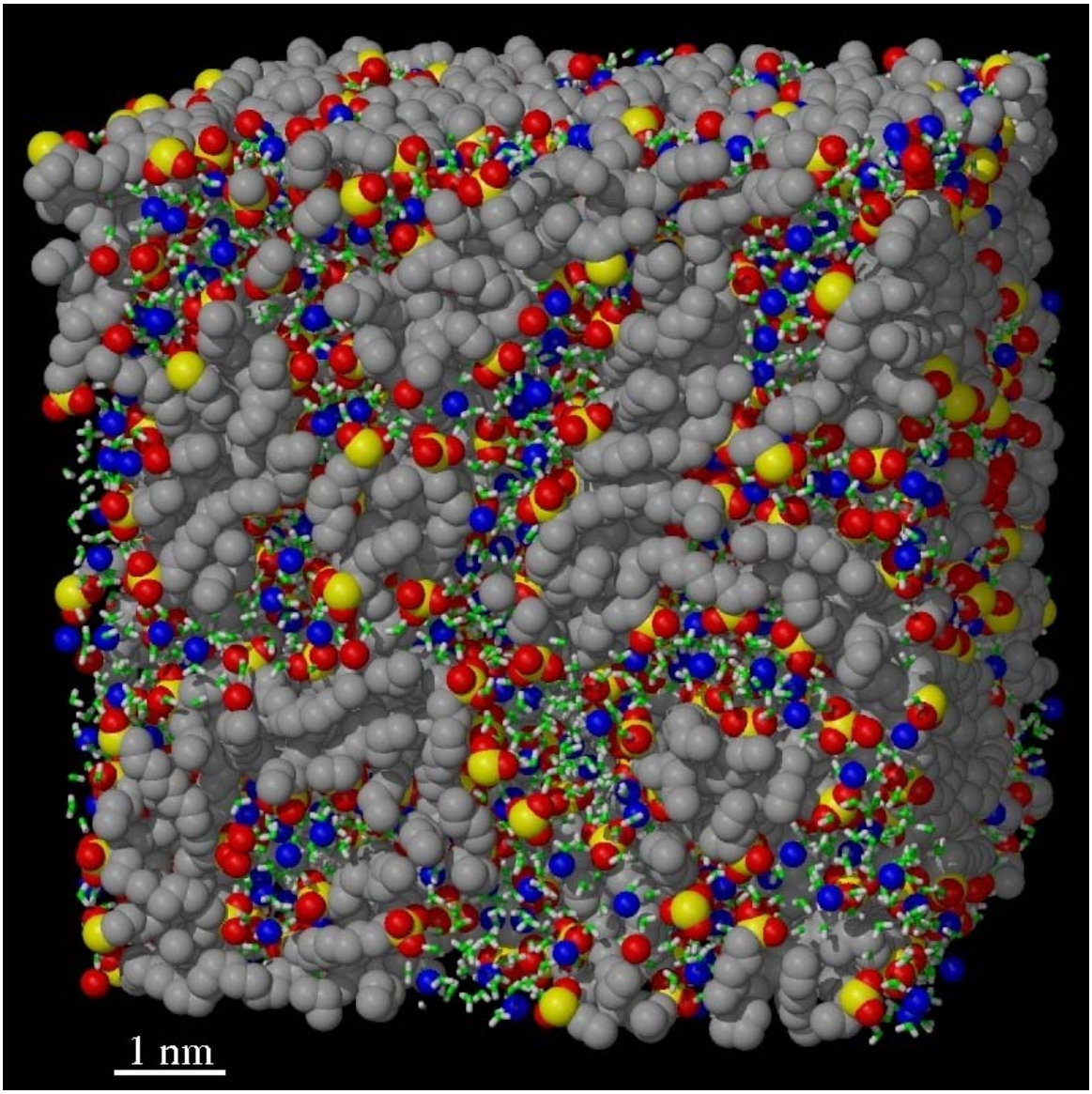

Figure 6.5. Structural view of equilibrated SPE from a snapshot of time and size converged system. Gray CH_2 or CH_3 groups of backbone; yellow, sulphur; red, oxygen atom of SO_3^- groups; green, oxygen atom of waters; white, hydrogen atoms of waters; blue, sodium ions. Linear box dimension is ~8nm and H_2O/SO_3^- ratio is 7.

This typical snapshot, depicted in Figure 6.5, for the water ratio 7 confirms the hypothesis that the hydrated SPE is segregated into hydrophobic and hydrophilic regions. The polymer backbone made up of carbon atoms constitutes the hydrophobic regions, and the hydrophilic regions are constituted by water molecules and the sodium ions. From the figure it is obviously seen that the sulphonate groups tend to be located at the interface between the water clusters and the hydrophobic regions. The sodium ions, indicated in blue in figure 6.5, are embedded in the water channels formed consequently from hydrophilic-hydrophobic phase segregation with hydrated and neutralized SPE system.

6.4.3. Swelling Behaviour:

Furthermore, both from figure 6.5 and the g(r) plot of carbon to carbon, the characteristic length scale was obtained as around 2 nm and the polyethylene backbones come together forming an approximately 1 nm thick structures. Moreover, as can be seen in figure 6.5, which is mentioned before, some of the carbon backbone chains also as in the case of many biosystems in which again the hydrophobicity or hydrophilicity drives the phase separation. In Figure 6.6, radial distribution functions were plotted for various water per SO_3^- ratio systems. In this plot while the first peaks P1 and P2 remain approximately at the same position, the distance between P2 and P3 increases with the rising water ratio and P3 shifts to larger scales. It can be seen that with the change in the water amount, characteristic length scale also shifts, indicating the water swelling.

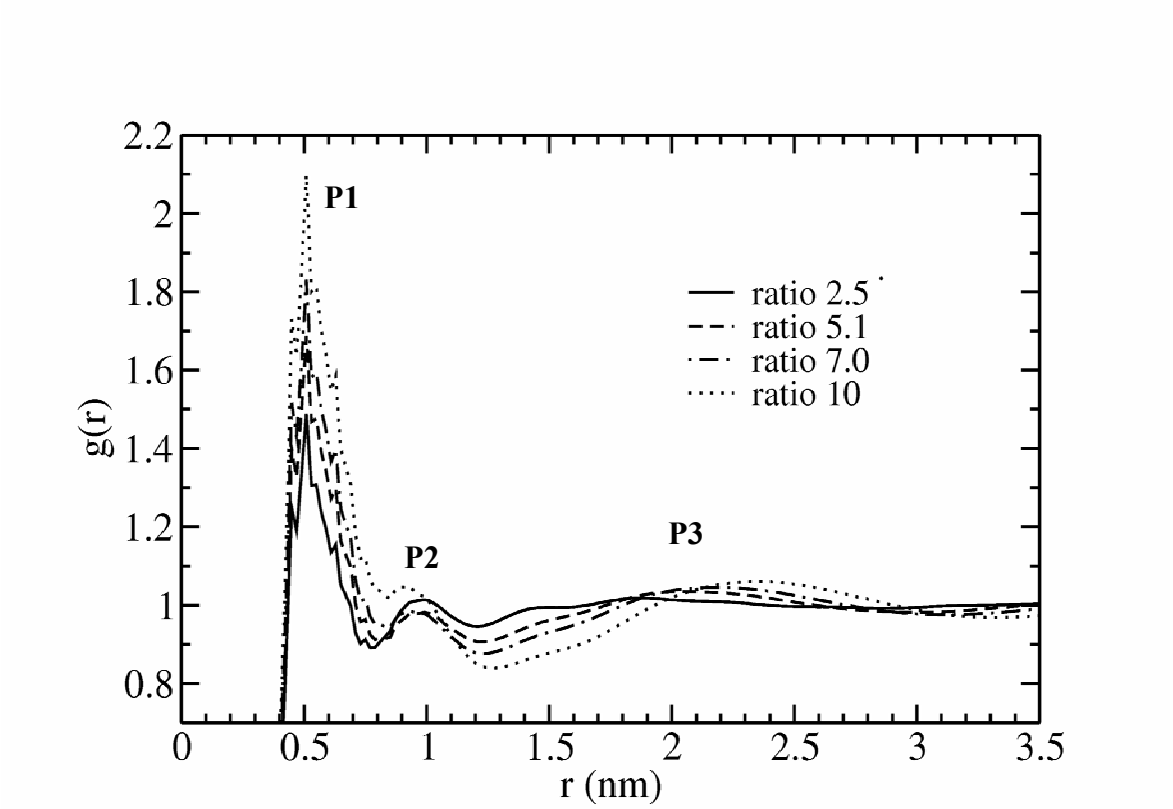

Figure 6.6. Carbon to carbon radial distribution functions at distance r for various water per SO_3^- ratios.

6.4.4. Diffusion coefficients:

In atomistic modelling the diffusion coefficient D can be determined by taking the slope of the mean square displacement (MSD) versus time curve and dividing by 6:

$$D = \lim_{t\to\infty} \frac{1}{6t} \left\langle (\vec{R}(t) - \vec{R}(0))^2 \right\rangle$$

However, for this calculation it is essential that the Einstein diffusion regime is reached. It means that MSDs should be linearly dependent on time. If the surroundings inhibit the free movement of the particle, for instance if it is confined a while to a small space

limited by the polymer chain, the diffusion is called anomalous diffusion. In this case $\left\langle [R_i(t) - R_i(0)]^2 \right\rangle \propto t^n$ where n <1, and mean square displacement MSD versus time curve is not linear.

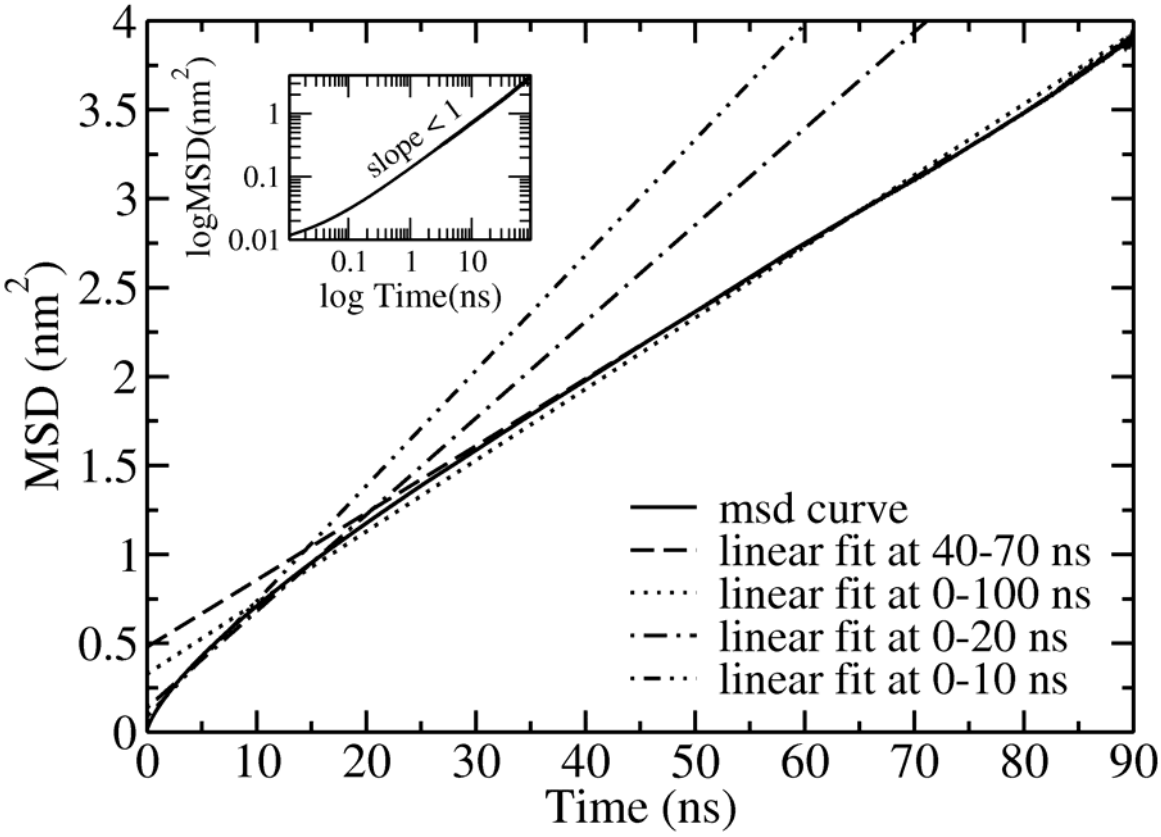

Figure 6.7. Mean Square displacement curve for ratio 2.5 at 298K with parameter type II and the linear fitting curves at different simulation times.

During the calculation of diffusion coefficients, the MSD for the oxygen in the water molecule was plotted as a function of time. MSD curve as a solid line and linear fitting curves belonging to the water ratio 2.5 system were plotted in Figure 6.7. By investigation of the linearity of the MSD curve for the lowest water-ratio system, the

correlation coefficient was calculated as 0.9998 for the part in between 40 ns and 70 ns. However, when only linear fitting between 0 to 10 ns plotted, there is 62 % variation in the diffusion coefficient (slope <1 on log-log scale). With a linear fit between 0 to 20 ns, this reduces to 36%. As it is shown in figure 6.7, also linear fit was done for all data, 0 to 100 ns, including the non-linear initial part. The difference in linearity causes the diffusion coefficient to have 6 % error in this case. In figure 6.8, the motions of a randomly chosen water molecule are shown to see whether the diffusion of the water molecules is limited by the polymer matrix. As it is shown in figure 6.8 part (a) it was observed that during the simulation time a water molecule can walk all through the box within the high water ratio 7.0 system whereas a water molecule may come across some obstacle effects within the lowest water ratio 2.5 system as it is shown in figure 6.8 part (b). As a result, for the low water ratios 20 ns is not enough to reach the Einstein type of diffusion. The diffusion coefficient should be calculated from the linear part of the MSD versus time curve without considering the initial non-linear portion.

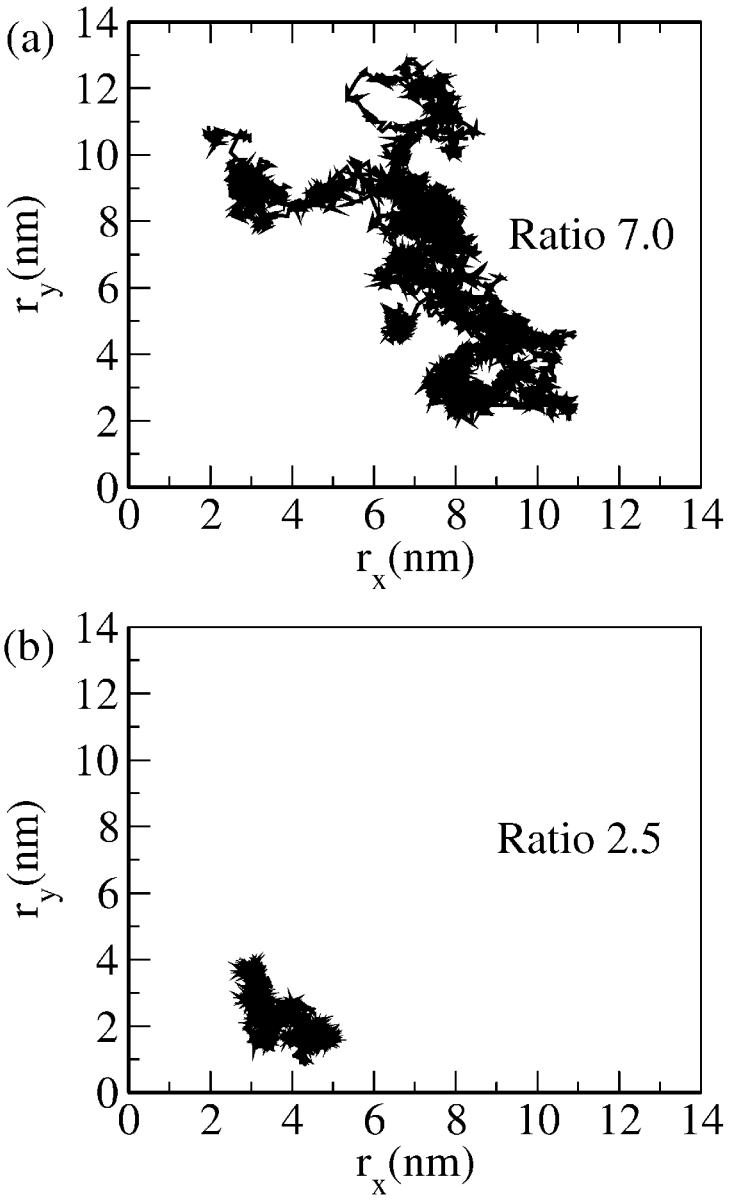

Figure 6.8. 100ns-Trajectory of motion of a water molecule on x-y plane part (a) in the ratio 7.0 system, part (b) in the ratio 2.5 system at 298K.

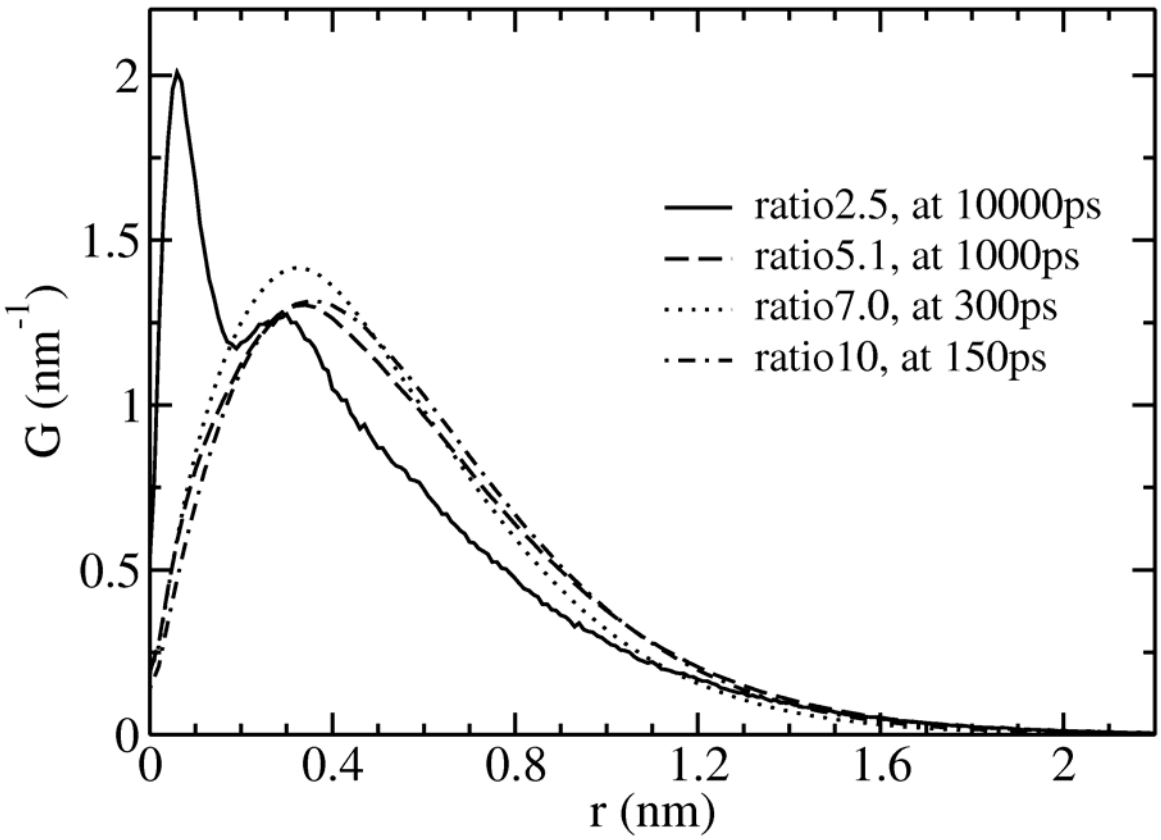

Figure 6.9. Van Hove functions for particles in group OW in different water ratio systems with parameter type II within different time periods.

To study the region where anomalous diffusion regime appearing in the self diffusion of water molecules in Na-SPE system, van Hove self-correlation functions $G_S(r,t)$ were used. The van Hove functions exhibit a shoulder or a double peak form in the anomalous regimes. $G_S(r,t)$ gives the probability density that a water molecule moves a distance r over a given time interval t:

$$G_S(r,t) = N^{-1}\left\langle \sum_{i=1}^{N} \delta[\vec{r} - (\vec{r}_i(t) - \vec{r}_i(0))] \right\rangle$$

$G_s(r,t)$ functions were plotted in Figure 6.9 for each different water ratio system simulations at 298K with type II parameter set. From these plots, it can be seen that for the lowest ratio, 2.5, system with lowest temperature 298K, even in time scales of 10 ns there are two peaks indicating that there are still some tightly bound water molecules in this system whereas in the higher water ratio systems there is only one peak within the same distance r range even for shorter time intervals. Therefore, we can conclude looking at both the snapshots, and the xy-projections of a water molecule within the matrix (fig 6.8), that when water ratio is high the hydrophilic channels are connected. This enables the water molecules to diffuse within the polymer matrix. However, at low water ratios (ratio 2.5) water molecules are mostly trapped in unconnected hydrophilic regions.

To investigate the motion of water molecules through the polymer matrix, the diffusivity of the water molecules in the polymer systems with different water content were studied at the three different temperatures. All the diffusion coefficients at each different ratio and temperature, and obtained with different parameters are tabulated in Table 6.3. The diffusion coefficients calculated were shown in Figure 6.10 in the form of an Arrhenius plot. Activation energies obtained from the slope of this curve are tabulated in Table 6.4. In Figure 6.10, the diffusion coefficients obtained from our simulations by applying different force field parameters were compared with the previously published experimental diffusion coefficients obtained by pulsed-gradient spin-echo NMR (PGSE-NMR).[150] Thus, in such a complex ionomer system, it can be seen that it was achieved in this study to reach the real behaviour of diffusion coefficients in the same order of magnitude as the experimental.

Table 6.3. The diffusion coefficient data used for the Arhenius plots

H_2O/ SO_3^- ratio	Temperature (K)	Parameter Type	$D_{OW}*10^5$ (cm^2/s)
2.5	298	I	0.0050(±0.0005)
	298	II	0.0064(±0.0004)
	315	II	0.0146(±0.0002)
	330	I	0.0210(±0.0007)
	330	II	0.0274(±0.0001)
5.1	298	I	0.0396(±0.001)
	298	II	0.0745(±0.002)
	315	II	0.1521(±0.0)
	330	I	0.1767(±0.006)
	330	II	0.2526(±0.0007)
7	298	I	0.1291(±0.0001)
	298	II	0.2227(±0.004)
	298	III	0.2506(±0.005)
	315	II	0.3689(±0.002)
	330	I	0.3767(±0.02)
	330	II	0.5574(±0.01)
	330	III	0.6862(±0.02)
7	298	II	0.2190(±0.002)
10	298	II	0.5334(±0.002)
	315	II	0.8184(±0.01)
	330	II	1.1193(±0.02)

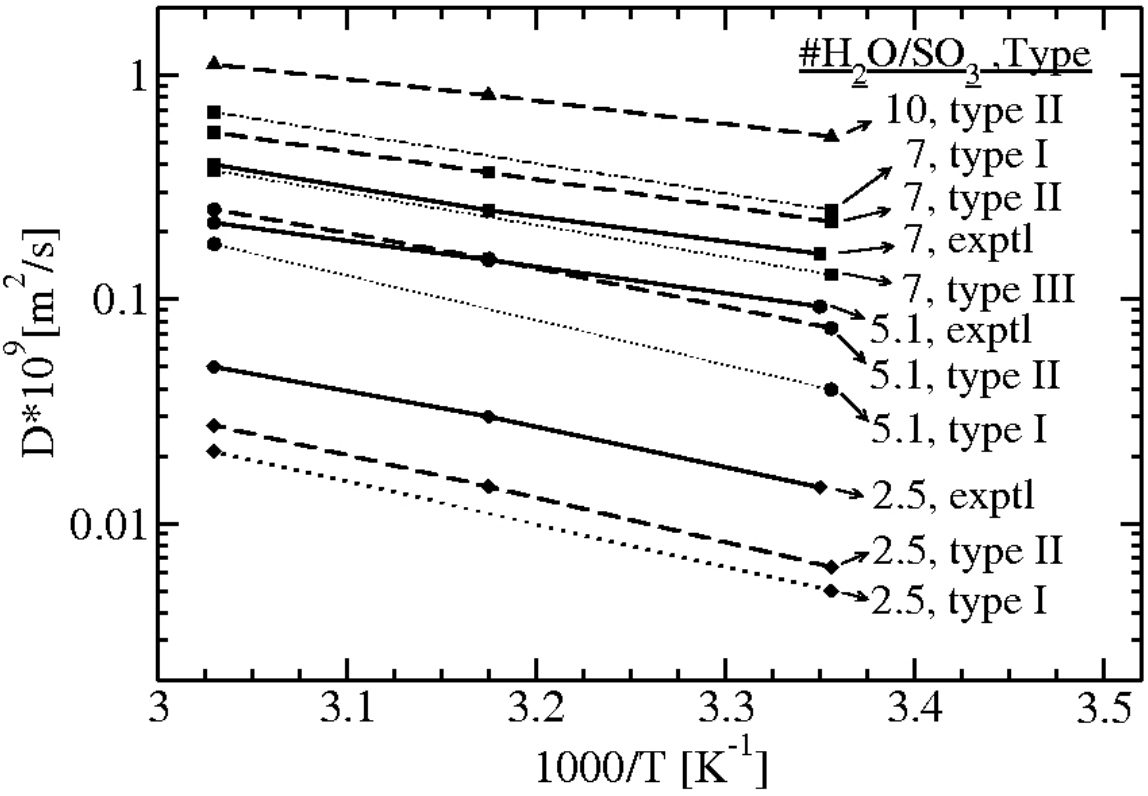

Figure 6.10. Arhenius plots showing the diffusion coefficients of water molecules obtained both experimentally and from the simulations done with different parameter sets and for different water ratios.

Table 6.4. Activation energies obtained by considering the simulation runs with the type II, modified SO_3^- parameters.

H_2O/ SO_3^- ratio	**E_A calculated (kJ/mol)**	**E_A experimental (kJ/mol)**
2.5	37.19	36.1 ± 1.1
5.1	35.17	25.8 ± 0.3
7	23.43	22.4 ± 0.2 (extrapolated)
10	18.97	no data
Bulk water		~17

6.4. Conclusions

In this study, water-swollen ionomer SPE systems with 4 different ratios of water per sulphonic group were simulated atomistically at three different temperatures with three different parameter sets. First of all, for the initial structure preparation we have done a few force field parameterizations. Then, the efforts put on to obtain a structurally equilibrated system with time convergence and without any size effects. Lateron results were analysed in details to observe the structure formation and swelling behaviour of the SPE ionomer. Finally, the studies were done on the diffusion of water through the ionomer and the restriction conditions were discussed.

For the proper choice of box size to reach a convergence, three different systems were generated with ratio 7 at 298K, including a small box, a 8 times bigger and a 27 times bigger of the small one. From the slope of MSD versus time curves, it is seen that the size convergence was reached with the middle-size whereas the first box was too small having different slope from the other two bigger systems. As a result, it is concluded that at least a system box with 80 chains of 120C long having totally 34680 atoms was large enough for the system of interest to obtain data comparable to experimental ones.

While performing structural analysis, the variation in the micro structures, such as swelling of the water channels and characteristic length scales increases with the increase in the water amount is easily observable by looking at the radial distribution functions and simulation snapshots. Furthermore, information on the local structural behaviours could be obtained. With the decreasing water to SO_3^- group ratio, inhomogeneities

increase resulting in two different groups of waters. As concluded from the Van Hove plots, there are some restricted water molecules even in 10 ns time scales since there are relatively less-connected water channels when the water amount is low. Together with the MSDs, it is observed that for high water ratios at least 20 ns equilibration time is required to obtain accurate diffusion coefficients in the normal regime whereas for low water ratios as 2.5 even longer equilibration times were required of up to 60ns. By looking at the linear fitting curves at different time scales in the MSD curves, it is observed that, especially in the low water contents, there might be errors in diffusion coefficients up to 60 % when only 10 ns simulation results were used. Requirement to reach the Einstein behaviour becomes important in these cases.

When the diffusivity of water through the water channels formed within the polymer was investigated, it is seen that the diffusivity of water shows a strong dependence on the water content and also on temperature. The diffusion coefficients are in the same order of magnitude as the experimental ones and also the activation energies fit quite well. For the universal behaviour the activation energy has to be close to that in the bulk solvent, (ca 17 kJ/mol). A significant increase of the activation energy is normally an indication that the polymer matrix becomes closely involved in the diffusion process.

For this kind of MD simulations, it must be remembered that the accuracy of the force field and other approximations embodied can affect the diffusion of water or any other particle in the system. In this study, even when different force field parameters were used, the diffusion coefficients remain predictive by being in the same order of magnitude with a similar slope which gives information about the activation energies.

From the overall study, the importance of size and time convergence requirements for this kind of water-swollen ionomer systems is seen obviously. As all our simulations have a length of 100 ns, we can conclude that they have converged at least for the properties we have analyzed in details so that predictive results for the system come out.

Consequently, in this chapter by an extensive study on hydrated SPE system, a comprehensive analysis of the global morphology and the local structure has been performed and the consequences of these configurations on diffusion of water molecules were discussed. Besides that the challenges in atomistic MD of this kind of systems were explained.

CHAPTER 7

Conclusion and Outlook

In this thesis we studied solvation and transport of various small molecules in both liquid mixtures and polymeric systems to understand polymer permeation process via atomistic computer simulations. To achieve that we have started with a study on solvation thermodynamics of a non-polar solute in a binary solution by splitting the solvation free energy term into its individual components. Furthermore, we discussed the relations between these energy contributions and the solvent equation of state data in solute transfer thermodynamics in low molecular weight systems. Since free energy and its components are the key aspects of solvation phenomena, we provided a comparative study on recently developed advanced methodologies to obtain free energy differences in polymeric solvents as well. Finally, taking into account that the diffusion is the second aspect in polymer permeation, we performed detailed analysis on the transport behavior of water molecules through ionic polymer systems. In this study, verification of computational techniques was achieved by reproducing the experimental diffusivity data of water molecules.

The first part of this thesis deals with a study on the methane solvation in terms of the free energy, enthalpy and entropy with two contributions of solute-solvent interaction and solvent reorganization interaction in various dimethyl sulfoxide (DMSO) and water concentrations (chapter 3). We presented that the entropy change of methane transfer

from water to aqueous solutions of DMSO is positive while DMSO molecules preferentially solvate the non polar solute. During this process DMSO molecules release some of their hydration waters to the bulk resulting in the increase in entropy. However, we claimed that the entropy change should not be used just by itself to describe the preferential interaction of methane with DMSO molecules since the solvent reorganization process is enthalpy-entropy compensating in the free energy.

In this thesis, we have investigated the entropy of small molecules in a solvent media. To have a complete view on the solvation thermodynamics, free energy terms and its components up to macromolecules in different solvents both in liquids and polymeric melts can be investigated further. Then the available methods we used for entropy calculations are not applicable anymore. Throughout our studies, we made use of the fact that for the free energy differences between two different states extensive sampling of the relevant parts where two states differ is sufficient instead of evaluating the complete partition function. However, to compute either absolute entropies or entropy differences from MD simulations it is necessary to simulate the system as a whole. Based on principles of statistical thermodynamics, finite-difference approximation is applicable for computation of the entropy of methane solvation in the binary mixture assuming a constant difference in the heat capacity, c_V (or c_P for NPT) over the temperature range sought. On the other hand, for the entropy calculations of macromolecules, e.g. in a case where folded and unfolded conformations of a peptide involved, considering only internal (conformational) non-diffusive degrees of freedom is not sufficient to understand the underlying forces that drive peptide or protein folding. In such cases, inclusion of solvent degrees of freedom is necessary. For similar studies where the solvation shell is

inaccessible to straight forward application of established entropy estimation methods, a recent method introduced by Grubmuller et al [151] can be an alternative way for computation. By exploiting the permutation symmetry of the solvent, it may be possible even to investigate the individual contributions from the rotational and intramolecular degrees of freedom in close future. Performing similar studies on the solvation thermodynamics for a variety of molecules in various solvent media will improve the knowledge on the underlying interactions.

A further detailed study in this thesis (in chapter 4) was performed on solvent reorganization contributions to solvation entropies and enthalpies of methane in mixtures of DMSO and water. Although the solvation entropies and enthalpies, more than the free energies, depend sensitively on proper description of solvent-solvent, solvent-cosolvent, cosolvent-cosolvent interactions a direct validation of the force-field parameterization was not possible due to lack of corresponding experimental data. Interestingly, however we have showed that the solvent reorganization enthalpy can be directly obtained from solvent equation of state data (i.e. the solvent internal pressure) via the relation

$$\left(\Delta E_{VV}\right)_P \cong \left(T\left(\frac{\alpha_P}{\kappa_T}\right)\Delta V_S^* \right) = \left[\left(\frac{\partial U}{\partial V}\right)_T + P \right] \Delta V_S^* \qquad (7.1)$$

In this relation, α_p is the isobaric thermal expansion coefficient of the solvent, κ_T is the solvent isothermal compressibility, ΔV_S^* is the solvation volume of solute S and $\left(\frac{\partial U}{\partial V}\right)_T$ is the solvent internal pressure.

Taking into account that the solvent internal pressure term is directly related to thermal expansion coefficient and isothermal compressibility constant which totally depends on the parameterization of the solvent, performing a systematic study similar to

Hess et al performed on the hydration thermodynamic properties of amino acid anologues for a systematic comparison of biomolecular force fields and water models [152] could be a good practice to check the performance of the water model descriptions in solvation studies of DMSO-water binary mixtures.

In the following part of the thesis (chapter 5), after showing how to obtain free energy differences and its individual components in binary mixtures and discussing the knowledge accessible from these terms, we switch to free energy computation methodologies for polymeric materials. We presented the resultant data from classical TI or Fast growth TIs by comparing to the ones we obtained from one step perturbation method. We illustrated within a BPA-PC system that the latter method works quite well for the computation of solvation free energy of molecules with sizes which exceed existing free volume available within the polymer matrix. Introduction of various methods such as the one we used or the another recent method, e.g. Jarzynski's Fast Growth TI, is obviously quite important for the theoretical studies since by these means there is a decrease in the computational effort and thus an increase in the efficiency.

Finally, after the discussions and comments via the solvation studies performed in this thesis, we close up with an investigation on diffusion part of the polymer permeation process in chapter 6. In this part, starting with an artificially constructed simulation system of SPE chains together with ions and water involved, we observed the microphase separation and the dependence of the dynamics of water molecules on the amount of water in the hydrophilic channels, on the temperature and also on the force-field parameters employed. Considering all the convergence problems, we achieved to reproduce the experimental diffusivity data in such an ionomeric polymer system. To go

further in this last study, the simulation system can be constructed in various other ways to see whether the results comparable to the experimental data is sensitive to the initial construction of the system or when the system is behind the percolation limit atomistic details are less affective anymore. Besides that to go deeper than the atomistic scale, for example in order to understand the mechanisms in proton conductivity, performing some other multiscale studies from atomistic to electronic (i.e. QM) level research can enlighten the behavior of water or the other components in such systems at a more magnified scheme since proton is a quantum particle.

To sum up, atomistic molecular dynamics on polymer permeation can be taken as a useful tool to understand the interactions within the polymeric materials. With the application of the methodologies discussed in this thesis on various other cases and comparison of the results with the experimental outcomes development in computational means will open a new era.

BIBLIOGRAPHY

1. Peter, C.; van der Vegt, N.F.A. *J. Phys. Chem. B* **2007**, 111, 7836.

2. Makrodimitri, Z.A.; Dohrn, R.; Economou, I.G. *Macromolecules* **2007**, 40 (5), 1720.

3. Neyertz, S.; Douanne, A.; Brown, D. *Macromolecules* **2005**, 38 (24), 10286.

4. Luder, K.; Lindfors, L.; Westergren, J.; Nordholm, S.; Kjellander, R. *J. Phys. Chem. B* **2007**, 111 (25), 7303.

5. Schmid, N.; Zagrovic, B.; van Gunsteren, W.F. *Biochemistry* **2007,** 46 (22), 6500.

6. Muller Plathe, F. *Acta Polymerica*, **1994**, 45 (4), 259.

7. Zhang, R.S.; Mattice, W.L. *J. Membr. Sci.* **1995,** 108 (1-2), 15.

8. Neyertz, S.; Douanne, A.; Brown, D. *J. Membr. Sci.* **2006**, 280 (1-2), 517.

9. Schepers, C.; Hofmann, D. *Mol. Simul.* **2006**, 32 (2), 73.

10. Moly, K.A.; Bhagawan, S.S.; George, S.C.; Thomas, S. *J. Mater. Sci.* **2007**, 42 (12), 4552.

11. Suresh, G.; Pandey, A.K.; Goswmi, A. *J. Membr. Sci.* **2007**, 295 (1-2), 21.

12. Bingol, B.; Meyer, W.H.; Wagner, M.; Wegner, G. *Macromol. Rapid Commun*. **2006**, 27 (20), 1719.

13. Kremer, K. *Macromol. Chem. Phys*., 204:257, **2003**.

14. Muller-Plathe, F. *Chem. Phys. Chem*., 3:754, **2002**.

15. Pople, J.A. *Acc. Chem. Res*. **1970**, 3, 217

16. Hehre, W.J; Radom, L.; Schleyer, P.v.R.; Pople, J.A. *Ab Initio Molecular Orbital Theory* ,Wiley-Interscience: New York **1986**

17. Szabo, A.; Ostlund, N.S. *Modern Quantum Chemistry: Introduction to Advanced Electronic Structure Theory*, McGraw-Hill: New York **1985**

18. Clark, T.A. *Handbook of Computational Chemistry: A practical guide to chemical structure and energy calculations,* Wiley-Interscience: New York **1985**

19. Cook, David B. *Handbook of Computational Quantum Chemistr*y, Oxford University Press, **1998**

20. Møller, C.; Plesset M.S. *Phys. Rev* **1934**, 46, 61

21. Leininger, M.L.; Allen, W.D.; Schaefer, H.F.; Sherrill, C.D. *J. Chem. Phys.* **2000**, 112, 21, 9213

22. Trygve, H.; Jorgensen, P.; Olsen, J.; *Molecular Electronic Structure Theory,* Wiley-Interscience: New York **2000**

23. De Frees, D.J.; Levi, B.A.; Pollack, S.K.; Hehre, W.J.; Binkley, S.J.; Pople, J.A. *J. Am. Chem. Soc.* **1979** 101, 4085

24. Davidson, E.R.; Feller, D. *Chem. Rev.* **1986** 86, 681

25. Feller, D.; Davidson, E.R. *"Basis sets for Ab Initio Molecular Orbital Calculations and intermolecular interactions'' Reviews in Computational Chemistry*, VCH: New York **1990**, 1-43

26. Boyd, D.B. *Aspects of Molecular Modeling Reviews in Computational Chemistry*, VCH: New York **1990**, 321-354

27. Metropolis, N.; Rosenbluth, A.W.; Rosenbluth, M.N.; Teller, A.H.; Teller, E. J. *Chem. Phys.* **1953**, 21, 1087

28. Binder, K.; *Monte Carlo and Molecular Dynamics Simulations in Polymer Sciences*, Oxford Univ. Press., **1995**

29. Alder, B.J.; Wainwright T.E. *J. Chem. Phys*. **1959**, 31(2), 459

30. Gilson, M.K. *Curr. Opin. Struct. Biol.* **1995**, 5, 216

31. Schreiber, H.; Steinhauer, O. *Biochemistry* **1992**, 31, 5856

32. Berendsen, H.J.C.; In Van Gunsteren, W.F.; Weiner, P.K.; Wilkinson A.J. *Computer Simulation of Biomolecular Systems Theoretical and Experimental Applications*, ESCOM, Leiden, **1993**, 161-181

33. Luty, B.A.; Davis, M.E.; Tironi, I.G.; Van Gunsteren, W.F. *Mol. Simul*. **1994**, 14, 11

34. Saito, M. *J. Chem. Phys.* **1994**, 101, 4055

35. Cheatham, I.T.E.; Miller, J.L.; Fox, T.; Darden, T.A.; Kollman, P.A. *J. Am. Chem. Soc.* **1995**, 117,4193

36. Tironi, I.G.; Sperb, R.; Smith, P.E.; Van Gunsteren, W.F. *J. Chem. Phys.* **1995**,102, 5451.

37. Berendsen, H.J.C.; van der Spoel, D.; van Drunen R. *Comput. Phys. Commun*. **1995**, 91, 43

38. Lindhal, E.; Hess, B.; van der Spoel, D. *J .Mol. Model.* **2001**, 7, 306

39. Van der Spoel, D.; Lindhal, E.; Hess, B.; Groenhof G.; Mark A.E., Berendsen H.J.C., *J. Comput. Chem.* **2005** 26,1701

40. Hockney, R.W. *Methods in Computational Physics*, **1970**, Vol. 9

41. Verlet L. *Phys.l Rev.* **1967**, 159,98

42. Swope, W.C.; Andersen H.C.; Berens, P.H.; Wilson, K.R. *J. Chem. Phys.* **1982**, 76, 637

43. Ryckaert, J.P.; Ciccotti, G.; Berendsen, H.J.C. *J. Comput. Phys.***1977**, 23, 327

44. Hess, B.; Bekker, H.; Berendsen, H.J.C.; Fraaije, J.G.E.M. *J. Comput. Chem.* **1997**, 18, 1463

45. Berendsen, H.J.C.; Postma, J.P.M.; Van Gunsteren, W.F.; Dinola, A; Haak, J.R., *J. Chem. Phys* **1984**, 81, 3684.

46. Nose, S.; Klein, M.L. *Mol. Phys.*.**1983**, 50, 1055

47. Nose, S. *Mol. Phys*, **1984**, 52, 255

48. Soddemann,T.; Dunweg,B.;Kremer,K. *Phys. Rev. E* **2003**,68,046702

49. Parinello, M.; Rahman, A. *Phys. Rev. Lett.* **1980**, 45, 1196

50. Parinello, M.; Rahman, A. *J. Appl. Phys.* **1981**, 52, 7182

51. Kolb, A.; Dunweg, B. *J. Chem. Phys.* **1999**,111,10,4453

52. Onsager, L. *J. Am. Chem. Soc.* **1936**, 58, 1486

53. Tironi, I.G.; Sperb, R.; Smith, P.E.; Van Gunsteren, W.F. *J. Chem. Phys.* **1995**, 102, 5451

54. Ewald, P.P. *Ann. Rev*, **1921**, 64, 253

55. De Leeuw, S.W.; Perram, J.W.; Smith, E.R. *Proc. R. Soc. London*, **1980**, 373, 27

56. Smith, P.E.; Van Gunsteren, W.F.; Computer Simulation of Biomolecular Systems ESCOM, Leiden, **1993**

57. Darden, T.; York, D.; Pedersen, L. *J. Chem. Phys.* **1993**, 98, 10089

58. Deserno, M.; Holm, C. *J. Chem. Phys.*, **1998**, 109, 7678

59. Essmann, U.; Perera, L.; Berkowitz, M.L.; Darden, T.; Lee, H.; Pedersen, L.G. *J. Chem. Phys.* **1995**, 103, 8577

60. Widom, B. *J. Chem. Phys.* **1963**, 39, 2808

61. Widom, B. *J. Phys. Chem.* **1982**, 86, 869

62. Frenkel, D.; Smit, B. *Understanding Molecular Simulation* Academic Press. New York **1996**

63. Mezei, M.; Beverdige, *Ann. N.Y. Acad. Sci.* **1986**, 482, 1

64. Jarzynski, C. *Phys. Rev. Lett.* **1997**, 78, 14, 2690

65. K.A. Dill, *Protein Sci.* **1999**, 8, 116

66. Gallicchio, E.; Kubo, M.M.; Levy, R.M. *J. Phys. Chem.* **2000**, *104*, 6271.

67. Matubayasi, N.; Reed, L.H.; Levy, R.M. *J. Phys. Chem*. **1994**, *98*, 10640.

68. Paschek, D. *J. Chem. Phys.* **2004**, *120*, 6674.

69. Paschek D. http://ganter.chemie.uni-dortmund.de/~pas/pics/xe.png

70. Schravendijk, P.; Van der Vegt, N.F.A. *J. Chem. Theory Comp*. **2005**, *1*, 643.

71. Lee, M. E.; Van der Vegt, N.F.A. *J. Chem. Phys.* **2005**, 122, 114509-13

72. Lee, M. E., Van der Vegt, N.F.A *J. Chem. Theory Comp*. **2007**, 3, 194-200

73. Lee, M. E., Van der Vegt, N.F.A *J. Am. Chem. Soc* **2006**, 128, 4948-4949

74. Grunwald, E.; Steel, C. *J. Am. Chem. Soc.* **1995**, *117*, 5687

75. . Sanchez, I.C.; Truskett, T.M.; In 't Veld, P.J. *J. Phys. Chem*. B **1999**, *103*, 5106.

76. Yu, H.-A.; Karplus, M. *J. Chem. Phys.* **1988**, *89*, 2366.

77. Guillot, B.; Guissani, Y. *J. Chem. Phys.* **1993**, *99*, 8075.

78. Ben-Amotz, D.; Raineri, F.O.; Stell, G. *J. Phys. Chem*. B **2005**, *109*, 6866.

79. Stone, M.T.; In 't Veld, P.J.; Lu, Y.; Sanchez, I.C. *Mol. Phys*. **2002**, *100*, 2773.

80. Peter, C.; Oostenbrink, C.; Van Dorp, A.; Van Gunsteren, W.F. *J. Chem. Phys*. **2004**, *120*, 2652.

81. Van der Vegt, N.F.A. *J. Membr. Sci.* **2002**, *205*, 125.

82. Van der Vegt, N.F.A.; Van Gunsteren, W.F. *J. Phys. Chem*. B **2004**, *108*, 1056.

83. Van der Vegt, N.F.A.; Trzesniak, D.; Kasumaj, B.; Van Gunsteren, W.F. *Chem. Phys. Chem.* **2004**, *5*, 144.

84. Ben-Naim, A. *Solvation Thermodynamics*; Plenum Press: New York, 1987.

85. Ben-Naim, A.; *J. Phys. Chem*. **1965**, *69*, 3240.

86. Lee, B.; Graziano, G. *J. Am. Chem. Soc.* **1996**, *118*, 5163.

87. Geerke, D.P.; Oostenbrink, C.; Van der Vegt, N.F.A.; Van Gunsteren, W.F. *J. Phys. Chem.* B **2004**, *108*, 1436.

88. Berendsen, H.J.C.; Postma, J.P.M.; Van Gunsteren, W.F.; Hermans, J. in *Intermolecular Forces*; Pullman, B., Ed.; Reidel: Dordrecht, **1981**, 331-342.

89. Hoover, W.G. *Phys. Rev.* A **1985**, *31*, 1695.

90. Widom, B. *J. Chem. Phys*. **1963**, *39*, 2808.

91. Ben-Naim, A.; Marcus, Y. *J. Chem. Phys*. **1984**, *81*, 2016.

92. Dymond, J.H. *J. Phys. Chem.* **1967**, *71*, 1829.

93. Ben-Naim, A. *Statistical Thermodynamics for Chemists and Biochemists* Plenum: New York, **1992**, 448-457.

94. Southall, N.T.; Dill, K.A.; Haymet, A.D.J. *J. Phys. Chem. B* **2002**, *106*, 521.

95. Symons, E.A. *Can. J. Chem.* **1971**, *49*, 3940.

96. Hummer, G.; Garde, S.; García, A.E.; Pohorille, A.; Pratt, L.R. *Proc. Natl. Acad. Sci. USA* **1996**, *93*, 8951.

97. Garde, S.; Hummer, G.; García, A.E.; Paulaitis, M.E.; Pratt, L.R. *Phys. Rev. Lett.* **1996**, *77*, 4966.

98. MacDonald, D.D.; Hyne, J.B. *Can. J. Chem*. **1971**, *49*, 611.

99. Kell, G.S. *J. Chem. Eng. Data* **1967**, *12*, 66.

100. Riddick, J.A.; Bunger, W.B.; Sakand, T.K. *Organic Solvents: Physical Properties and Methods of Purification* John Wiley and Sons: New York, **1986**.

101. Wilhelm, E.; Battino, R.; Wilcock, R.J. *Chem. Rev*. **1977**, *77*, 219.

102. Krouskop, P.E.; Madura, J.D.; Paschek, D.; Krukau, A. *J. Chem. Phys.* **2006**, *124*, 016102.

103. Frenkel, D.; Smit, B. *Understanding molecular simulation* Academic Press, 2002.

104. Müller-Plathe, F. *Macromolecules* **1991,** *24*, 6475.

105. Sok, R.M.; Berendsen, H.J.C.; Van Gunsteren, W.F. *J. Chem. Phys*. **1992**, *96*, 4699

106. Gusev, A.A.; Suter, U.W. *J. Chem. Phys*. **1993**, *99*, 2228.

107. Tamai, Y.; Tanaka, H.; Nakanishi, K. *Macromolecules* **1995**, *28*, 2544.

108. Van der Vegt, N.F.A.; Briels, W.J.; Wessling, M.; Strathmann, H. *J. Chem. Phys*. **1996**, *105*, 8849.

109. Cuthbert, T.R.; Wagner, N.J., Paulaitis, M.E. *Macromolecules* **1997**, *30*, 3058.

110. Hofmann, D.; Fritz, L.; Ulbrich, J.; Schepers, C.; Bohning, M. *Macromol. Theory Sim*. **2000**, *9*, 293.

111. Stapleton, M.R.; Panagiotopoulos, A.Z. *J. Chem. Phys*. **1990**, *92*, 1285.

112. Siepmann, J.I.; Frenkel, D. *Mol. Phys.* **1992**, *75*, 59.

113. Spyriouni, T.; Economou, I.G.; Theodorou, D.N. *Macromolecules* **1997**, *30*, 4744.

114. Fukuda, M. *J. Chem. Phys*. **2000**, *112*, 478.

115. Raptis, V.E., Economou, I.G.; Theodorou, D.N.; Petrou, J.; Petropoulos, J.H. *Macromolecules* **2004**, *37*, 1102.

116. Kirkwood, J.G. *J. Chem. Phys*. **1935**, *3*, 300.

117. Zwanzig, R.W. *J. Chem. Phys.* **1954**, *22*, 1420.

118. Hummer, G. *J. Chem. Phys*. **2001**, *114*, 7330..

119. Hess, B.; Peter, C.; Özal, T.A.; Van der Vegt, N.F.A., Submitted.

120. Boulougouris, G.C.; Economou, I.G.; Theodorou, D.N. *Mol. Phys*. **1999**, *96*, 905.

121. Boulougouris, G.C.; Economou, I.G.; Theodorou, D.N. *J. Chem. Phys*. **2001**, *115*, 8231.

122. Siegert, M.R.; Heuchel, M.; Hofmann, D. *J. Comput. Chem*. **2007**, *28*, 877.

123. Van der Vegt, N.F.A.; Briels, W.J. *J. Chem. Phys*. **1998**, *109*, 7578.

124. Schafer, H.; Van Gunsteren, W.F.; Mark, A.E. *J. Comput. Chem*. **1999**, *20*, 1604.

125. Leon, S.; Van der Vegt, N.; Delle Site, L.; Kremer, K. *Macromolecules* **2005**, *38*, 8078.

126. Hahn, O.; Mooney, D.A.; Müller-Plathe, F.; Kremer, K. *J. Chem. Phys.* **1999**, *111*, 6061.

127. Schuler, L.D.; Daura, X.; Van Gunsteren, W.F. *J. Comput. Chem*. **2001**, *22*, 1205.

128. Allen, M.P.; Tildesley, D.J. *Computer Simulations of Liquids,* Clarendon Press, Oxford, 1998.

129. Goswami, M.; Kumar, S.K.; Bhattacharya, A.; Douglas, J.F. *Macromolecules* **2007**, 40, 4113-4118

130. Muller-Plathe, F. *Macromolecules*, **1996**, 29, 4782-4791

131. Muller-Plathe, F. *Chem. Phys. Lett.* **1996**, 252, 419-424

132. Muller-Plathe, F. *J. Chem. Phys.* **1998**, 108, 8252-8263

133. Vishnyakov, A.; Neimark, A.V. *J. Phys. Chem. B* **2001**, 105, 7830-7834

134. Yang, H.; Huang, Q.; Hua, C.; Lan, Y.; Chen, C. *J. Chinese Chem. Soc.*, **2003**, 50, 529-538

135. Ennari, J.; Neelov, I.; F.Sundholm, F. *Polymer* **2001**, 42, 8043-8050

136. Ennari, J.; Elomaa, M.; Sundholm, F. *Polymer* **1999**, 18, 5035-5041

137. Urata et al., *J. Phys. Chem. B* **2005**, 109, 4269-4278

138. Urata et al., *J. Phys. Chem. B* **2005**, 109, 17274-17280

139. Banaszak, M.; Clarke, J.H.R. *Phys. Rev. E* **1999**, 60, 5753-5756

140. Muller-Plathe, F. *Macromolecules* **1998**, 31, 6721-6723

141. Masubuchi, Y.; Nishioka, A.; .Takimoto, J.; Koyama, K. *Polymer* **2002**, 43, 239-242

142. Roudgar, A.; Narasimachary, S.P.; Eikerling, M. *J. Phys.Chem. B.* **2006** 110, 20469-20477

143. Freger, V.; Korin, E.; Wisniak, J; . orngold, E.K. *J. Membr. Sci.* **1997**, 133, 255-267

144. Freger, V.; Korin, E.; Wisniak, J.; Korngold, E. *J. Membr. Sci.* **1997**, 128**,** 151-162

145. Schuler, L.D.; Daura, X.; van Gunsteren, W.F. *J. Compt. Chem.* **2001**, 22, 1205-1218

146. Frisch M. J.et al, *Gaussian 98 User's Reference*, Gaussian, Inc., Pittsburgh, **1998**

147. Besler, B.H.; Merz, K.M.;Kollman, P.A. *J. Comput. Chem.* **1990**, 11, 431-439

148. Berendsen, S. *J. Chem. Phy*s. 1988, 89, 5876

149. Weerasinghe, S.; Smith, P.E. J. Chem. Phys. **2003**, 119, 11342-11349

150. Freger, V.; Korin, E.; Wisniak, J.; Korngold, E.; Ise, M.; Kreuer, K.D. *J. Membr. Sci.* **1999**, 160, 213-224

151. Reinhard, F.; Grubmüller,H. *J. Chem.Phys*. **2007**, 126, 014102-014102-7

152. Hess, B.; van der Vegt, N.F.A., *J.Phys.Chem.B* **2006**, 110, 17616-17626